THE UNIVERSITY OF OKLAHOMA

GRADUATE COLLEGE

A LIFTING LINE ANALYSIS OF NONPLANAR WINGS

A DISSERTATION

SUBMITTED TO THE GRADUATE FACULTY

in partial fulfillment of the requirements for the

degree of

DOCTOR OF PHILOSOPHY

by

WILLIAM A. EDGINGTON

Norman, Oklahoma

1972

A LIFTING LINE ANALYSIS OF NONPLANAR WINGS

APPROVED BY

Edward T. Bluth

Maurice Rasmussen

Arthur Bernhart

Martin C. Jischke

Darrell G. Harden

DISSERTATION COMMITTEE

ACKNOWLEDGMENT

The author sincerely appreciates the guidance and assistance given by Dr. Edward F. Blick, of the School of Aerospace and Mechanical Engineering, and also gives a special note of thanks to Dr. Martin C. Jischke and Dr. Maurice L. Rasmussen, of the School of Aerospace and Mechanical Engineering, for their assistance.

The author also wishes to express his gratitude to his wife, Nancy, and his three sons, Richard, John, and William, for their patience and understanding during this period of research.

TABLE OF CONTENTS

LIST OF ILLUSTRATIONS

LIST OF ILLUSTRATIONS (Cont'd.)

LIST OF ILLUSTRATIONS (Cont'd.)

LIST OF SYMBOLS

a	semi-minor axis of ellipse
a_0	two dimensional lift curve slope
AR	aspect ratio
b	semi-major axis of ellipse
B_n	Fourier coefficients
c	wing chord
c'	wing chord between wing tip and first collocation point
C_D	wing drag coefficient
C_{D_i}	wing induced drag coefficient
C_L	wing lift coefficient
$\bar{d}$	vector from vortex to the point at which downwash is calculated
$D(y,n)$	function, see equation 2.19
$D(\phi,n)$	function, see equation 3.23
e	eccentricity
$\hat{e}_l$	unit vector normal to $\bar{d}$
$\hat{e}_r, \hat{e}_\phi$	unit vectors, polar coordinates
$E(\phi)$	function, see equation 3.21
$f(y)$	function, see figure 2.2
$F(y,z)$	function, see equation 2.11
$F(r,\phi)$	function, see figure 3.1
H_n	function, see appendix B

$\hat{i},\hat{j},\hat{k}$	unit vectors, Cartesian coordinates
I_n	function, see appendix B
J_n	function, see appendix B
k	efficiency factor
K	b/a
K_{np}	function, see equation A.2
ℓ	two dimensional lift
M	function, see equation 3.16
N	function, see equation 3.17
P	locus, see figure 2.3
P_1	locus, see figure 2.3
$\bar{q}$	induced velocity vector
Q(n)	function, see equation 3.15
$\bar{r}$	radius vector
r_1	function, see equation A.6
r_{00}	function, see equation A.7
$\bar{R}$	radius vector
s	arc-span coordinate, see figure A.1
s_1,x_1	variables of integration, see equation A.1
S	wing reference area
U	free stream velocity
$\bar{w}$	downwash vector
x,y,z	Cartesian coordinates
x_0	function, see equation A.3
y_0	function, see equation A.4

z_0	function, see equation A.10
z_{00}	function, see equation A.5

Greek Letters

α_a	geometric angle of attack
α_c	geometric angle of attack at wing center-line
α_i	induced angle of attack
α_o	effective angle of attack
α_z	angle of attack for zero lift
β	angular displacement of first collocation point
γ	rate of change of circulation
Γ	circulation
Γ_0	circulation at center-line
δ	c/R
η	variable of integration, see equation 3.6
λ	$\eta-\phi$ (appendix C)
ξ	$\eta-\phi$ (appendix A)
ρ	density (radius of curvature in appendix A)
ϕ	collocation point, polar coordinates
ψ	function, see equation A.9

Subscripts

n	normal component
x,y,z	components along the x,y,z axes

A LIFTING LINE ANALYSIS OF NONPLANAR WINGS

CHAPTER I

INTRODUCTION

The motivation behind this endeavor has its beginning during the 1920's. It was then that Mr. Willard Custer conceived the idea of constructing a channel-wing aircraft. Since the first pilotless flight in 1927 Mr. Custer has continued to advance the concept and his latest model is the CCW-5 [1].

The channel wing concept has gained a certain amount of momentum in the last few years owing to the increased interest in developing a reliable short take-off and landing (STOL) aircraft. The concept takes advantage of the Bernoulli Principle by relying on an increased velocity over the upper surface of the channel. This increase in velocity lowers the static pressure on the upper surface and results in higher lift forces than can be obtained from using a planar wing.

This increase in velocity is attained by mounting the aircraft engine in the center of a semi-circular channel with the propeller mounted aft at the trailing edge of the

wing. Figure 1.1 illustrates the possibility of utilizing the concept on a Fairchild F-27.

Until recently, investigative efforts probing the feasibility of the concept have been primarily experimental in nature [2-8] and although a considerable amount of increased lift could be attributed to the channel the concept did not receive much enthusiasm. This lack of enthusiasm is partially attributable to the fact that a firm requirement for a STOL type aircraft did not exist at that time. A resurgence of interest in the concept has since been generated because of the realization that a STOL-type aircraft is indeed practical and feasible.

Theoretical investigations into the concept are still relatively few in number and are divided into two different approaches. The first approach [9] is a closed form solution requiring only airfoil data and the propeller thrust as inputs. Its relative simplicity is the major advantage since it compares very favorably with experimental data for a propeller mounted behind a semi-circular channel. A disadvantage of the approach is that it does not predict the effect of the channel section on the remainder of the wing. The second effort [10] uses lifting surface theory as its basis and, although the results compare well with experimental data, it requires a considerable amount of computer time for a solution. Unlike the Blick theory [9] the second method

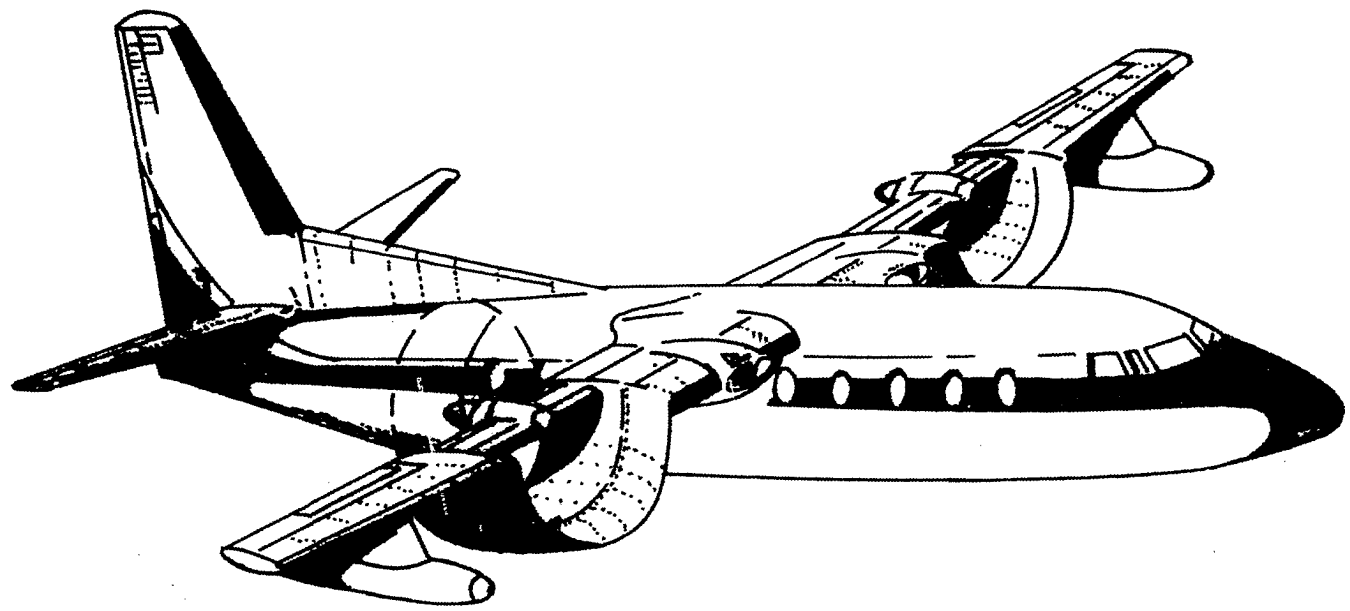

Figure 1.1 Possible Channel Wing Modification to a Fairchild F-27

does predict the effect of the channel section on the remainder of the wing. Both of the aforementioned methods have been applied only to semi-circular sections; the Blick theory being restricted to this type of section.

It is well known that Prandtl's lifting line theory [11] closely approximates the results from lifting surface theory for high or moderate aspect ratio planar wings. It will be the object of this dissertation to apply the same ideas to nonplanar wings, with the assumption that the channel sections are elliptical in shape. This will hopefully provide some basis for choosing an optimum channel shape.

Chapter II develops a lifting line theory for a nonplanar wing of a general shape. The applicability of this method for a general shaped wing will not be evaluated since the calculations will be restricted to elliptical wings.

Chapter III applies the previously developed theory to an elliptical wing. An extension of this development to include applications to wings of other shapes such as a planar wing with a channel inserted between the wing tips should be straightforward.

Chapter IV concerns itself with the aerodynamic properties that are derived from the circulation of elliptically shaped wings.

CHAPTER II

THEORETICAL DEVELOPMENT

The lifting line theory as formulated by Prandtl is the basis for this development. Prandtl's model of the flow past a finite wing does imply certain assumptions which will be iterated at this time.

The circulation, Γ, associated with the lift on the wing vanishes at the tips and is distributed symmetrically about the midsection of the wing. This circulation is equated to the outflow of vorticity and any variation in circulation will be accompanied by a shedding of vorticity from the wing. These vortex filaments are generated at the wing and proceed downstream to infinity (if the flow is assumed to be steady) from the trailing edge of the wing in the direction of the undisturbed flow. Unlike lifting surface theory, Prandtl's lifting line theory assumes the lift is concentrated along a single line to which the wing reduces as the aspect ratio tends to infinity. The vortex filaments originating at this line have a constant strength, $\frac{d\Gamma}{ds}$, where s is the distance measured along the lifting line as shown in figure 2.1.

The total velocity, $\overline{dq}$, induced by one of these elemental vortex filaments may be obtained by the use of

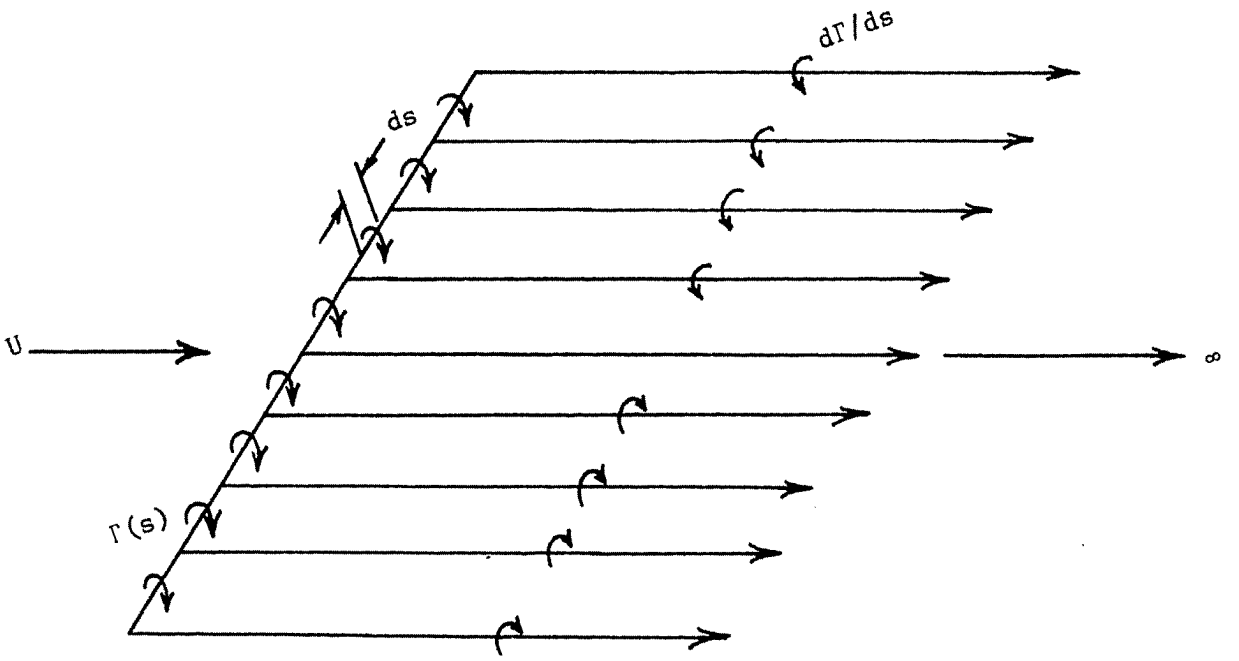

Figure 2.1 Vortex Filaments Originating from a Lifting Line

Biot-Savart law and integrating from the lifting line to infinity. This integration may be found in most textbooks on fluid dynamics and is omitted from this work.

The induced velocity, $\bar{q}$, resulting from the summation of all the elemental vortex filaments, has two components; one along the lifting line and the other normal to a plane passed through the lifting line and the undisturbed velocity. The component along the lifting line is zero for a planar wing and will be assumed to be very small compared to the normal component along a nonplanar wing with the possible exception of a small arc length very near the wing tip. The normal component is commonly referred to as the downwash, $\bar{w}$. After one makes the assumption that the component along the lifting line is negligible, each section of the wing is then assumed to behave as though it were a two dimensional section of the wing in the presence of the free stream plus the downwash.

BASIC EQUATIONS

The resultant force, ℓ_n, experienced by a unit span of the wing is given by the Kutta-Joukowski theorem which relates this force to the density, ρ, free stream velocity, U, and the circulation, Γ.

$$\ell_n = \rho U \Gamma \tag{2.1}$$

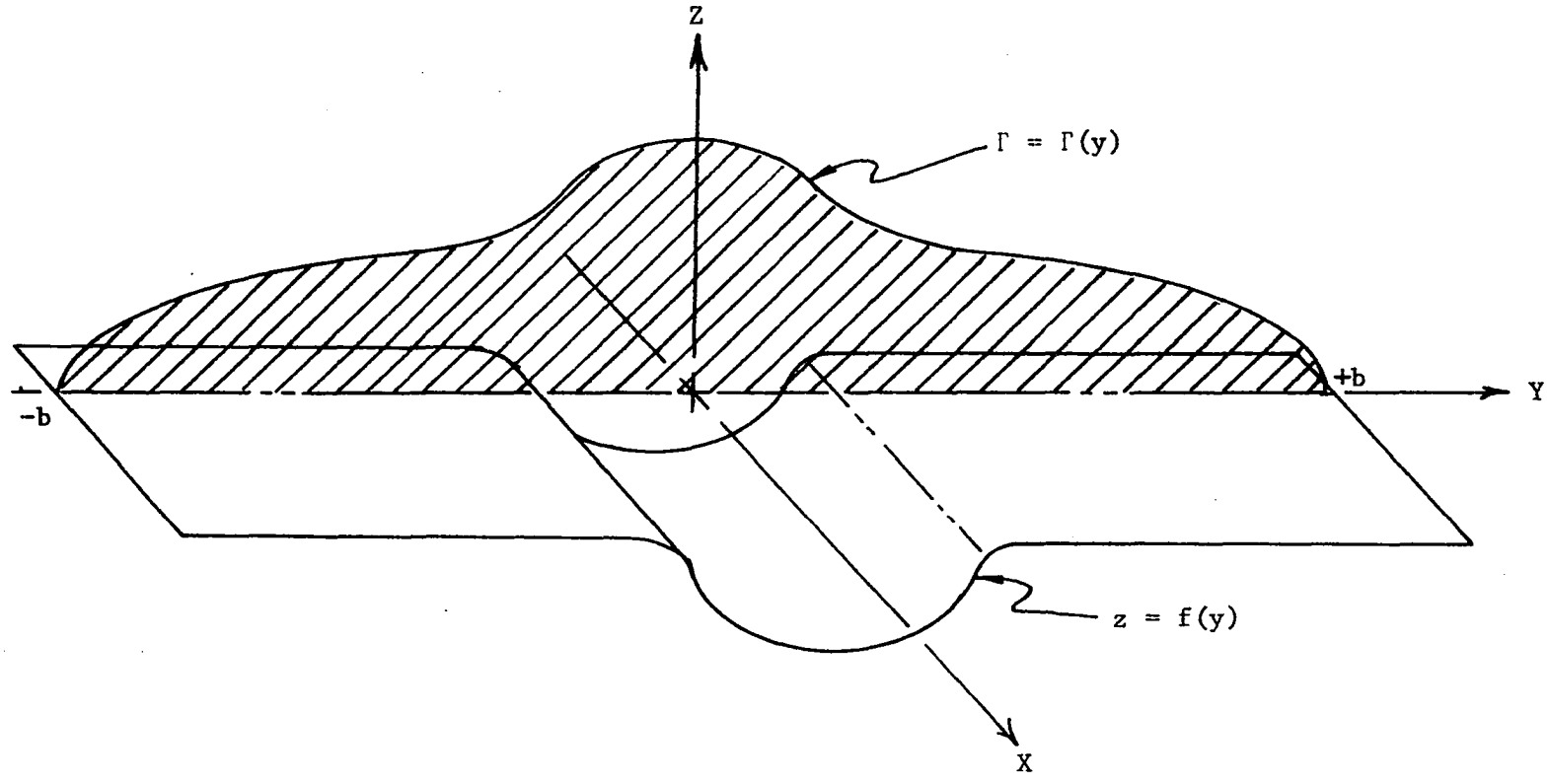

Figure 2.2 Lifting Line Representation of a Nonplanar Wing

From two dimensional airfoil theory, it is also known that

$$\ell_n = a_o \alpha_o \frac{1}{2} \rho U^2 c \tag{2.2}$$

where a_o is the lift curve slope associated with the two dimensional airfoil section, c is the airfoil chord, and α_o is the effective angle of attack. After the expression for ℓ_n that is given by the Kutta-Joukowski theorem is substituted into equation 2.2, an expression results which has two unknown values.

$$\Gamma = \frac{1}{2} a_o U c \alpha_o \tag{2.3}$$

These two unknown values are the circulation, Γ, and the effective angle of attack, α_o. The effective angle of attack may be related to the absolute angle of attack, α_a, in the following manner.

$$\alpha_o = \alpha_a - \alpha_i \tag{2.4}$$

The induced angle of attack, α_i, arises as a result of the downwash and may be expressed as

$$\alpha_i = \arctan \frac{w}{U} \simeq \frac{w}{U} . \tag{2.5}$$

Equation 2.3 now may be written in terms of the circulation and a new unknown quantity, downwash.

$$\Gamma = \frac{1}{2} a_o U c \left[\alpha_a - \frac{w}{U} \right] \tag{2.6}$$

The problem is now relegated to one of finding an expression for the downwash distribution on the wing and relating this downwash to the circulation distribution. The incremental downwash, dw, is that component of the induced velocity that is normal to the wing (see figure 2.3) and may be calculated in the following manner.

$$dw = \overline{dq} \cdot \frac{\text{grad } F}{|\text{grad } F|} \tag{2.7}$$

The function, F, describes the shape of the wing and is written in a manner such that grad F is in a downward direction normal to the wing.

From the Biot-Savart law the incremental induced velocity, $\overline{dq}$, was found to be

$$\overline{dq} = \frac{d\Gamma/ds}{4\pi d} \frac{(\overline{d} \times \hat{i})}{|\overline{d} \times \hat{i}|} ds \tag{2.8}$$

where $\overline{d}$ is the vector from the vortex to a point on the wing and $\hat{i}$ is the unit vector in the X direction as shown in figure 2.3. The incremental downwash then becomes

$$dw = \frac{\text{grad } F}{|\text{grad } F|} \cdot \frac{d\Gamma/ds}{4\pi d} \hat{e}_1 \, ds \tag{2.9}$$

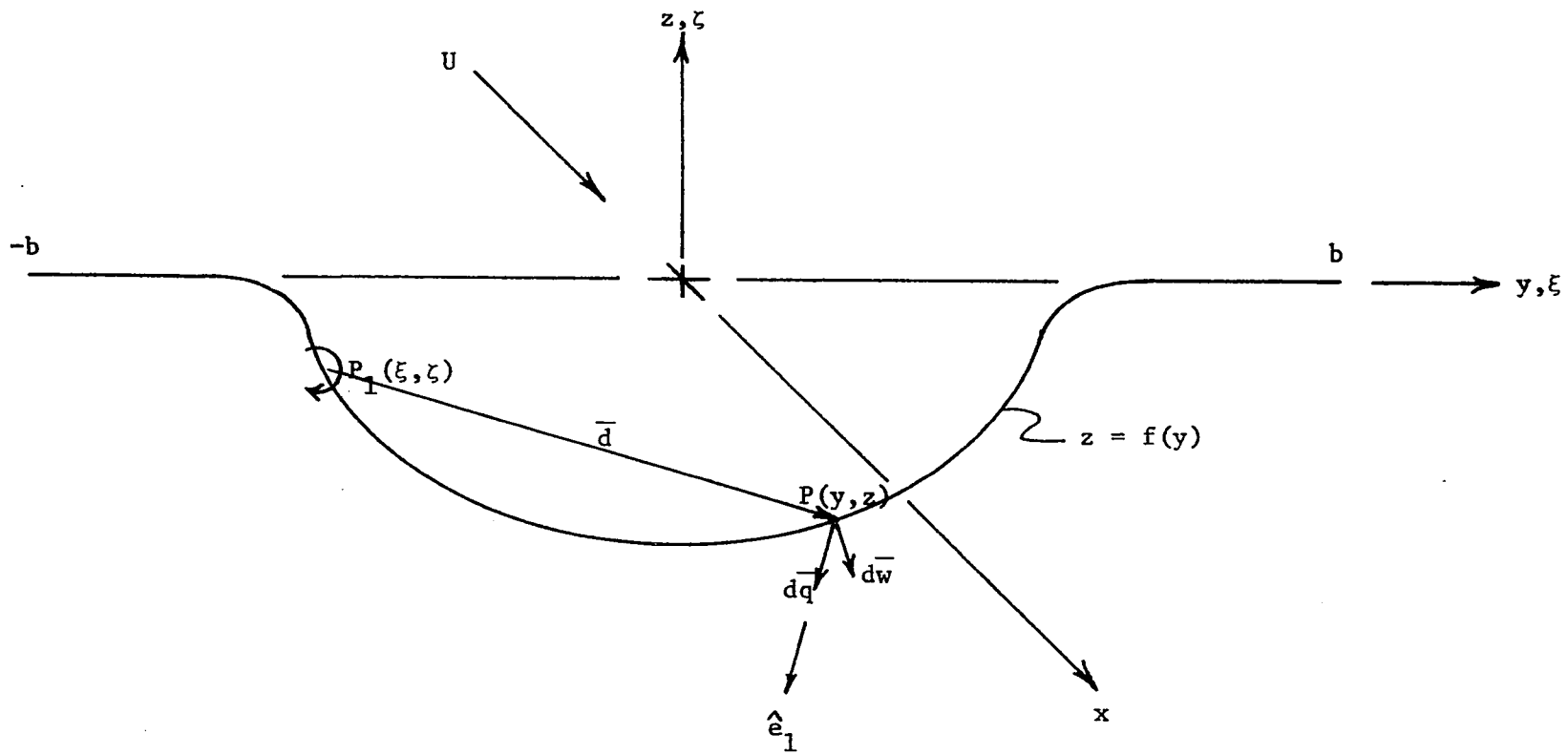

Figure 2.3 Induced Velocities on the Lifting Line

where

$$\hat{e}_l = \frac{(\bar{d} \times \hat{i})}{d} . \tag{2.10}$$

The total downwash at P(y,z) is obtained by integrating equation 2.9 over the entire span of the wing.

$$w = \frac{\text{grad } F}{|\text{grad } F|} \cdot \oint_{-b}^{b} \frac{d\Gamma/ds}{4\pi d} \hat{e}_l \, ds \tag{2.11}$$

This expression for the downwash can now be substituted into equation 2.6.

$$\Gamma = \frac{1}{2} a_o U c \left[\alpha_a - \frac{1}{4\pi U} \frac{\text{grad } F}{|\text{grad } F|} \cdot \oint_{-b}^{b} \frac{d\Gamma/ds}{d} \hat{e}_l \, ds \right] \tag{2.12}$$

There have been no restrictions placed upon either the chord, c, or the lift curve slope of the two dimensional airfoil, a_o, and in general they may be continuous functions of y.

The absolute angle of attack, α_a, is also a function of y and can be determined from the geometry of the wing and the angle of zero lift, α_z, for the airfoil section.

$$\alpha_a = \alpha - \alpha_z . \tag{2.13}$$

where α is the geometric angle of attack. If α_c is defined as the geometric angle of attack at the mid-section of the channel, then α can be determined in the following manner.

From figure 2.4 it can be seen that

$$V_x = U \cos \alpha_c \tag{2.14}$$

and

$$V_z = U \sin \alpha_c . \tag{2.15}$$

The geometric angle of attack, α, is then

$$\alpha = \arctan \left(\frac{V_n}{V_x} \right) \tag{2.16}$$

where V_n is that component of V_z that is normal to the surface of the wing. V_n is expressed as

$$V_n = -V_z \hat{k} \cdot \frac{\text{grad } F}{|\text{grad } F|} ; \tag{2.17}$$

the negative sign being required due to the direction of grad F. Therefore

$$\alpha_a = \arctan \left[- \frac{V_z}{V_x} \hat{k} \cdot \frac{\text{grad } F}{|\text{grad } F|} \right] - \alpha_z . \tag{2.18}$$

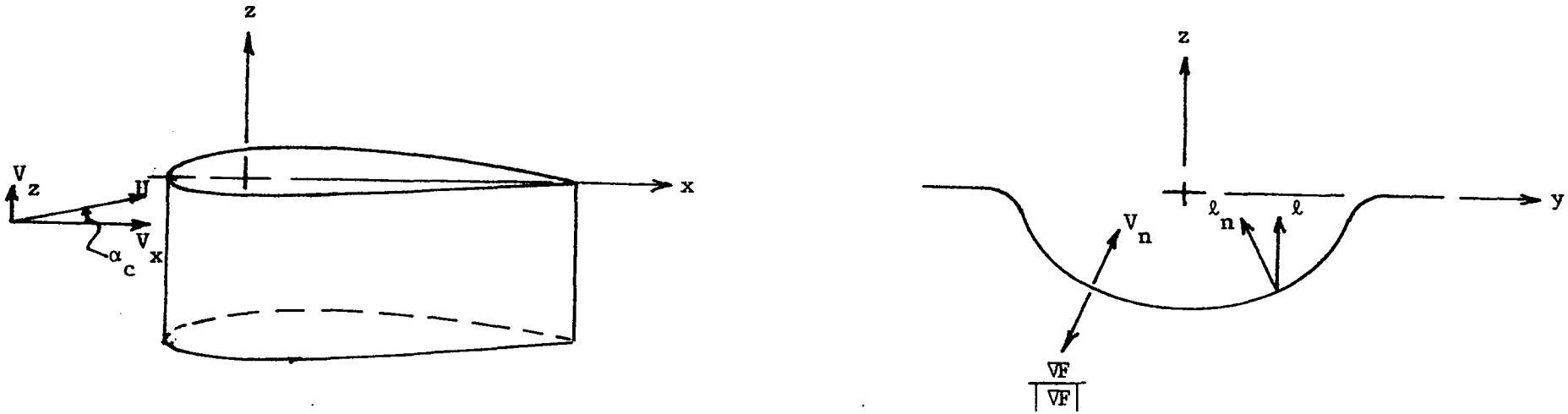

Figure 2.4 Angle of Attack

Equation 2.12 can now be expressed as

$$\Gamma + \frac{a_o c}{8\pi} \frac{\text{grad } F}{|\text{grad } F|} \cdot \oint_{-b}^{b} \frac{d\Gamma/ds}{d} \hat{e}_l \, ds =$$

$$\frac{1}{2} a_o U c \left\{ \tan^{-1} \left[-\tan \alpha_c \hat{k} \cdot \frac{\text{grad } F}{|\text{grad } F|} \right] - \alpha_z \right\} \qquad (2.19)$$

and becomes the equation which must be solved to determine the appropriate circulation distribution.

One method of solution is to assume a suitable series solution for the circulation distribution and evaluate the coefficients of the series by use of a collocation process. This method is pursued in the following chapter to evaluate the coefficients of a Fourier series that is used to represent the circulation distribution associated with wings that have an elliptical shape.

CHAPTER III

ELLIPTICAL WING SECTIONS

The special case of elliptical channels will be investigated in this chapter. Due to the nature of the geometry (see figure 3.1) where

$$r = \frac{ab}{\{\, b^2 \sin^2\phi + a^2 \cos^2\phi \,\}^{\frac{1}{2}}} \tag{3.1}$$

and

$$R = \frac{ab}{\{\, b^2 \sin^2\eta + a^2 \cos^2\eta \,\}^{\frac{1}{2}}} \tag{3.2}$$

it becomes advantageous to recast the general theory into polar coordinates.

If the assumption is made that the circulation, Γ, can be represented by a Fourier sine series, the coefficients of this series can then be determined by the method of collocation. The sine series is chosen since it automatically forces the circulation to zero at the wing tips thus satisfying that boundary condition. In addition only the odd terms of the series are considered since the even terms lead to an asymmetrical circulation distribution. For simplicity in the following integration the circulation is assumed to be only a function of the spanwise coordinate, ϕ.

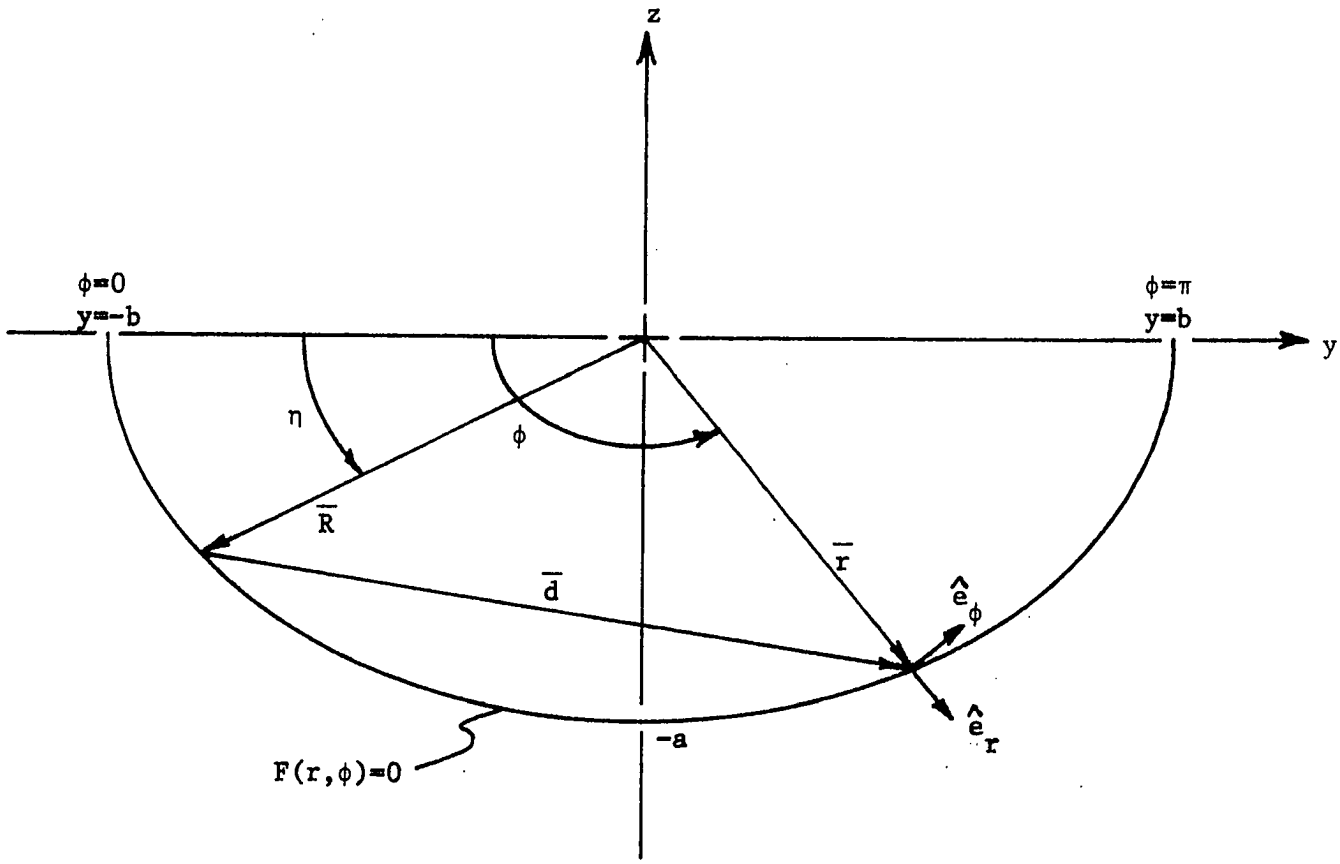

Figure 3.1 Polar Coordinates for an Elliptical Wing

The circulation sine series is then written as

$$\Gamma = Ub \sum_{n=1}^{\infty} B_n \sin n\phi \qquad (n \text{ odd}) \tag{3.3}$$

The rate of change of the circulation is now expressed as

$$\frac{d\Gamma}{ds} ds = \frac{d\Gamma}{d\phi} d\phi \tag{3.4}$$

and

$$\frac{d\Gamma}{d\phi} = Ub \sum_{n=1}^{\infty} nB_n \cos n\phi \tag{3.5}$$

since Γ is only a function of ϕ.

Equation 2.19 can now be expressed in polar coordinates as

$$\sum_{n=1}^{\infty} B_n \left\{ \sin n\phi + \frac{a_o c}{8\pi} \frac{\text{grad } F}{|\text{grad } F|} \cdot \oint_0^{\pi} \frac{n}{d} \cos n\eta \, \hat{e}_i \, d\eta \right\} =$$

$$\frac{a_o c}{2b} \left\{ \tan^{-1} \left[-\tan \alpha_c \hat{k} \cdot \frac{\text{grad } F}{|\text{grad } F|} \right] - \alpha_z \right\} \tag{3.6}$$

From equation 3.6 it can be seen that the argument of the integral is singular in the limit as d goes to zero. The solution for the coefficients for the circulation distribution by the collocation method involves the evaluation of n squared singular integrals if one uses the present form of equation 3.6. The number of

singular integrals can be reduced to n by removing the dependency upon n from the singular integral. This is accomplished by adding and substracting an identical quantity in the following manner.

$$\sum_{n=1}^{\infty} B_n \left\{ \sin n\phi + \frac{a_o c}{8\pi} \frac{\text{grad } F}{|\text{grad } F|} \cdot \left[n \int_0^{\pi} \frac{\hat{e}_i}{d} \left(\cos n\eta - \cos n\phi \right) d\eta + \cos n\phi \oint_0^{\pi} \frac{\hat{e}_i}{d} d\eta \right] \right\} = \frac{a_o c}{2b} \left\{ \tan^{-1} \left[-\tan \alpha_c \hat{k} \cdot \frac{\text{grad } F}{|\text{grad } F|} \right] - \alpha_z \right\} \tag{3.7}$$

The first integral of equation 3.7 is now non-singular and the limit as d goes to zero will depend upon the geometric shape of the wing. The second integral of equation 3.7 remains singular but is independent of n thus reducing the number of singular integrals to n. From equation 3.7 it can be seen that the only remaining variables that need to be recast into polar coordinates are $\hat{e}_i$, d and grad F.

The vector, $\bar{d}$, is expressed as

$$\bar{d} = \bar{r} - \bar{R} \tag{3.8}$$

where

$$\bar{r} = r\hat{e}_r \tag{3.9}$$

and

$$\bar{R} = R\{\cos(\phi-\eta)\hat{e}_r - \sin(\phi-\eta)\hat{e}_\phi\}. \tag{3.10}$$

Therefore

$$\bar{d} = \left[r - R\cos(\phi-\eta)\right]\hat{e}_r + R\sin(\phi-\eta)\,\hat{e}_\phi \tag{3.11}$$

and

$$d = \left[r^2 + R^2 - 2rR\cos(\phi-\eta)\right]^{1/2}. \tag{3.12}$$

The unit vector, $\hat{e}_l$, which is normal to $\bar{d}$, is then

$$\hat{e}_l = \frac{R\sin(\phi-\eta)\,\hat{e}_r + \left[R\cos(\phi-\eta) - r\right]\hat{e}_\phi}{\left[r^2 + R^2 - 2rR\cos(\phi-\eta)\right]^{1/2}}. \tag{3.13}$$

The gradient of F divided by its magnitude, which is the downward unit normal to the wing, is expressed as

$$\frac{\text{grad } F}{|\text{grad } F|} = \frac{\left[b^2\sin^2\phi + a^2\cos^2\phi\right]\hat{e}_r + \left[(b^2-a^2)\sin\phi\cos\phi\right]\hat{e}_\phi}{\left[b^4\sin^2\phi + a^4\cos^2\phi\right]^{1/2}}. \tag{3.14}$$

After substituting the values associated with the geometry of the wing into equation 3.7 it is found that

$$\sum_{n=1}^{\infty} B_n \left\{ \sin n\phi + \frac{a_o c}{8\pi b (K^4 \sin^2\phi + \cos^2\phi)^{1/2}} \left[n \int_0^{\pi} Q(\eta)(\cos n\eta - \cos n\phi)\, d\eta + \cos n\phi \oint_0^{\pi} Q(\eta)\, d\eta \right] \right\} =$$

$$\frac{a_o c}{2b} \left\{ \tan^{-1} \left[\frac{K^2 \tan \alpha_c \sin\phi}{(K^4 \sin^2\phi + \cos^2\phi)^{1/2}} \right] - \alpha_z \right\} \qquad (3.15)$$

where

$$Q(\eta) = \frac{MN^4 \sin(\phi-\eta) + \left[MN^2 \cos(\phi-\eta) - M^2 N \right] \sin\phi \cos\phi \, (K^2-1)}{M^2 + N^2 - 2MN \cos(\phi-\eta)} \qquad (3.16)$$

in which

$$M = (K^2 \sin^2\eta + \cos^2\eta)^{1/2}, \qquad (3.17)$$

$$N = (K^2 \sin^2\phi + \cos^2\phi)^{1/2}, \qquad (3.18)$$

and

$$K = \frac{b}{a} = 1/(1-e^2)^{1/2} \, . \qquad (3.19)$$

Except for the special case where the eccentricity, e, is zero (appendix B) a numerical solution for the integration is required. To facilitate the use of machine integration it becomes necessary to investigate both the limit of the non-singular integral as η approaches ϕ and the convergence of the singular integral in equation 3.15.

The integrand

$$Q(\eta)(\cos n\eta - \cos n\phi)$$

is non-singular and the limit as η approaches ϕ is

$$\lim_{\eta\to\phi}\left[Q(\eta)(\cos n\eta - \cos n\phi)\right] = \frac{nN^3 \sin n\phi\left[N^4-(K^2-1)^2\sin^2\phi\,\cos^2\phi\right]}{(K^2-1)^2\sin^2\phi\,\cos^2\phi + N^4}. \tag{3.20}$$

The singular integral in equation 3.15 converges and may be evaluated (appendix C) as follows.

$$\oint_0^{\pi} Q(\eta)d\eta = \int_0^{\phi-\varepsilon} Q(\eta)d\eta + \int_{\phi+\varepsilon}^{\pi} Q(\eta)d\eta + E(\phi) \tag{3.21}$$

where

$$E(\phi) = -\left[\frac{N \sin\phi \cos\phi \,(K^2-1)}{(K^2-1)^2 \sin^2\phi \cos^2\phi + N^4}\right]$$

$$\left[3N^4 + N^2(K^2-1)(\cos^2\phi - \sin^2\phi) + (K^2-1)\sin^2\phi \cos^2\phi\right] \varepsilon$$

$$+ \text{terms of order } \varepsilon^2. \qquad (3.22)$$

The Fourier coefficients in equation 3.15 are evaluated by the collocation method. This method requires that equation 3.15 be evaluated at n locations of ϕ and then this system of n simultaneous equations is solved to determine the value of the n Fourier coefficients that satisfy equation 3.15. After the Fourier coefficients are determined, equation 3.3 gives the expression for the circulation distribution. To render the circulation independent of the density and the free stream velocity, the spanwise values of circulation are normalized with respect to the value of the circulation, Γ_o, calculated at the wing center-line.

Figure 3.2 illustrates that an increase in eccentricity, for a given value of the two dimensional lift curve slope and the aspect ratio, increases the circulation distribution near the wing tips. The exhibited trend in circulation is not analagous to that of the planar wing wherein such a distribution would imply that as eccentricity increases the circulation distribution is approaching that of a wing which has an infinite span. The nonplanar wing, as eccentricity increases, has an increase in the force normal to the wing and an

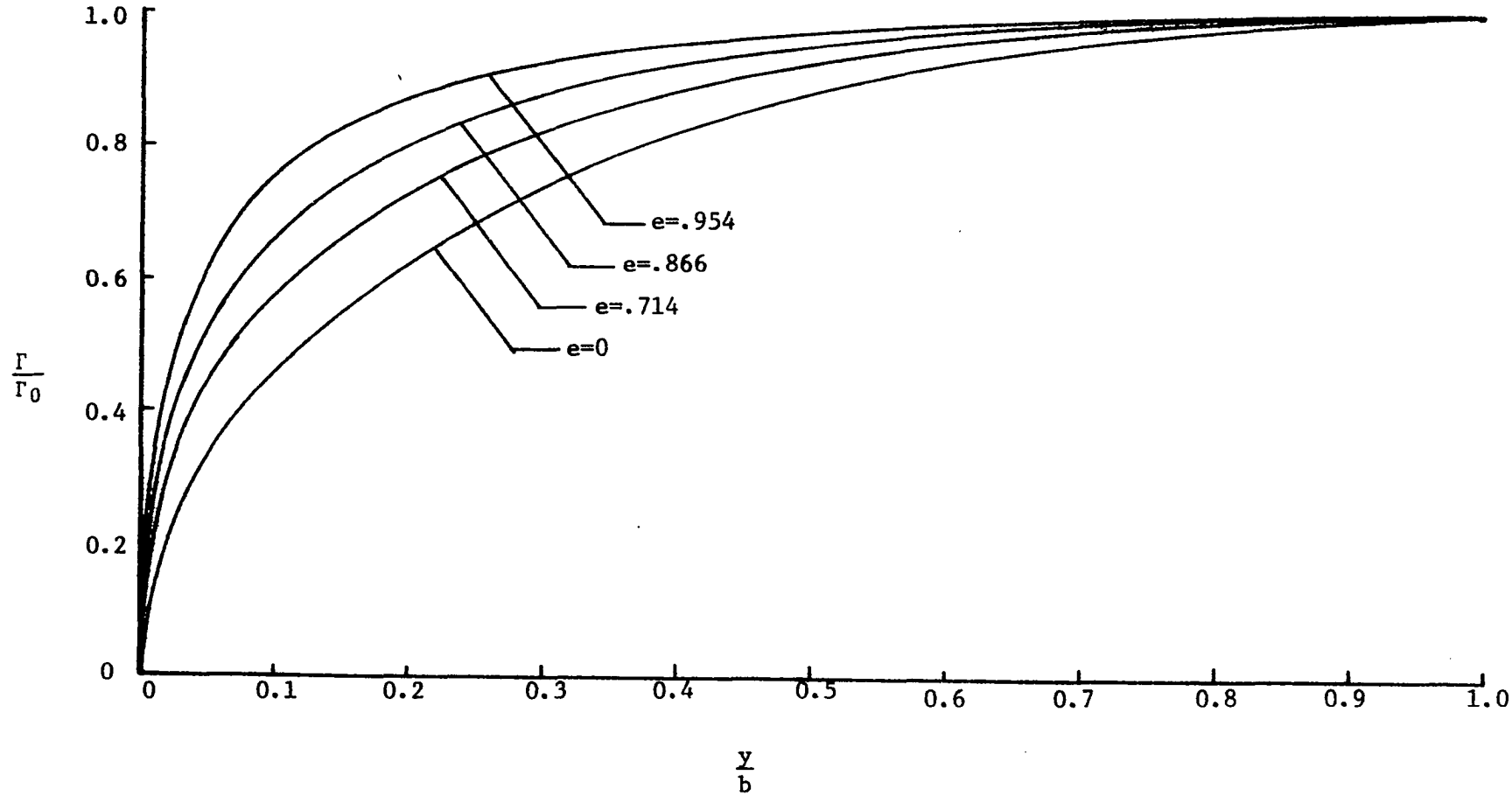

Figure 3.2 Circulation Distribution ($a_0=2\pi$)(AR=20)

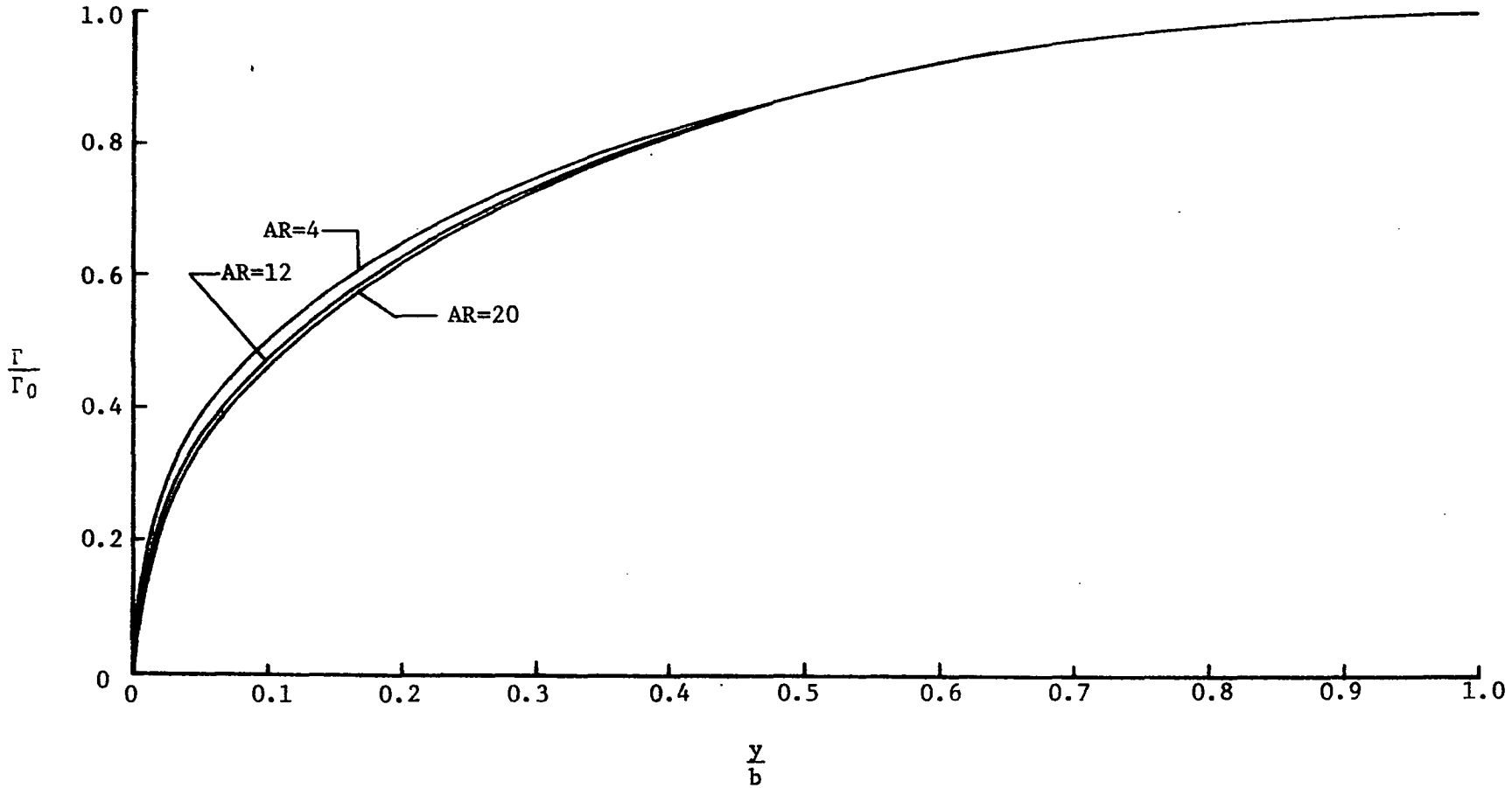

Figure 3.3 Circulation Distribution ($e=0$)($a_0=2\pi$)

increase in the induced drag. Due to the spanwise slope of the wing near the tip the lift (vertical force) does not increase at the same rate as the induced drag and the overall effect is to decrease the efficiency of the wing.

The wing aspect ratio is defined as

$$AR = \frac{4b^2}{S} \tag{3.23}$$

where the reference wing area, S, is taken as that area of a planar wing having a semi-span equal to the semi-major axis of the elliptical wing and the same chord distribution. It is shown in figure 3.3 that the circulation distribution decreases as the aspect ratio increases and the circulation distribution reaches an asymptotic limit for values of the aspect ratio near 20.

Figures 3.4 through 3.7 show the effect of changing the two dimensional section characteristics for elliptical wings of differing eccentricities. The section properties that were varied were the angle of zero lift and the lift curve slope. The NACA 2412 and 4412 airfoils have the same lift curve slope but different angles of zero lift. The angles of zero lift are -1.9^0 for the NACA 2412 and -3.9^0 for the NACA 4412 airfoil. Both airfoils have a lift curve slope of $.985(2\pi)$ per radian. The third wing was composed of airfoil sections having an angle of zero lift equal to zero and a lift curve slope of 2π. It is interesting to note that the circulation distribution is effected more by the angle of zero

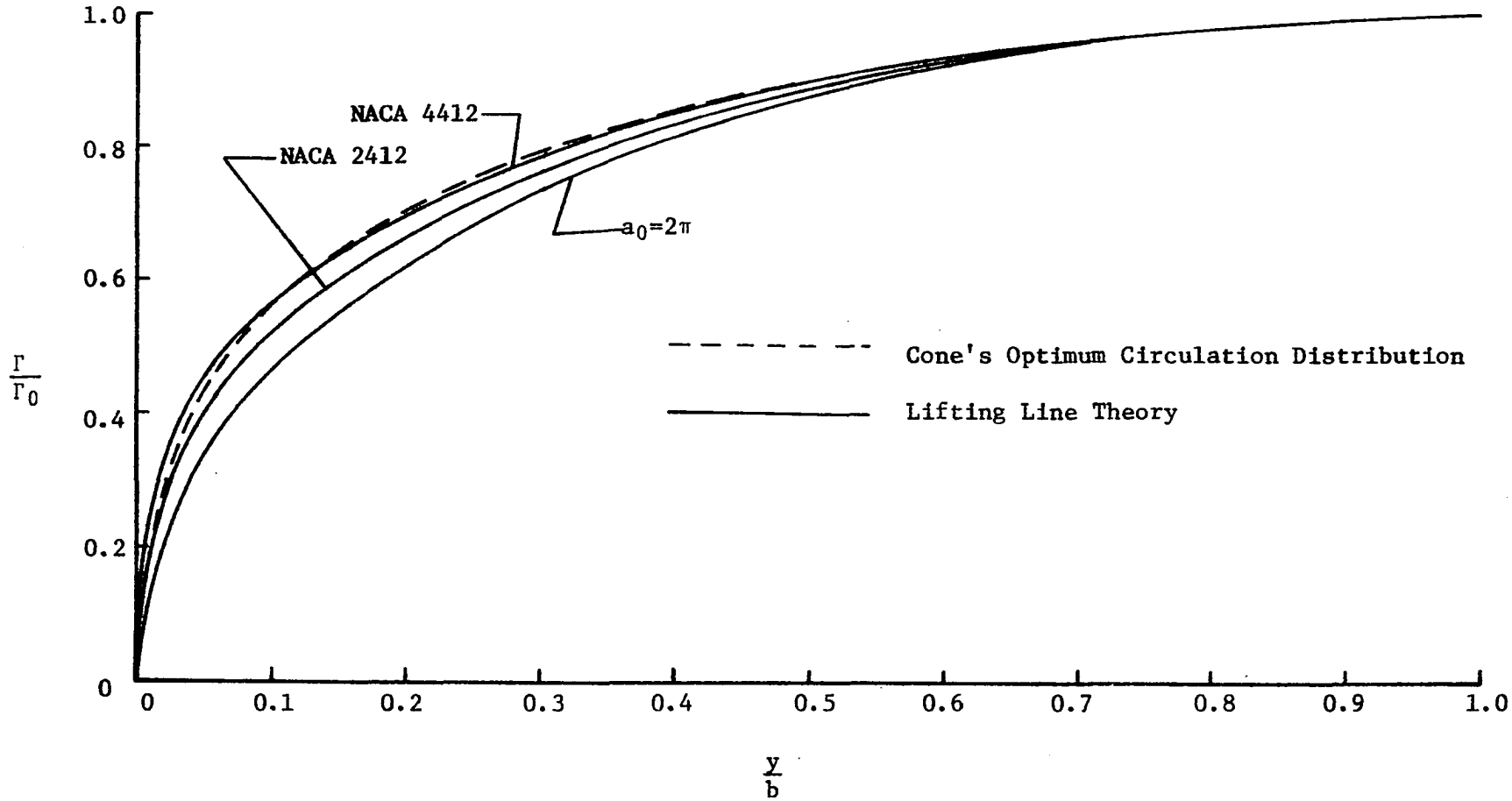

Figure 3.4 Circulation Distribution (e=0)(AR=20)

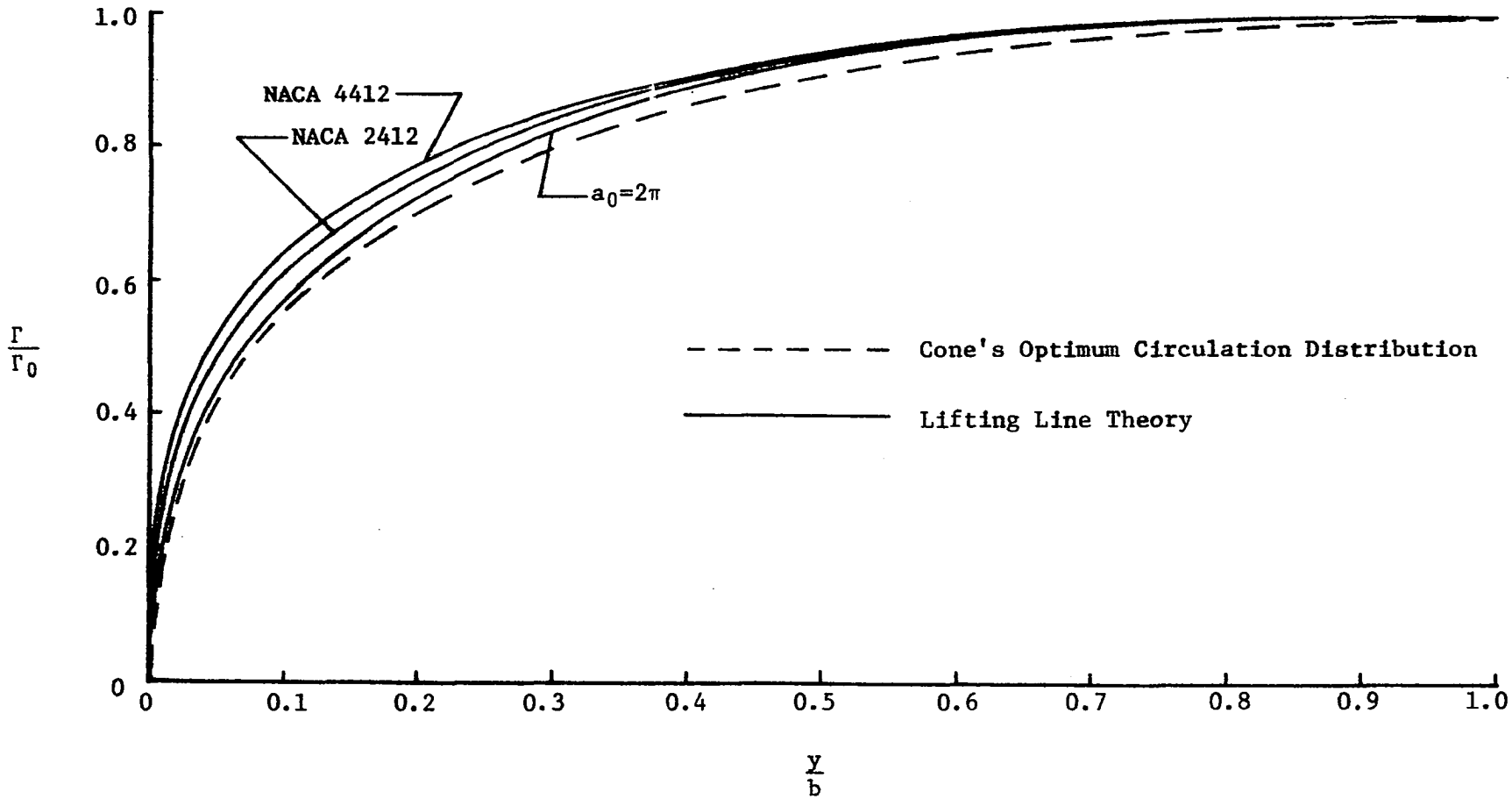

Figure 3.5 Circulation Distribution (e=.714)(AR=20)

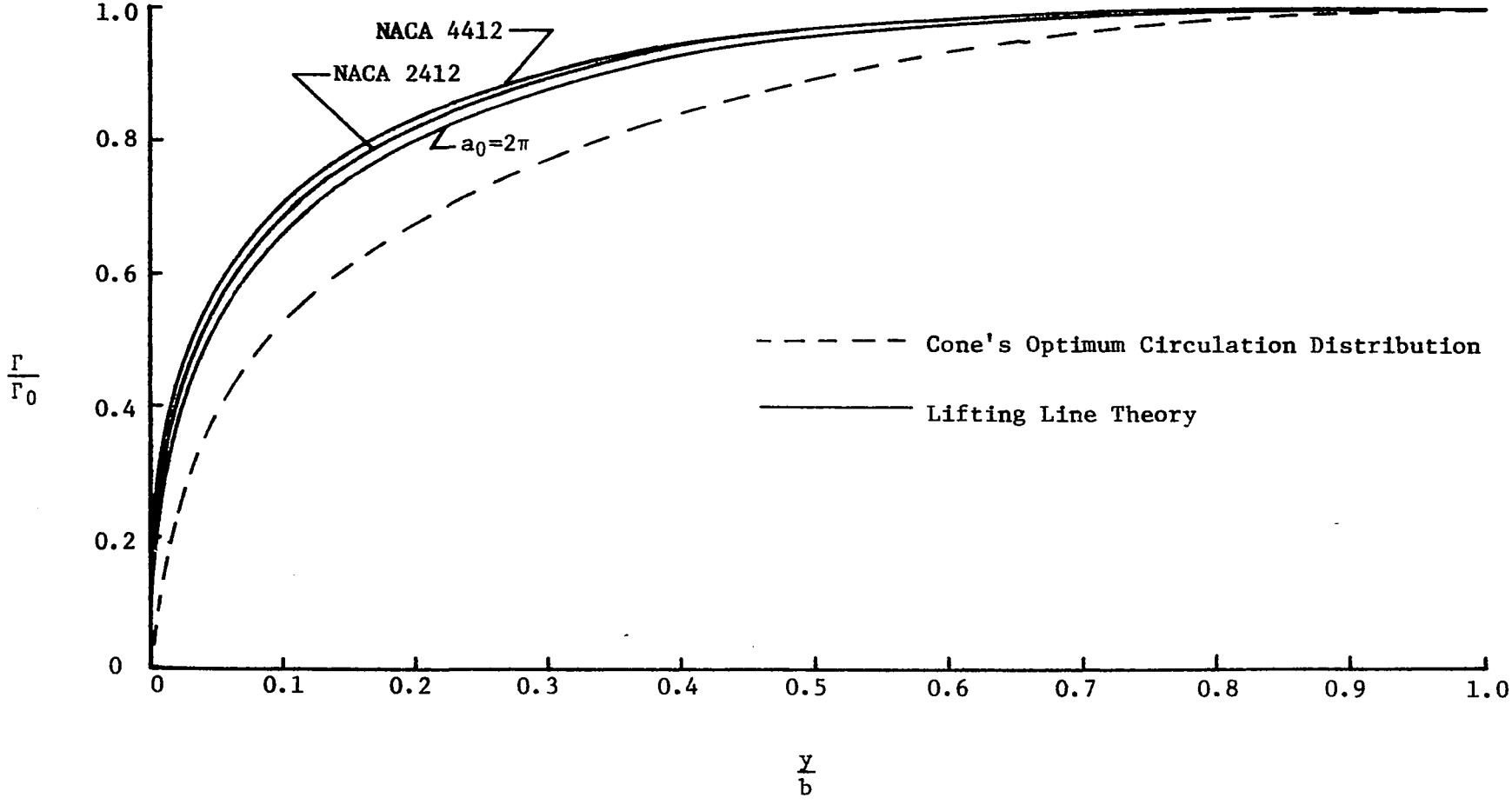

Figure 3.6 Circulation Distribution (e=.866)(AR=20)

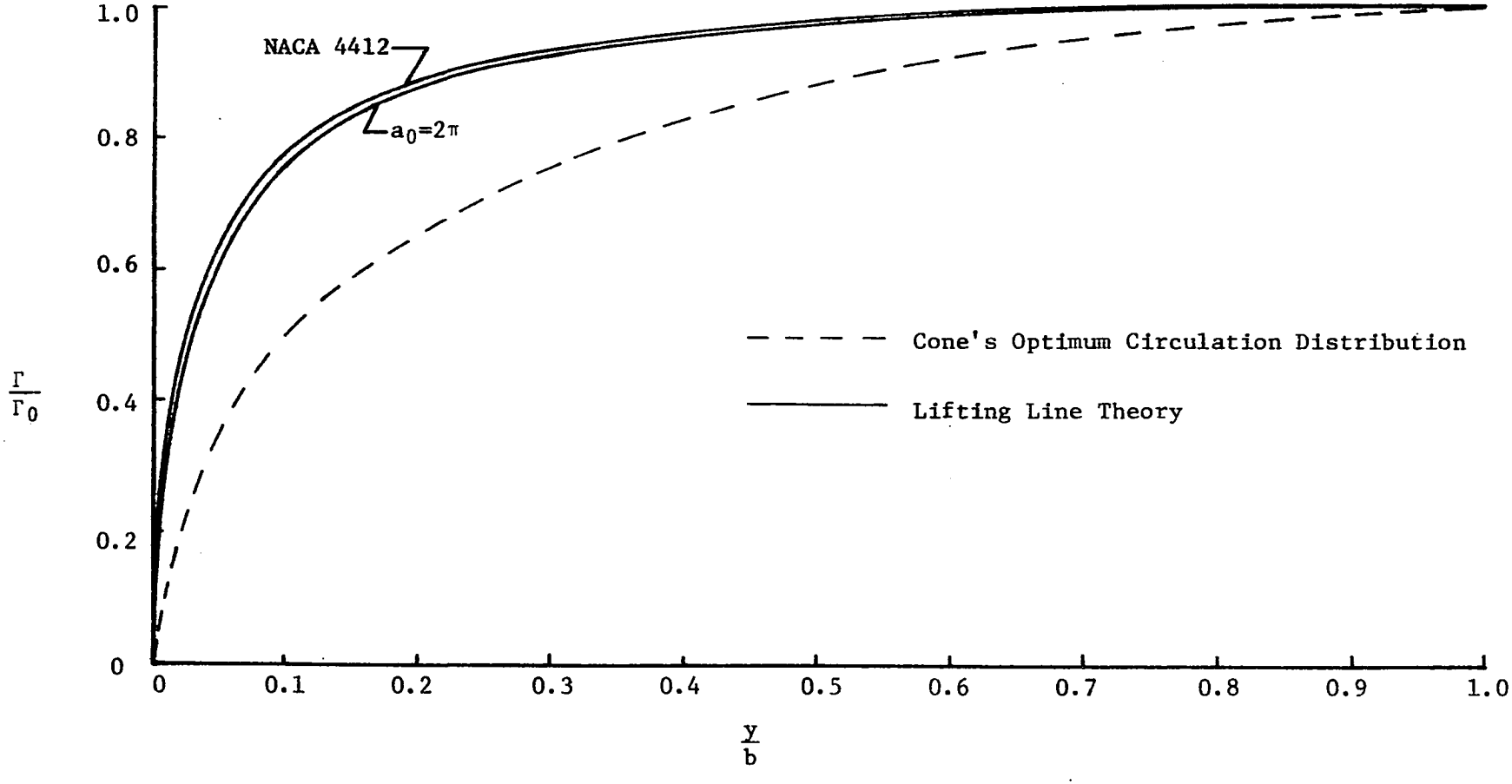

Figure 3.7 Circulation Distribution (e=.954)(AR=20)

lift than the lift curve slope. Decreasing the angle of zero lift on a nonplanar wing has the same effect upon the circulation distribution as giving positive twist to a planar wing.

Each wing is also compared to the optimum circulation distribution as described by Cone [13]. Cone's circulation distribution was optimized for minimum induced drag and a direct correlation between the two methods is not expected. The assumption that the chord remained constant was made prior to the development of any characteristic curves in this study. To obtain Cone's optimized distribution would require varying the chord, angle of attack and/or the two dimensional lift curve slope with the span. It is interesting to note that the circulation distribution for a semi-circular channel of constant chord and composed of NACA 4412 airfoil sections very nearly approximates the optimized distribution.

CHAPTER IV

AERODYNAMIC PROPERTIES

Coefficient of Lift

Once the circulation distribution is known, determination of the lift for the wing is straightforward. Making use of the fact that

$$\ell_n = \rho U \Gamma \tag{4.1}$$

where ℓ_n is the two dimensional force normal to the surface of the wing. The component of ℓ_n that is of interest is the component in the positive Z direction (see figure 3.1), the direction that is normally considered positive for the lift of a wing. The two dimensional lift, ℓ, in this direction is found by taking the scalar product of $\overline{\ell}_n$ and $\hat{k}$,

$$\ell = \overline{\ell}_n \cdot \hat{k} \tag{4.2}$$

where

$$\hat{k} = -\hat{e}_r \sin\phi - \hat{e}_\phi \cos\phi \tag{4.3}$$

in polar coordinates.

After an expression for ℓ is found, the result is then integrated across the span and the total lift, L, results.

For an elliptically shaped wing this becomes

$$L = \rho U^2 ab^4 \sum B_n \int_0^{\pi} \frac{\sin\phi \sin n\phi \, d\phi}{(b^2\sin^2\phi + a^2\cos^2\phi)^{3/2}} \tag{4.4}$$

Since all coefficients will be arbitrarily based upon the projected wing area as described in chapter III, the wing lift coefficient becomes

$$C_L = \frac{2L}{\rho S U^2} . \tag{4.5}$$

Figures 4.1 through 4.8 show how the wing lift coefficient varies with the angle of attack for different aspect ratios and eccentricities of an elliptically shaped wing. The wing coefficient of lift increases with both the aspect ratio and the eccentricity. For a given aspect ratio the coefficient of lift increases with eccentricity. From this result one may conclude that as the eccentricity approaches that of a planar wing the wing lift coefficient continues to increase, thus a planar wing of the same reference area produces greater lift.

Coefficient of Drag

The total drag of a wing is composed of two parts, the profile drag, D_p, and the induced drag, D_i.

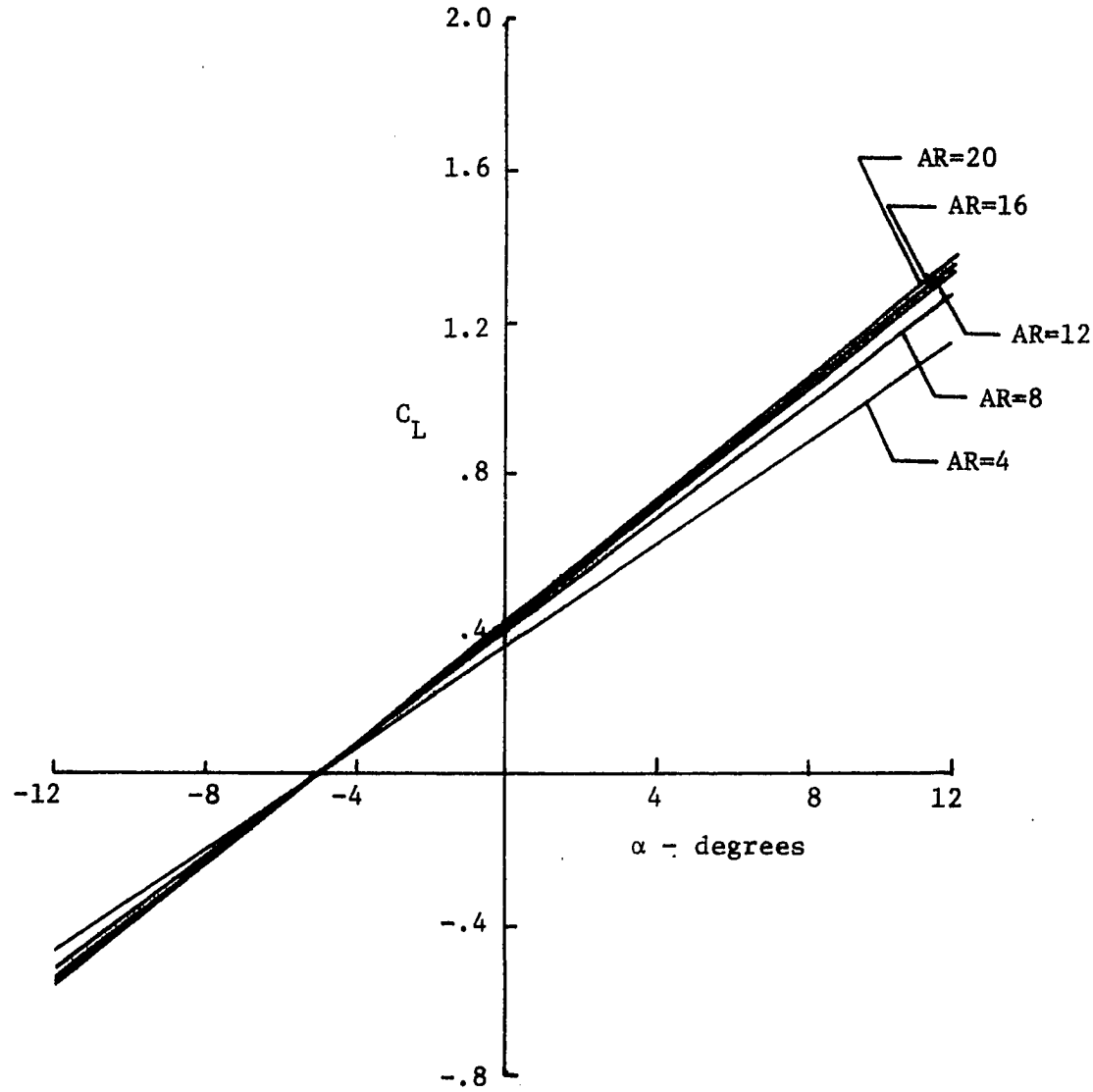

Figure 4.1 Wing Lift Coefficient (e=0)(NACA 4412 Airfoil)

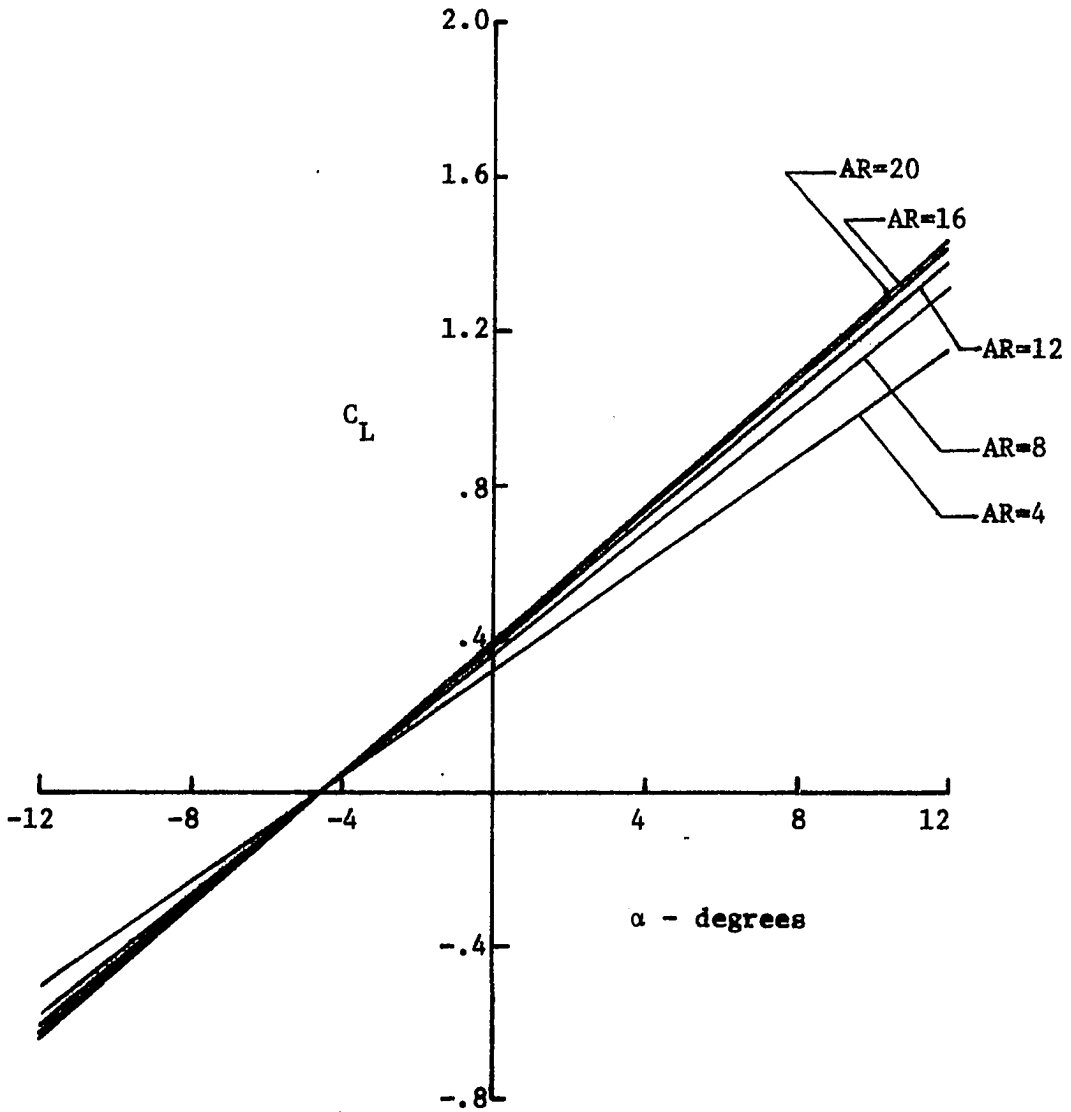

Figure 4.2 Wing Lift Coefficient (e=.714)(NACA 4412 Airfoil)

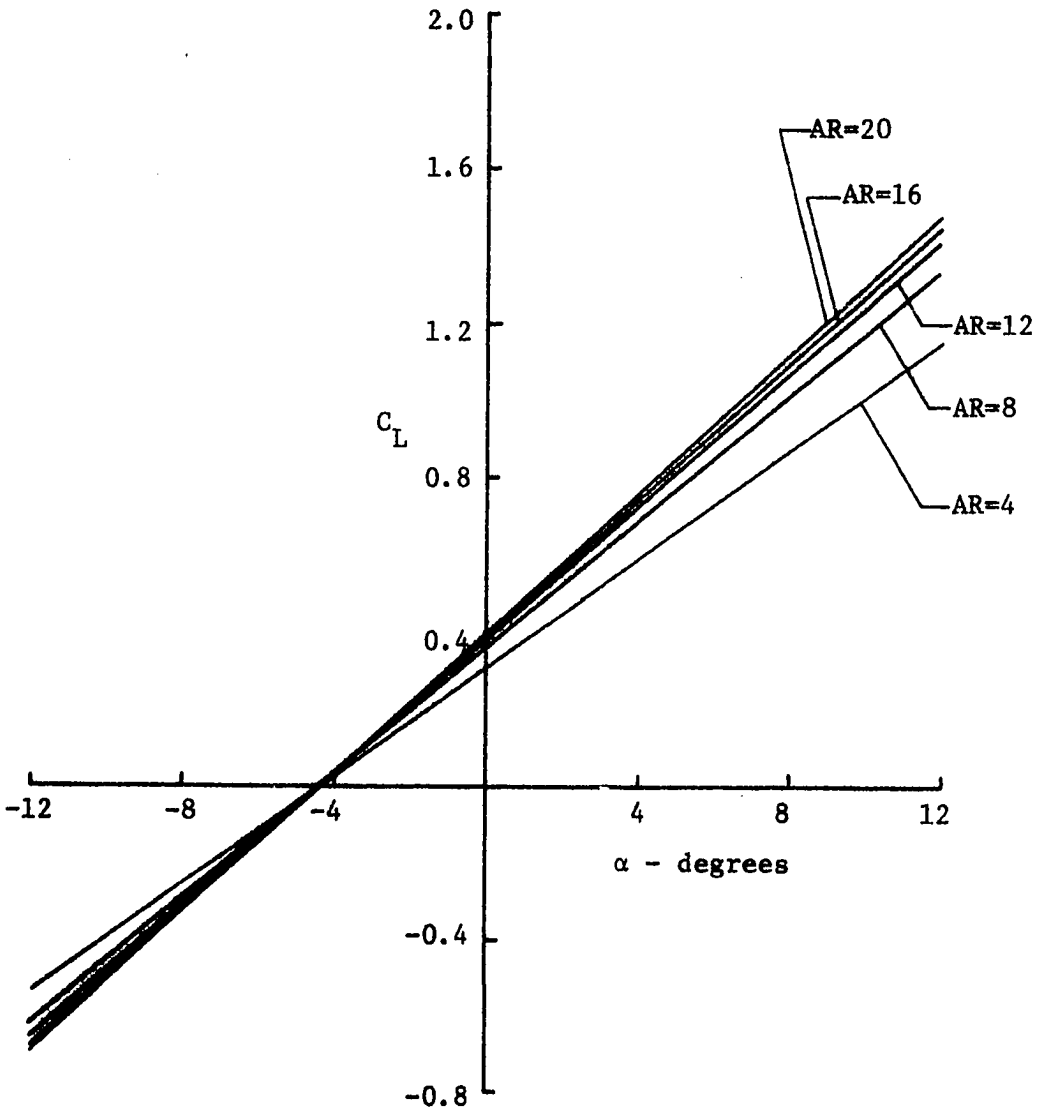

Figure 4.3 Wing Lift Coefficient (e=.866)(NACA 4412 Airfoil)

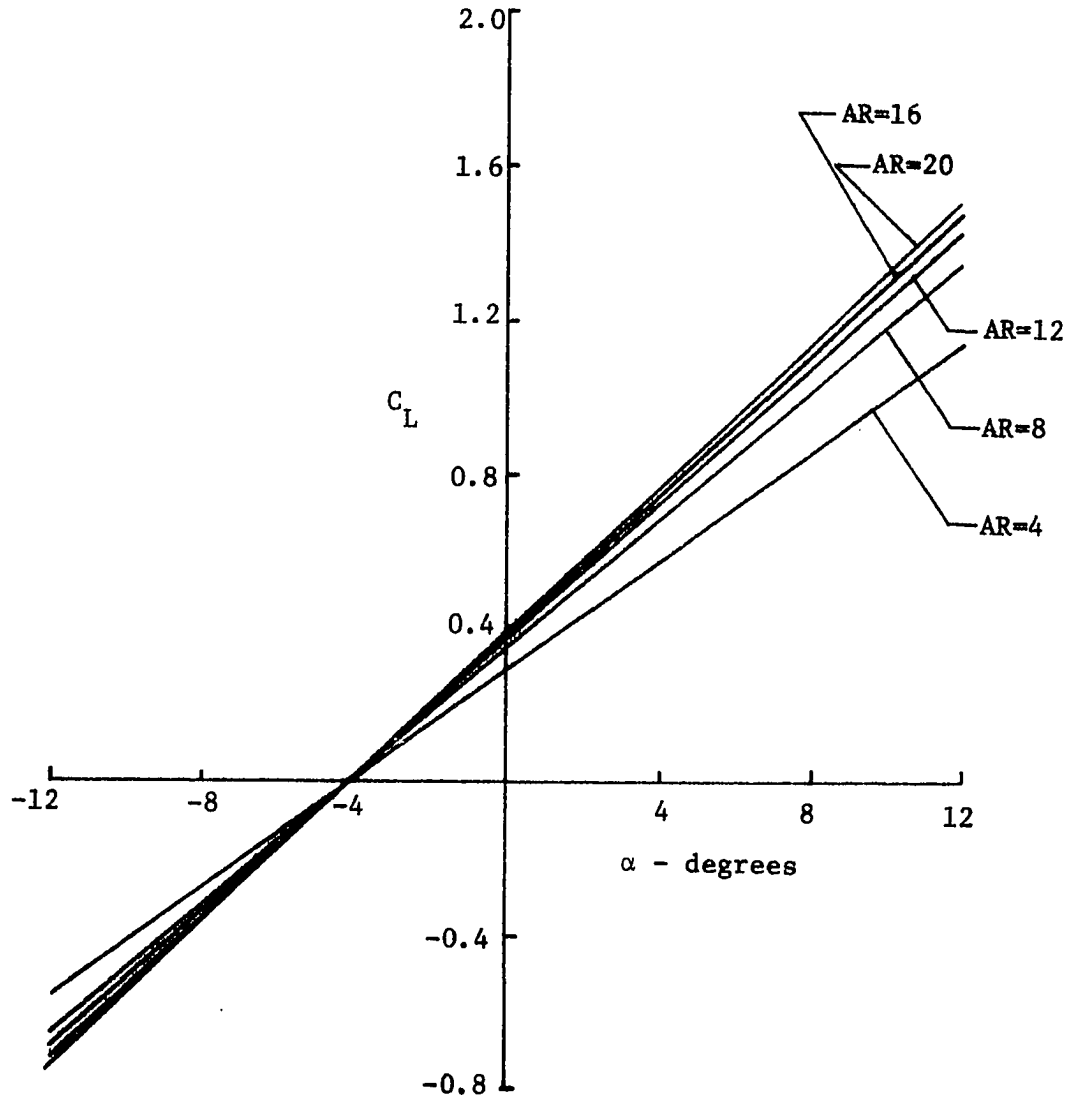

Figure 4.4 Wing Lift Coefficient (e=.954)(NACA 4412 Airfoil)

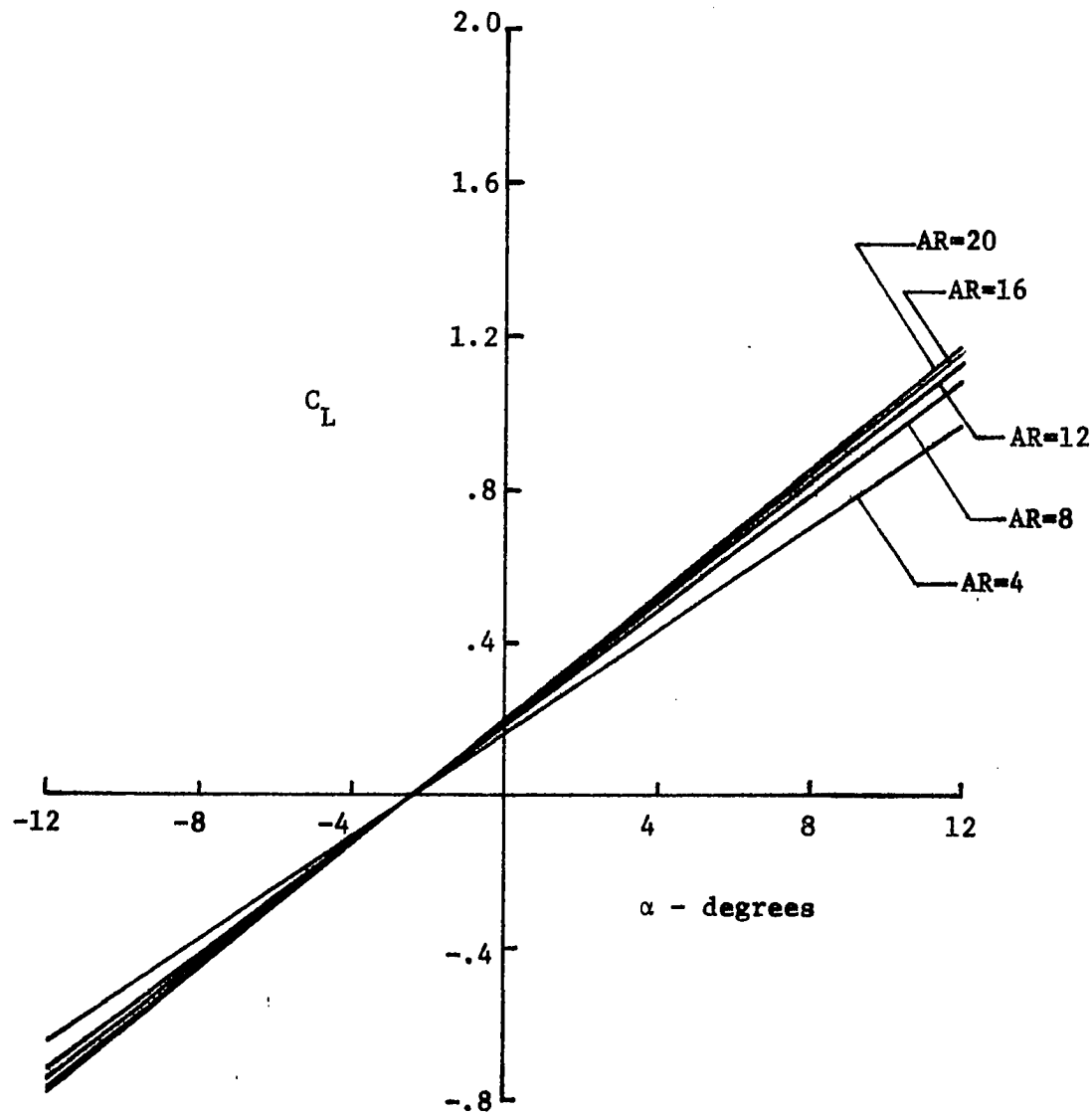

Figure 4.5 Wing Lift Coefficient (e=0)(NACA 2412 Airfoil)

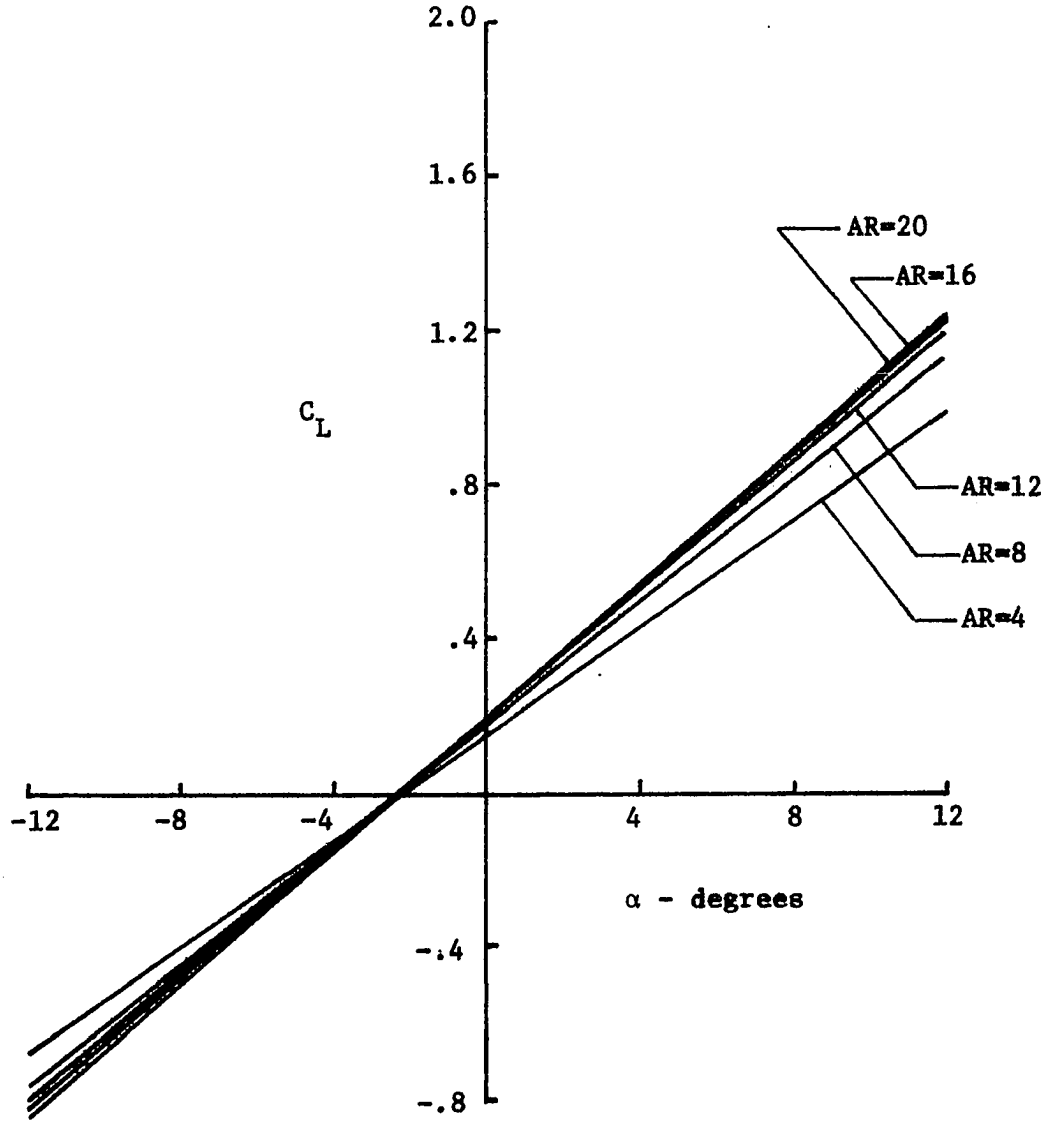

Figure 4.6 Wing Lift Coefficient (e=.714)(NACA 2412 Airfoil)

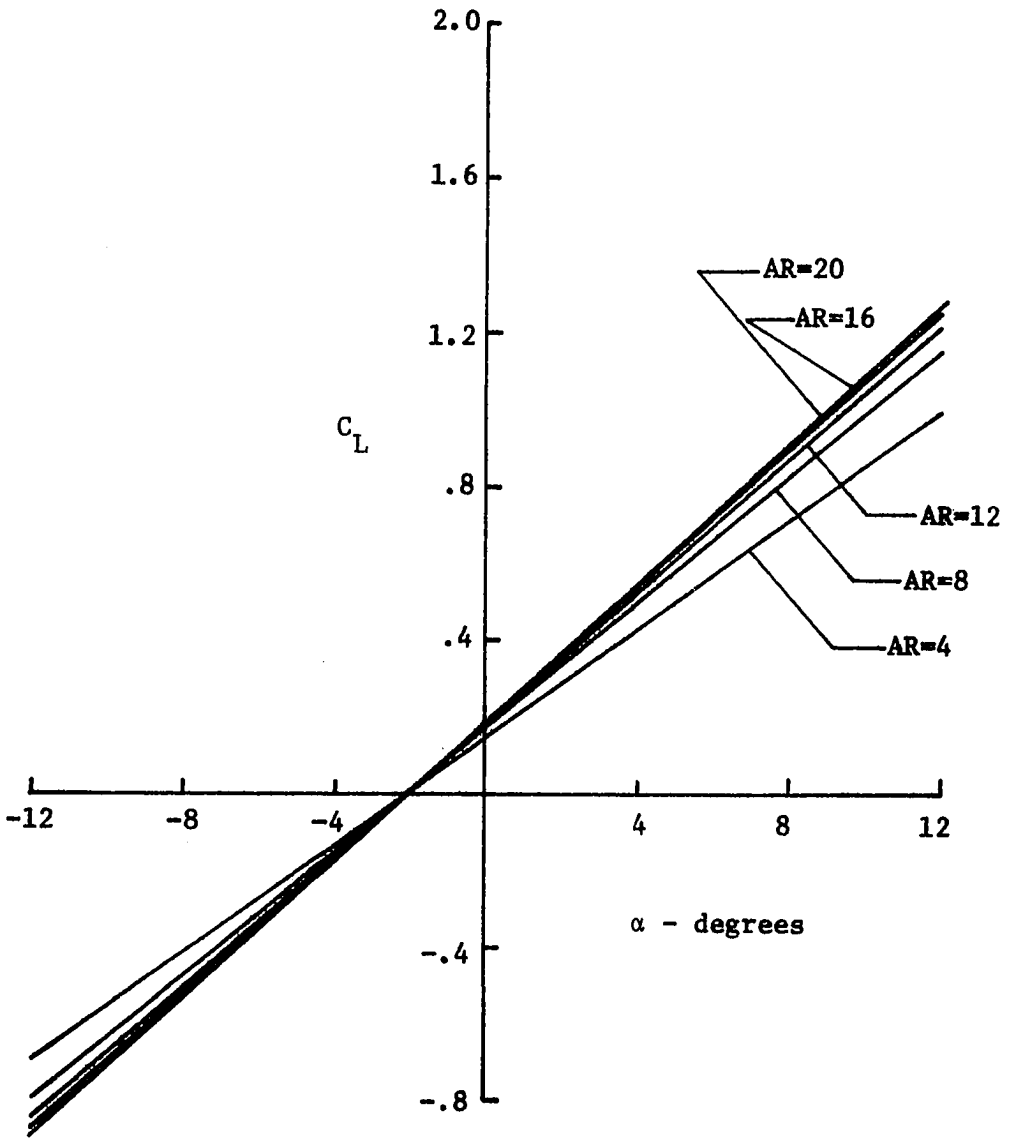

Figure 4.7 Wing Lift Coefficient (e=.866)(NACA 2412 Airfoil)

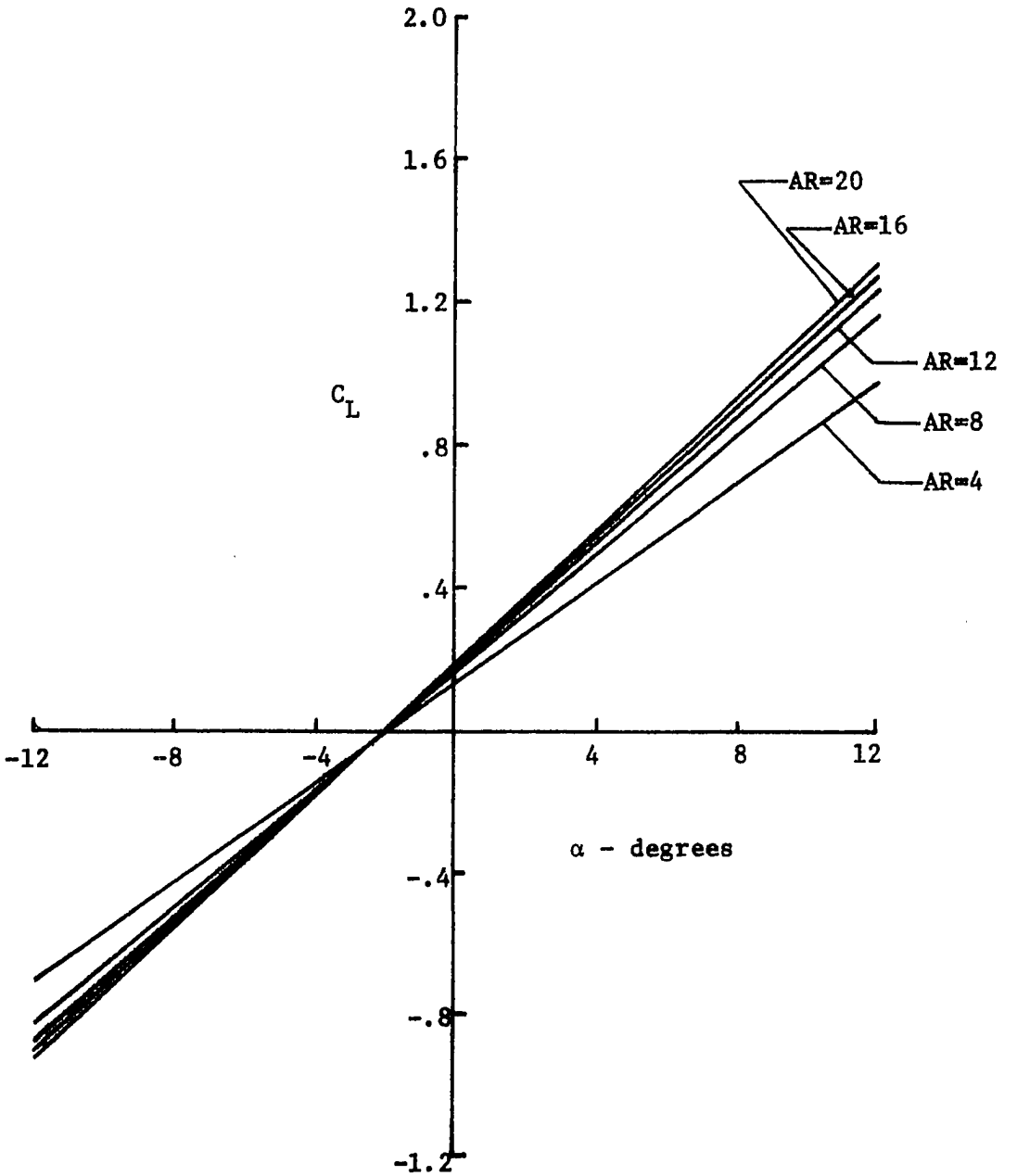

Figure 4.8 Wing Lift Coefficient (e=.954)(NACA 2412 Airfoil)

The induced drag was computed by means of the expression

$$D_i = \int_{-b}^{b} \ell_n \alpha_i \, ds \tag{4.6}$$

and from this

$$C_{D_i} = \frac{2D_i}{\rho S U^2} . \tag{4.7}$$

In the process of calculating the Fourier coefficients it is necessary to calculate a sufficient number of collocation points in order that the induced drag will have some measure of accuracy. The reason is that the induced angle of attack is only known at the collocation points. Five or six collocation points per semi-span appear to be sufficient for the circulation distribution but this does not give enough data points to accurately determine the downwash distribution. The data in this section were taken using twenty collocation points per semi-span.

The profile drag was computed by the use of data from airfoil sections [14]. The sectional profile drag was computed and then these values were summed across the total span of the wing to determine the total profile drag of the wing.

$$D_p = \frac{1}{2} \rho c U^2 \int_{-b}^{b} C_d \, ds \tag{4.8}$$

Again one makes use of the projected area, S, and finds that

$$C_{D_p} = \frac{c}{S} \int_{-b}^{b} C_d \, ds \tag{4.9}$$

where C_d is a function of the local angle of attack. After one combines equations 4.7 and 4.9 the result is

$$C_D = C_{D_p} + C_{D_i} \tag{4.10}$$

where C_D is based upon the projected wing area, S. Drag polars were then constructed for wings composed of two different airfoil sections. The results are presented in figures 4.9 through 4.16.

When one compares wings composed of the same airfoil sections and the same coefficient of lift the total drag coefficient decreases as eccentricity increases for low values of the lift coefficient. This is attributable to the fact that the profile drag is the most dominant form of drag within this range and as eccentricity decreases the wetted area of the wing increases. For higher values of the lift coefficient the induced drag becomes dominant and therefore the total drag coefficient increases with eccentricity.

After the coefficients of lift and drag are know it becomes a simple matter to plot the ratio L/D and these data are contained in figures 4.17 through 4.24.

For the wings that were considered the maximum value of L/D increases with increasing eccentricity. This is indicative of the fact that for these particular wings the maximum L/D occurs at relatively low values of the lift coefficient and thus within the range where the profile drag is dominant.

The wings composed of NACA 4412 airfoil sections have a higher maximum value of L/D than do those composed at NACA 2412 airfoil sections for a given aspect ratio. The maximum value for both wings occurs at low angles of attack where the predominant drag component is profile drag. Therefore the lift to drag ratios for the wing will be nearly proportional to that given for the two dimensional airfoil. In each case the wing will have a smaller L/D ratio than the airfoil due to a smaller lift coefficient. The NACA 4412 airfoil has a higher maximum L/D ratio than the NACA 2412 airfoil because of an increased camber thus increasing the lift coefficient.

For wings of the same aspect ratio and airfoil section the angle of attack at which the maximum L/D ratio occurs is affected only slightly by a change in eccentricity. This small change in angle of attack is the result of two factors. First, the rate of change of the drag coefficient with angle attack is very small for small angles of attack and second the lift curve slope changes only slightly with eccentricity.

The lift curve slope was calculated for two different wings which were composed of different airfoil sections and the results were plotted against eccentricity for different aspect ratios in figures 4.25 through 4.26.

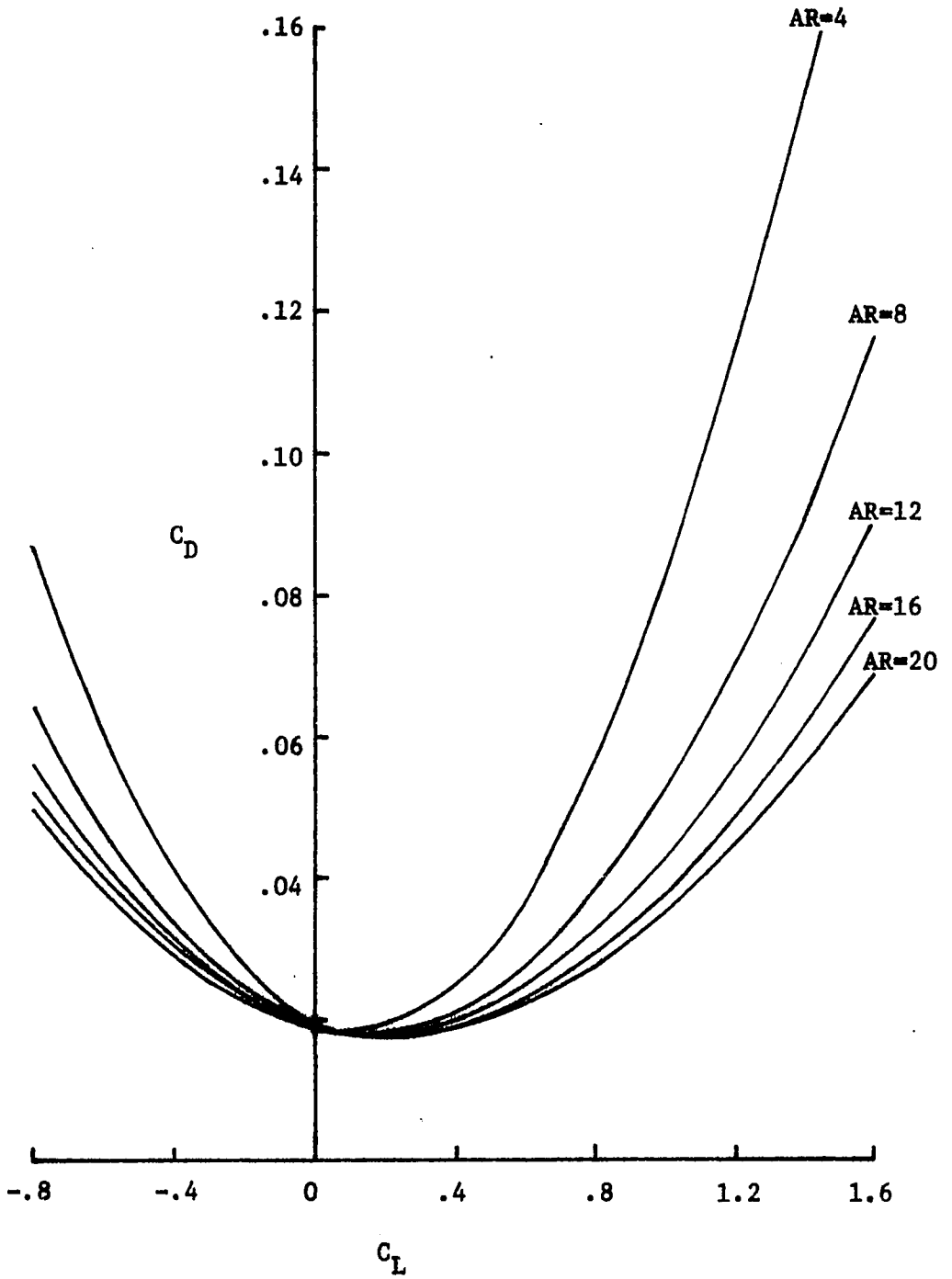

Figure 4.9 Drag Polar (e=0)(NACA 4412 Airfoil)

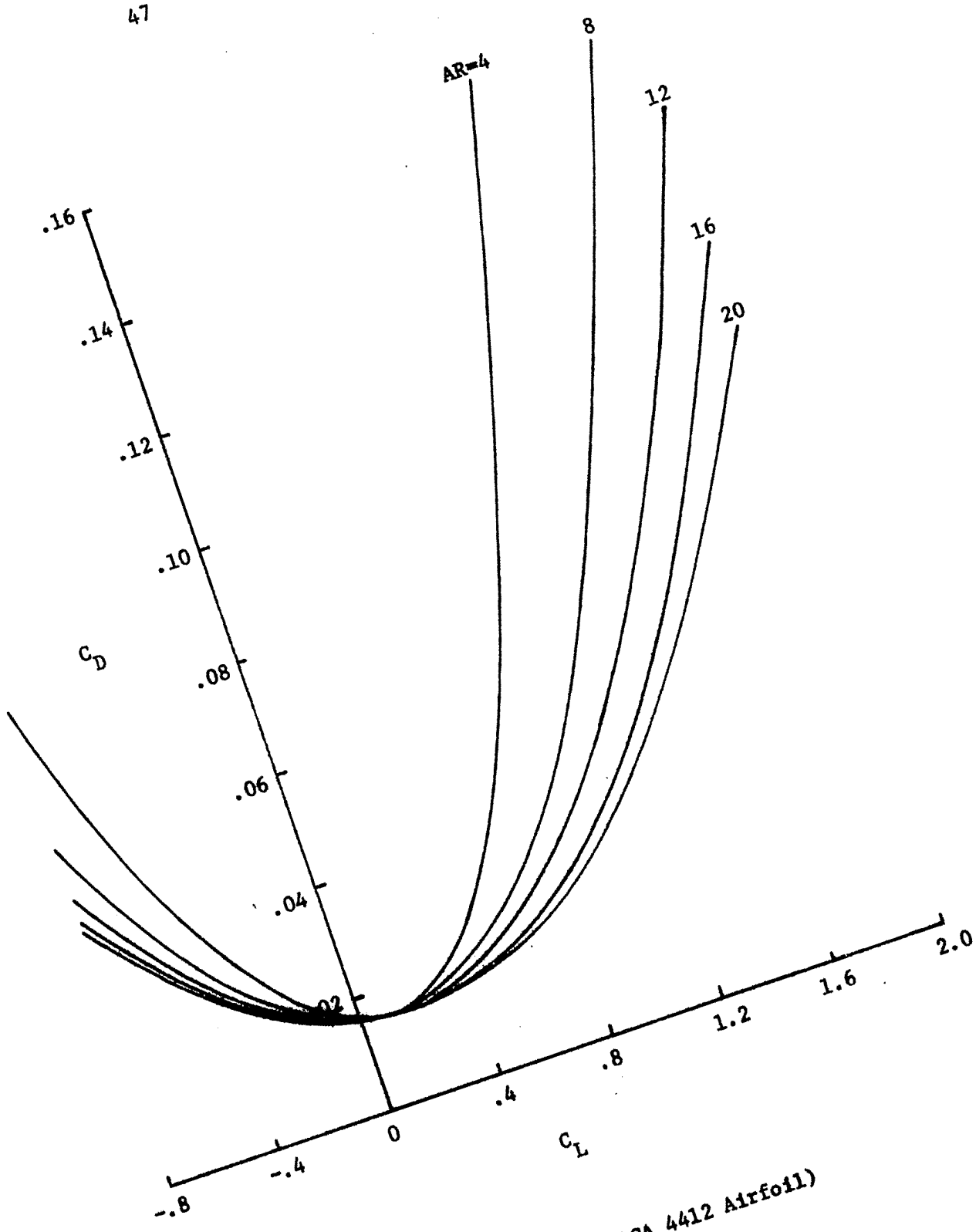

Figure 4.10 Drag Polar (e=.714)(NACA 4412 Airfoil)

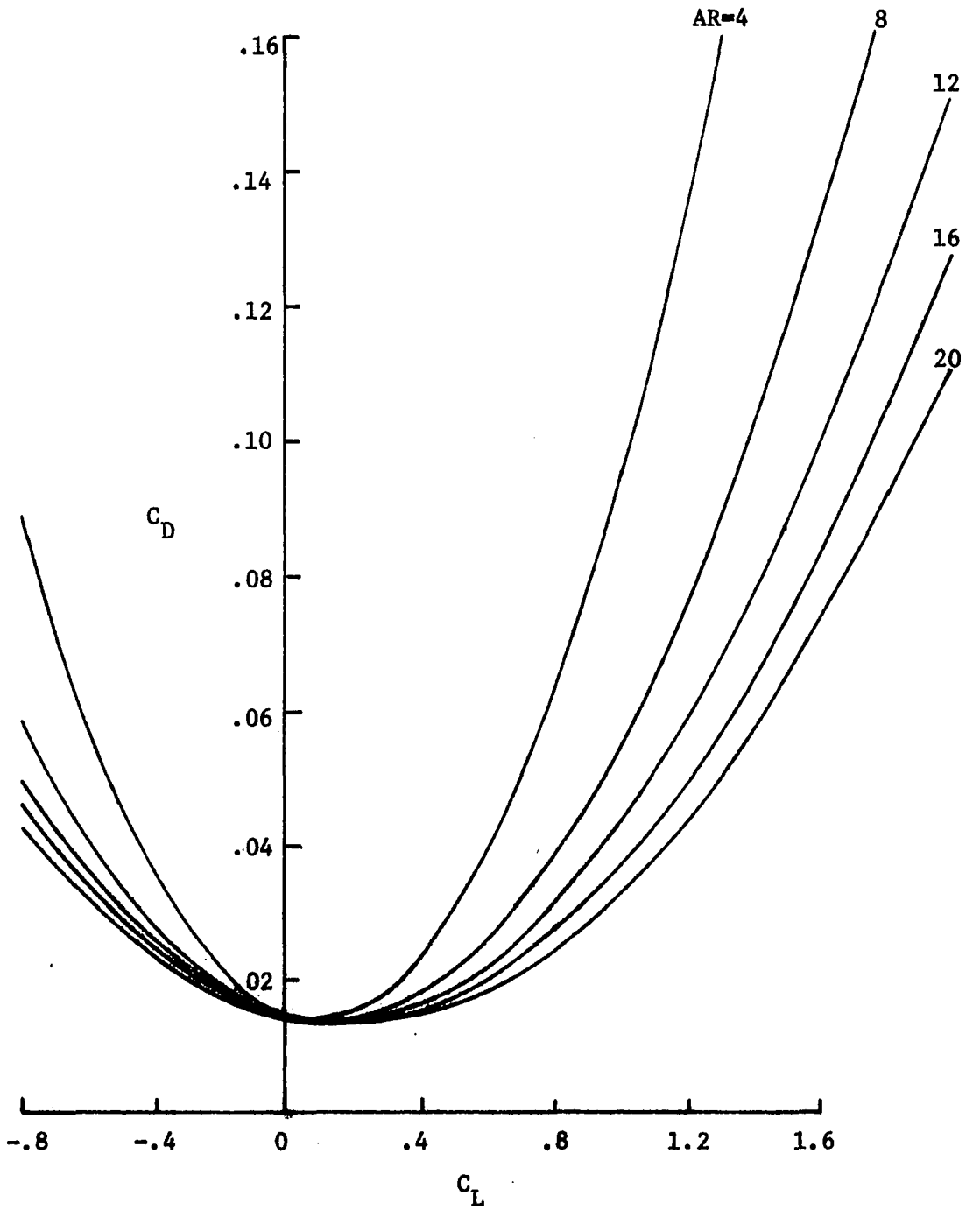

Figure 4.11 Drag Polar (e=.866)(NACA 4412 Airfoil)

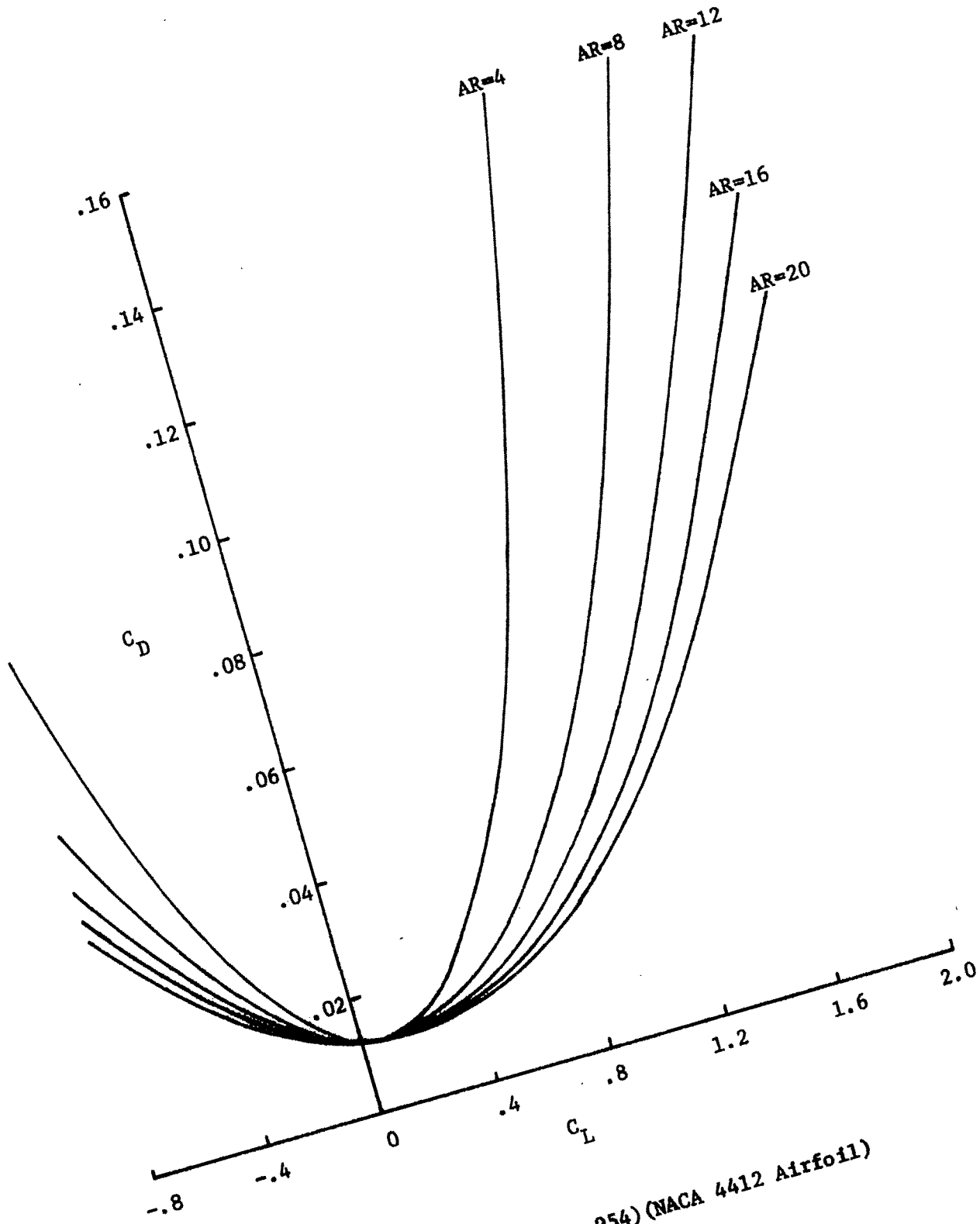

Figure 4.12 Drag Polar (e=.954)(NACA 4412 Airfoil)

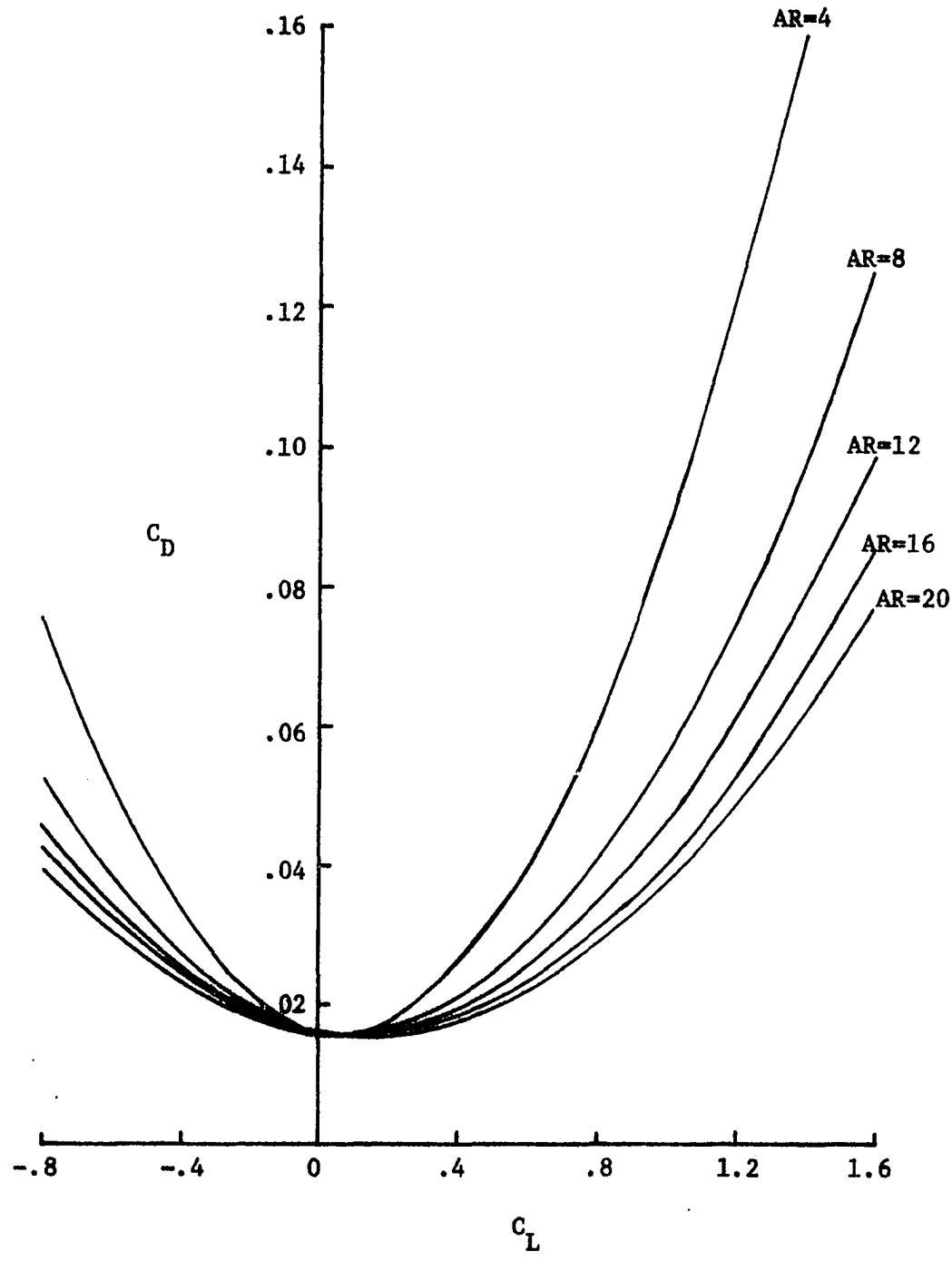

Figure 4.13 Drag Polar (e=0)(NACA 2412 Airfoil)

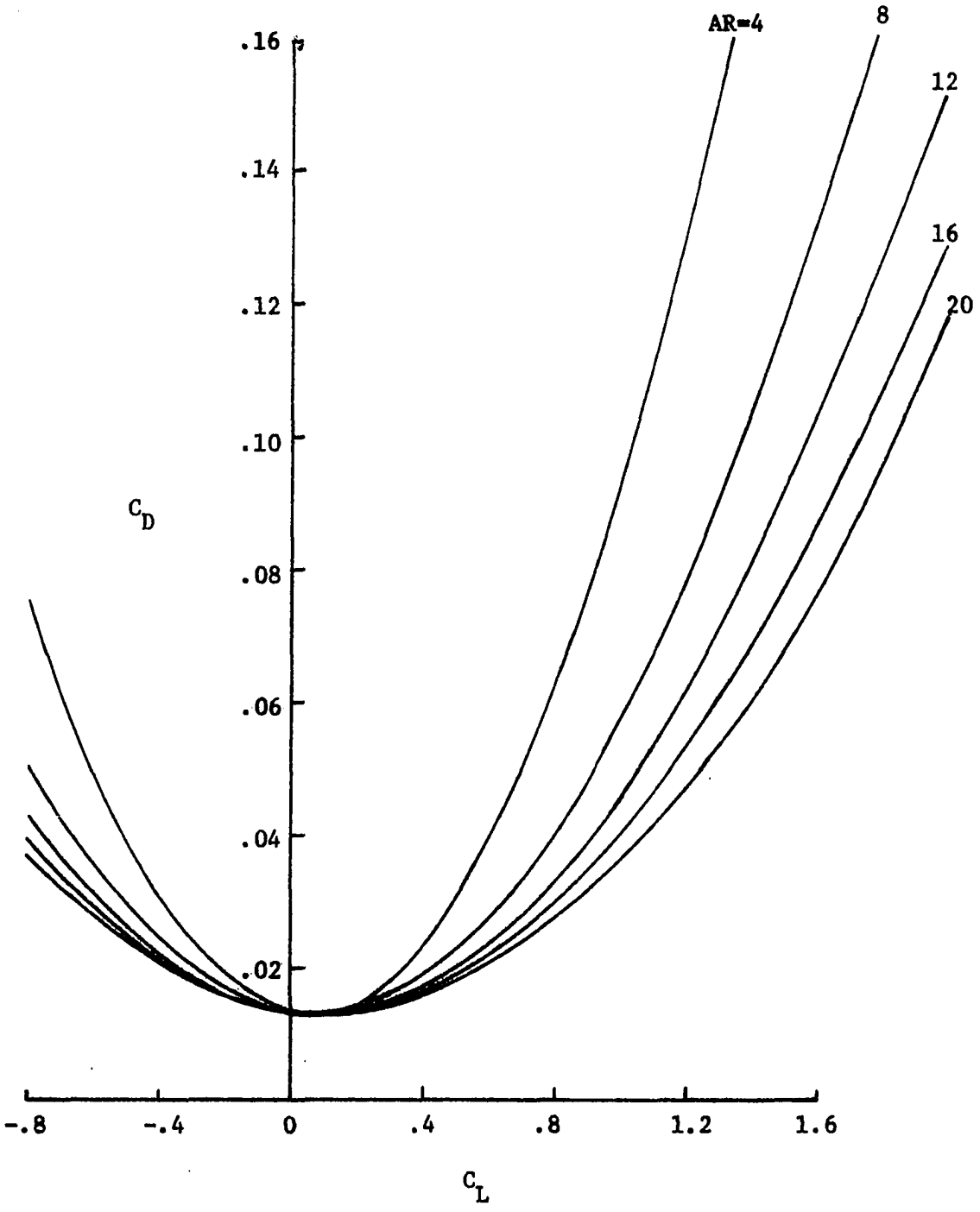

Figure 4.14 Drag Polar (e=.714)(NACA 2412 Airfoil)

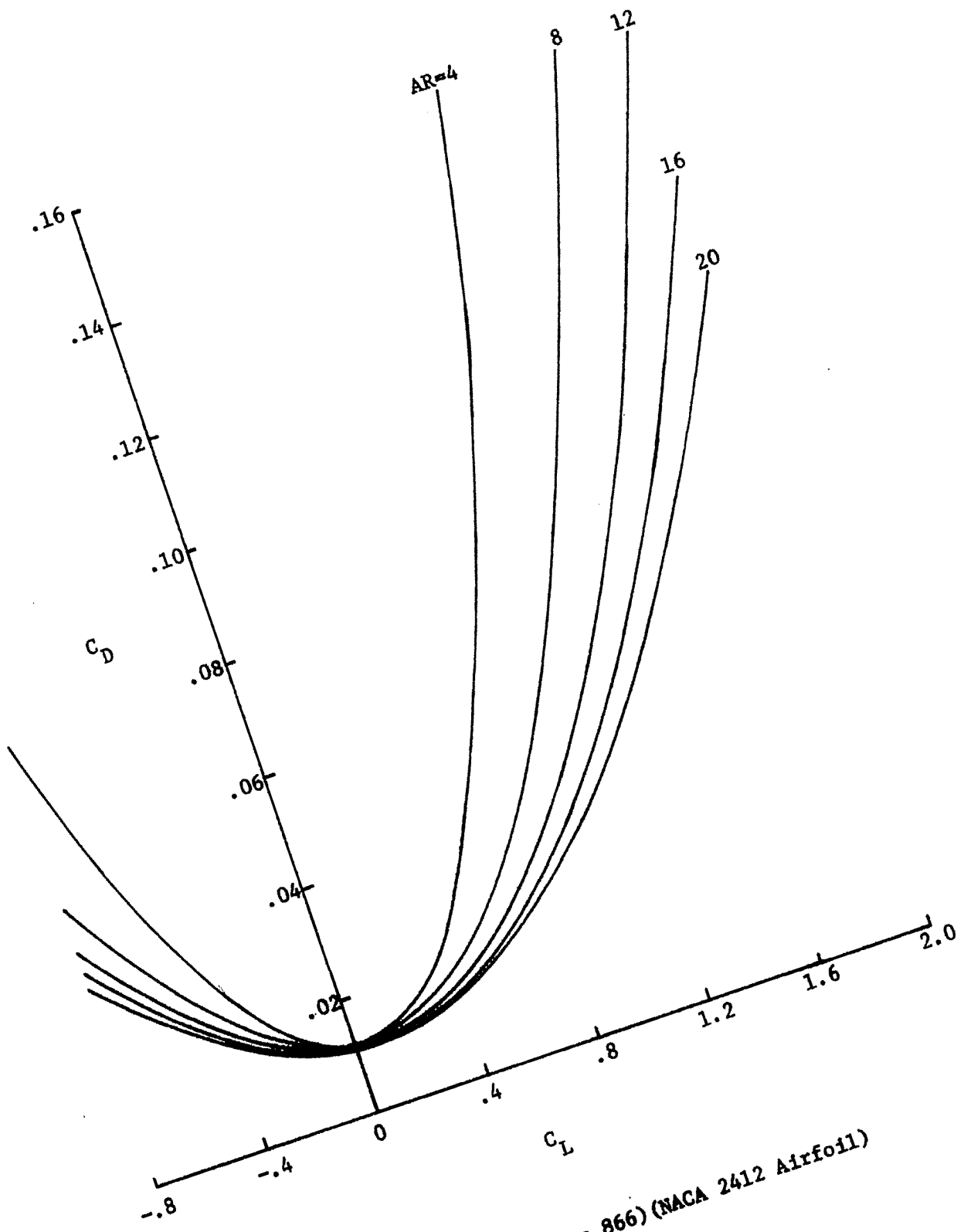

Figure 4.15 Drag Polar (e=.866)(NACA 2412 Airfoil)

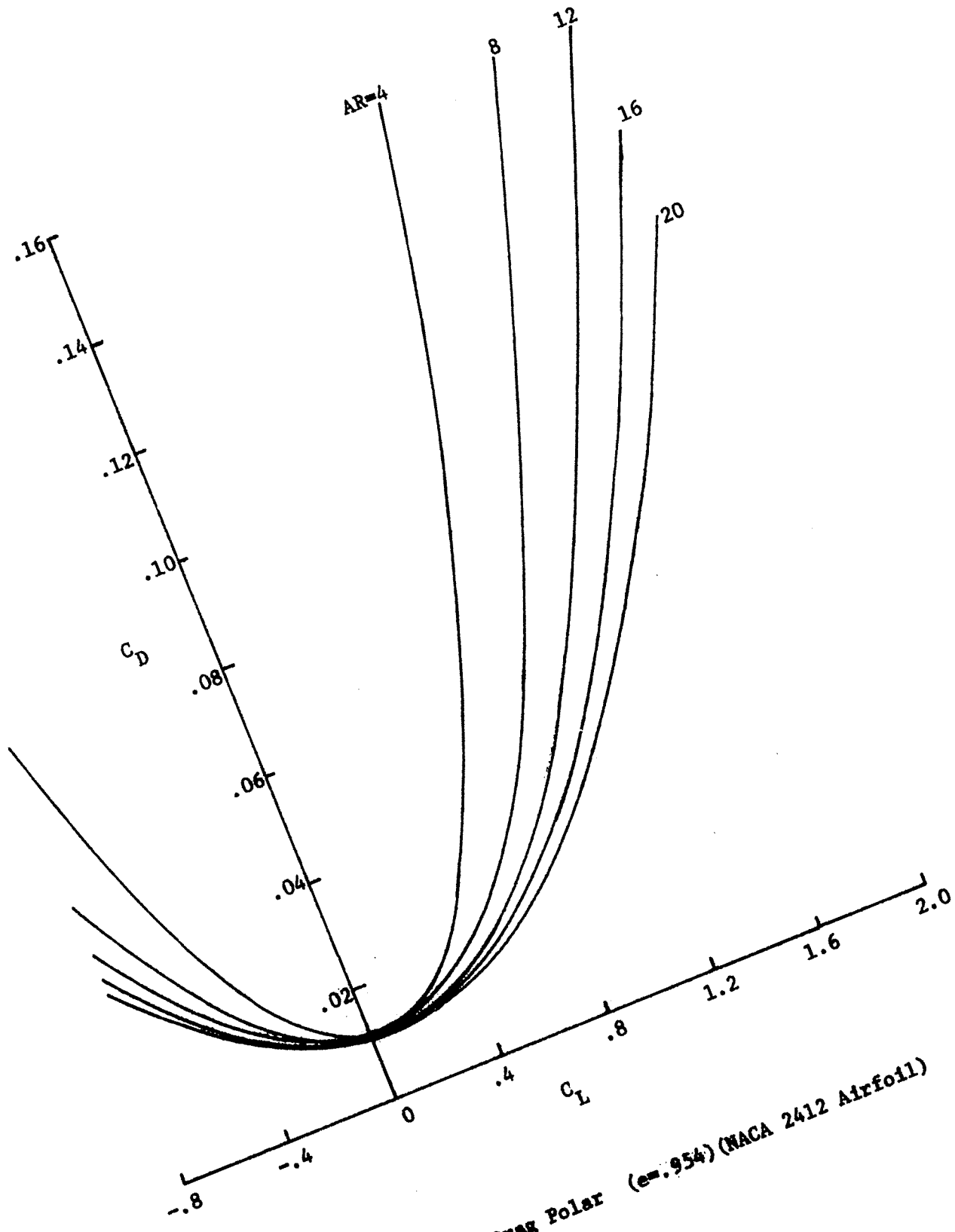

Figure 4.16 Drag Polar (e=.954)(NACA 2412 Airfoil)

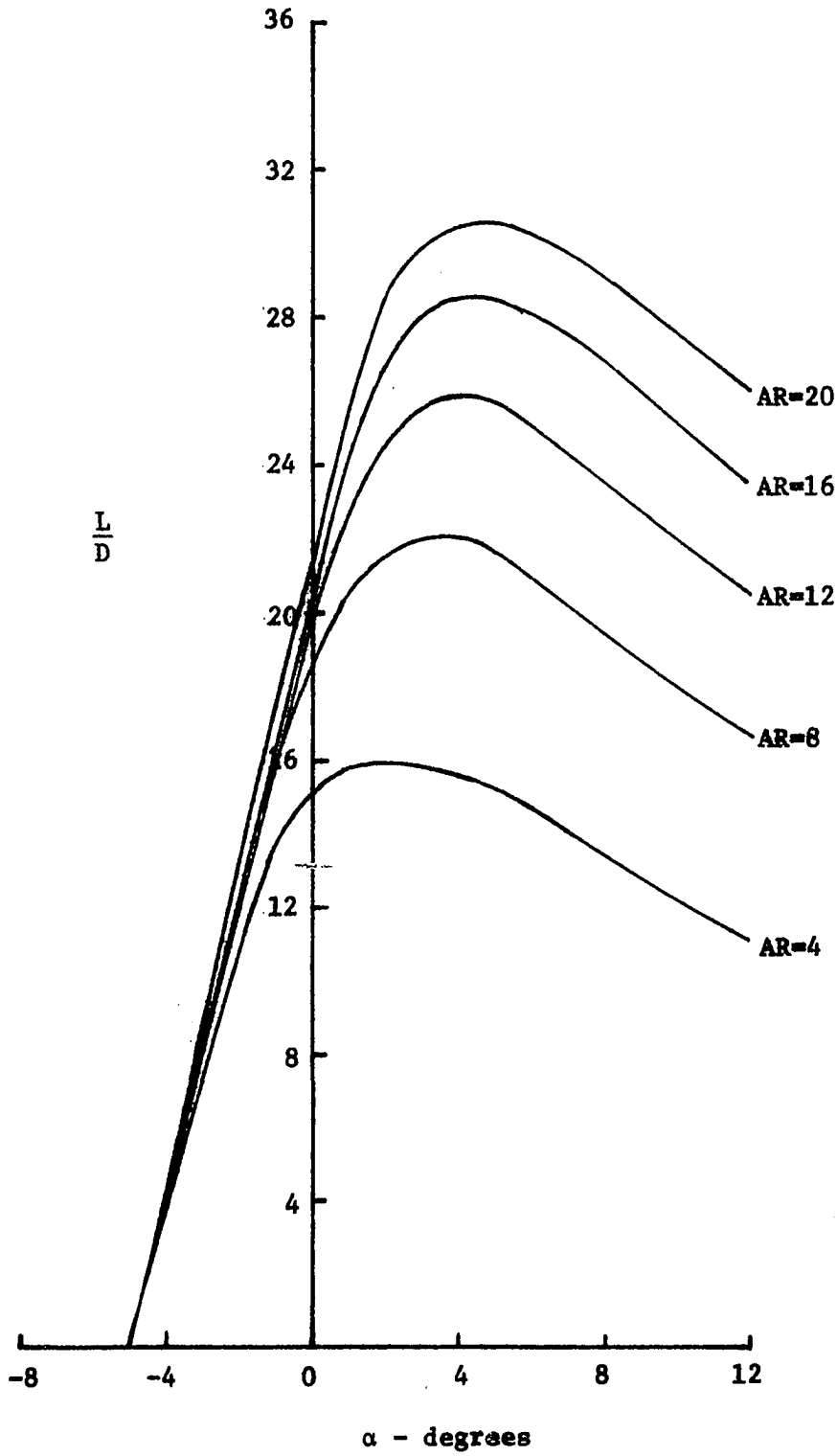

Figure 4.17 Wing L/D (e=0)(NACA 4412 Airfoil)

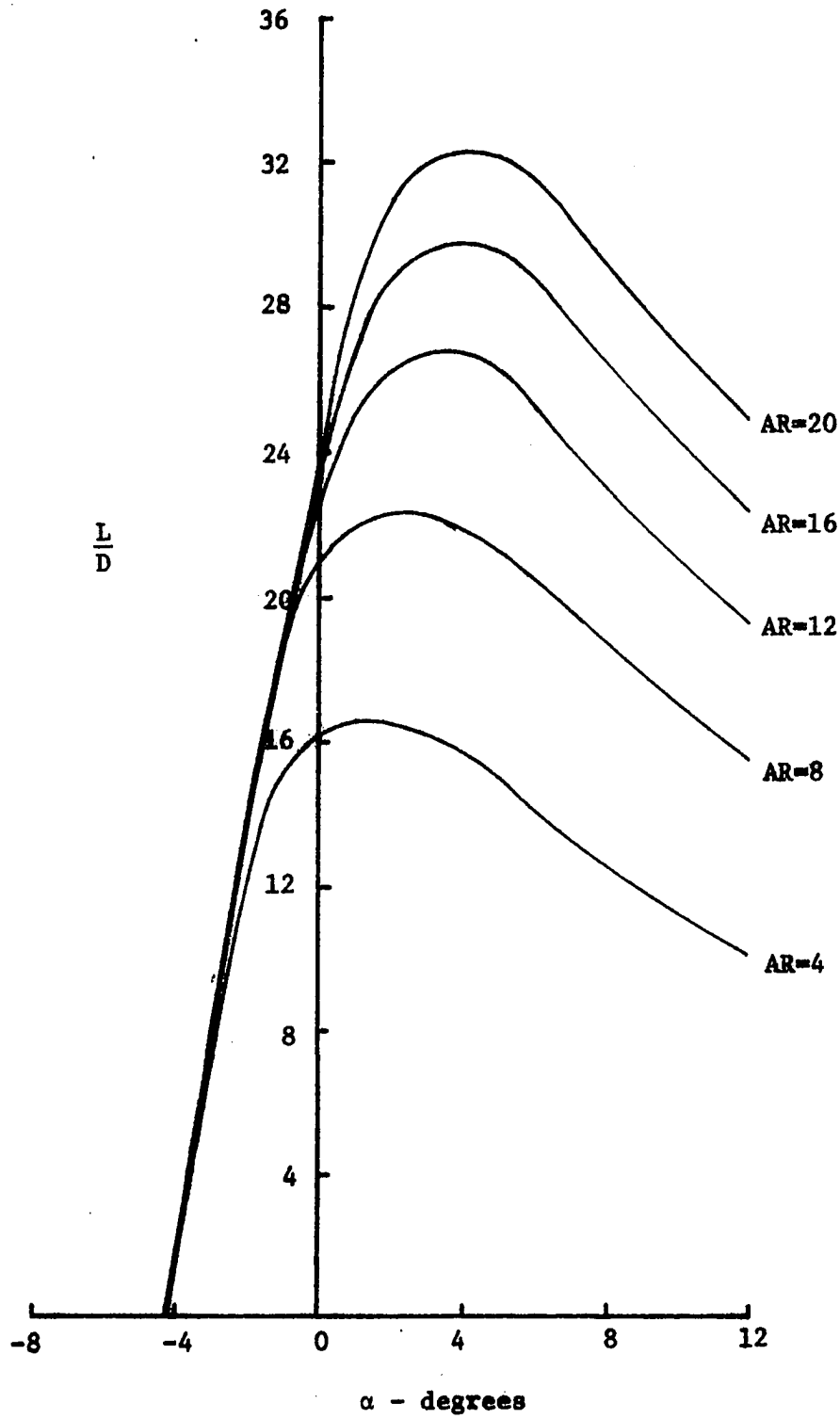

Figure 4.18 Wing L/D (e=.714)(NACA 4412 Airfoil)

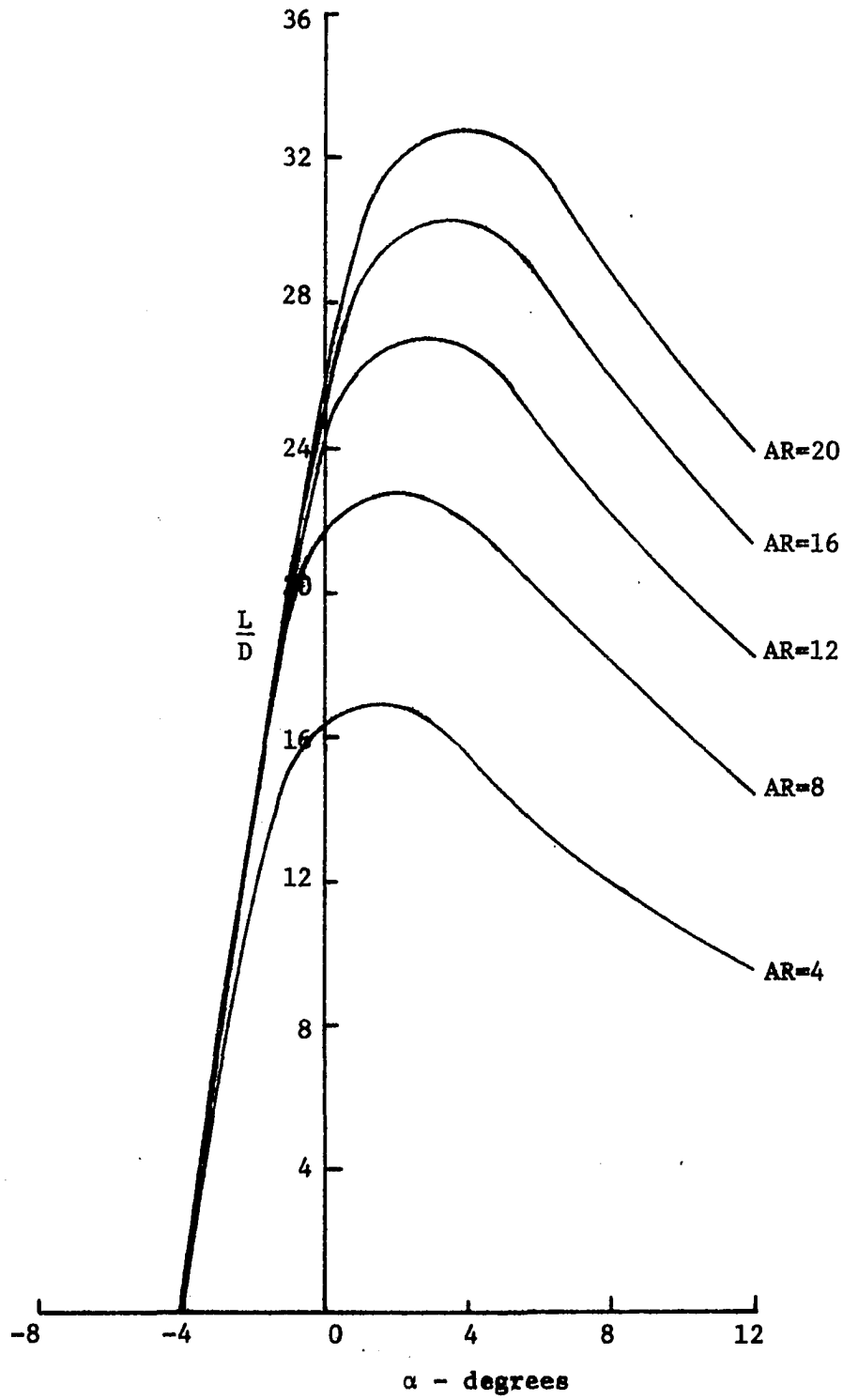

Figure 4.19 Wing L/D (e=.866)(NACA 4412 Airfoil)

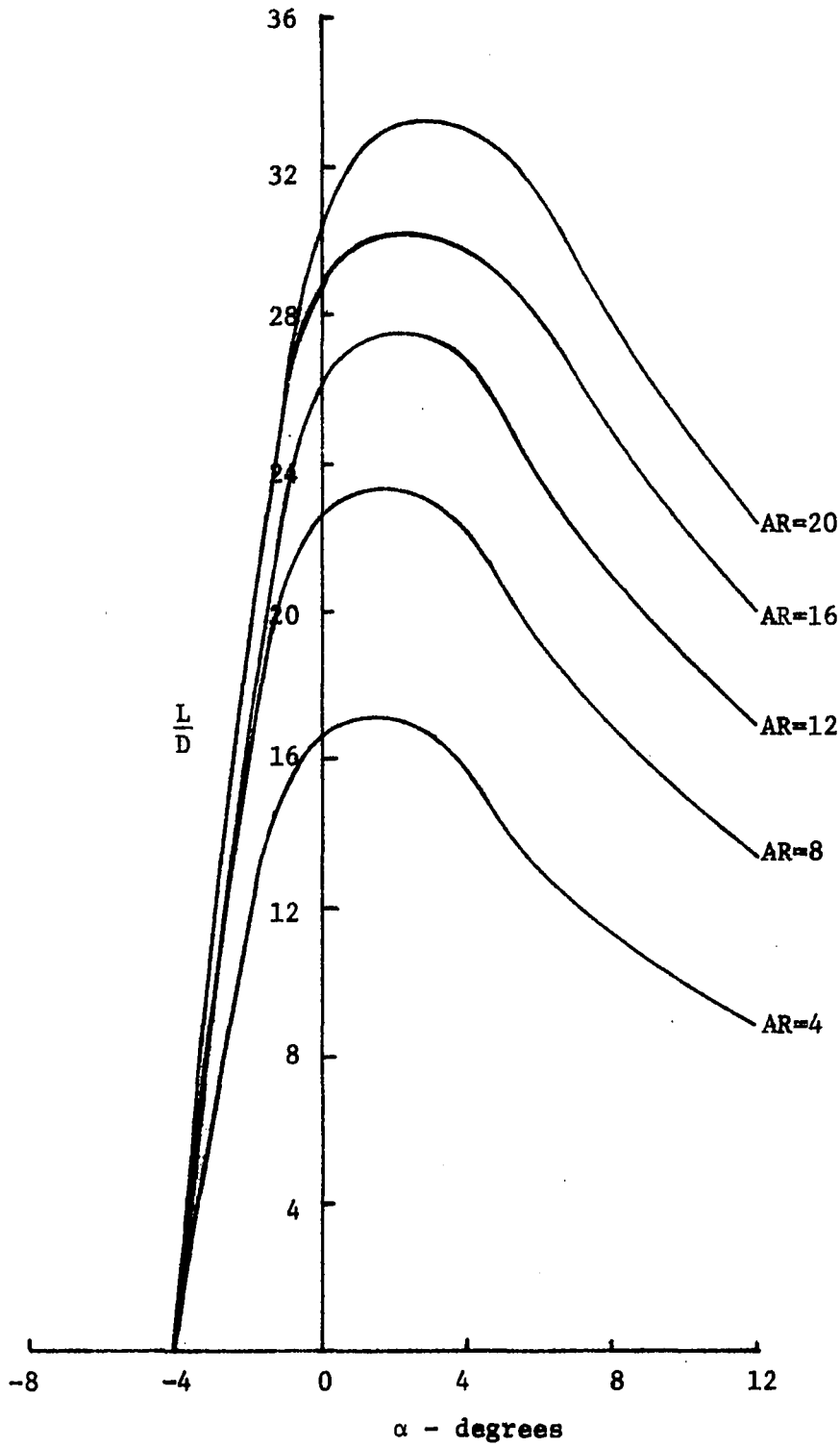

Figure 4.20 Wing L/D (e=.954)(NACA 4412 Airfoil)

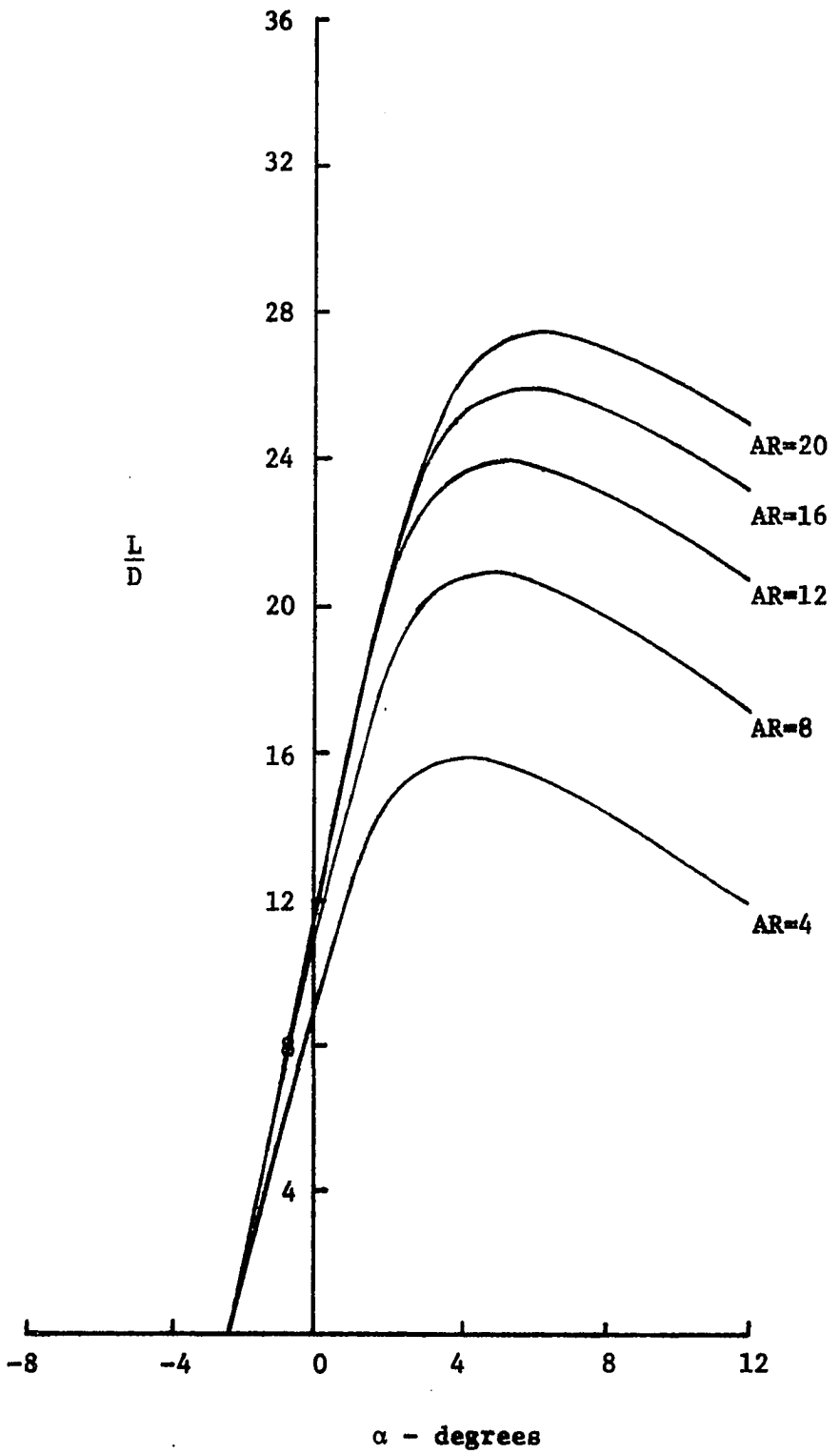

Figure 4.21 Wing L/D (e=0)(NACA 2412 Airfoil)

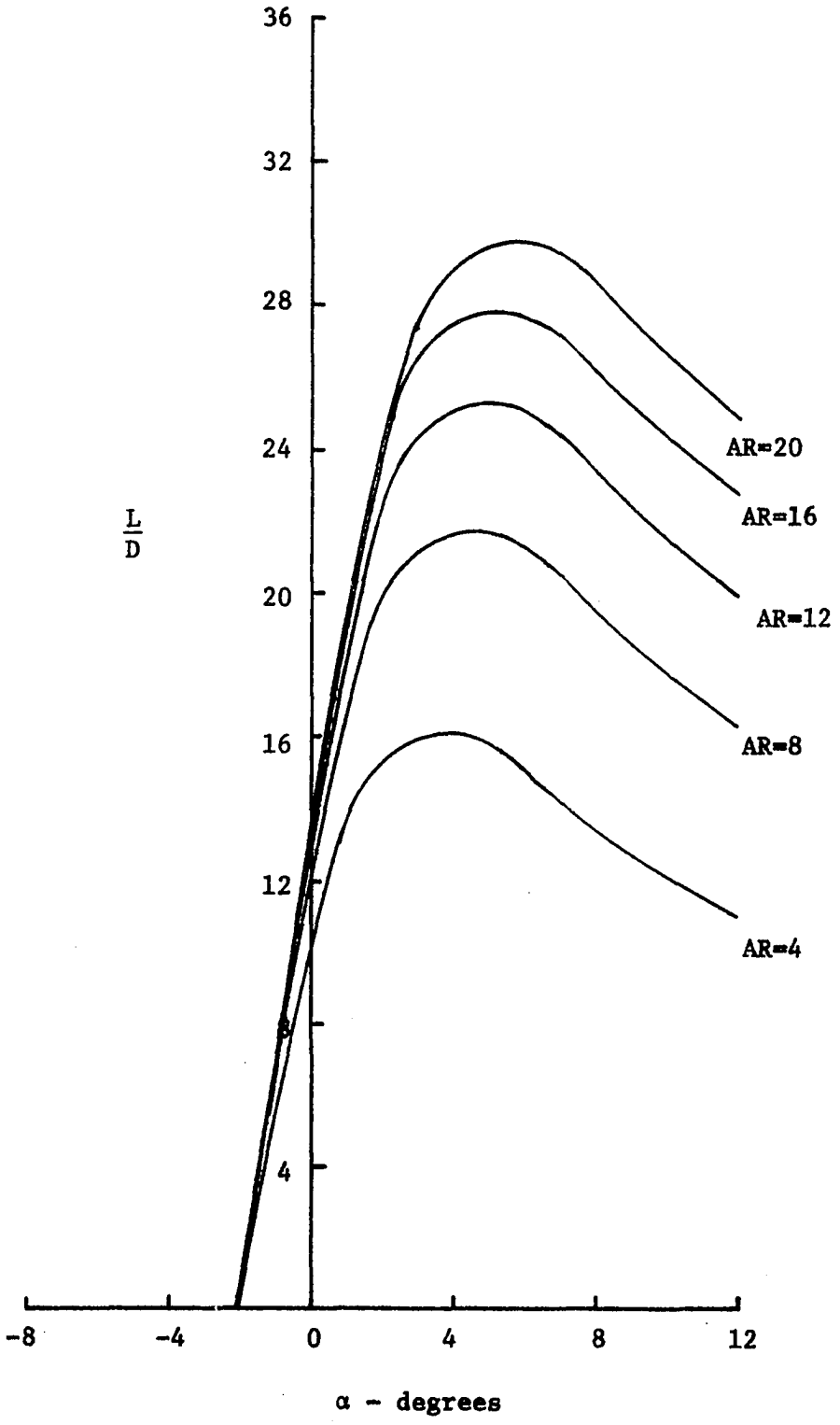

Figure 4.22 Wing L/D (e=.714)(NACA 2412 Airfoil)

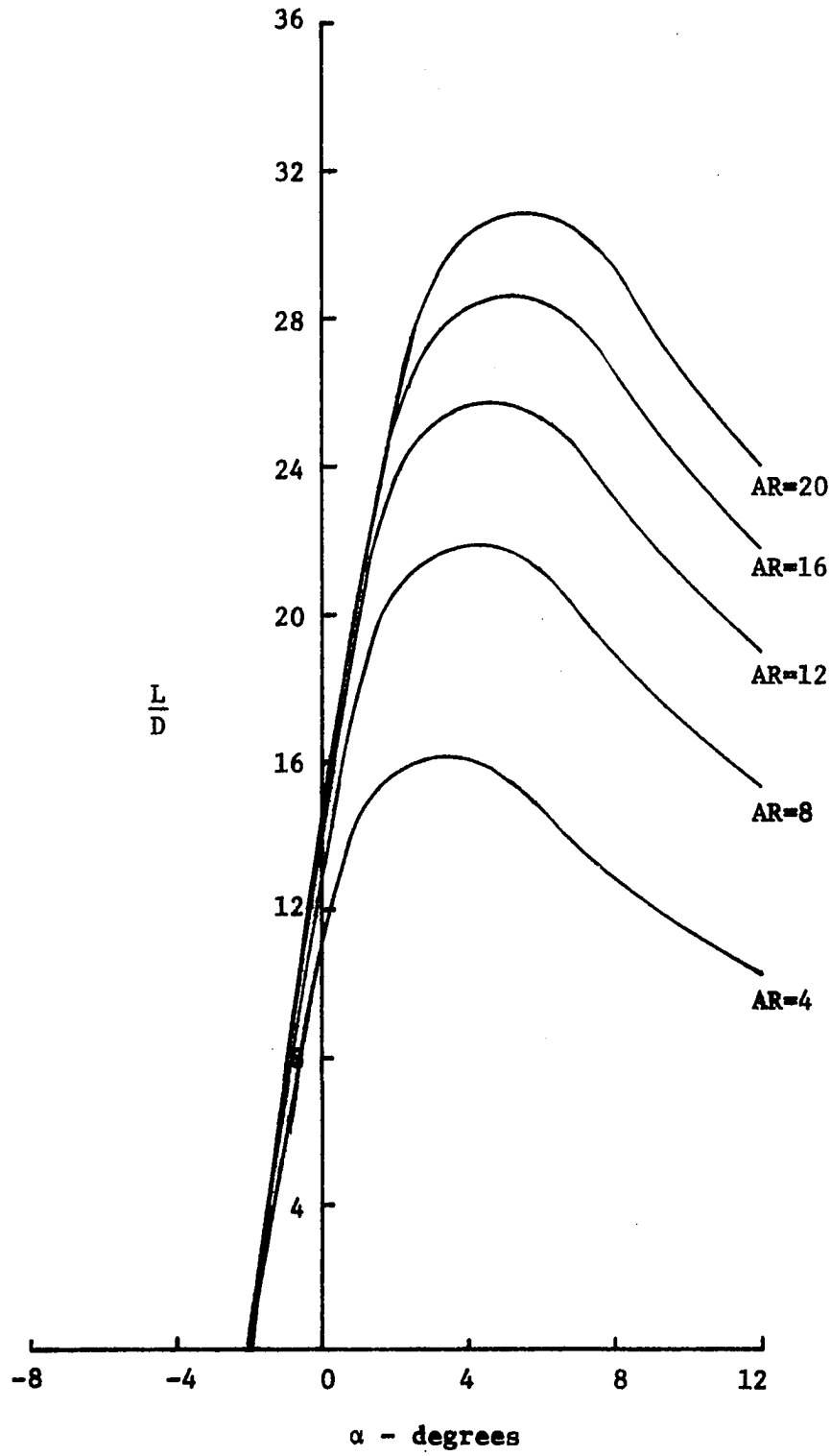

Figure 4.23 Wing L/D (e=.866)(NACA 2412 Airfoil)

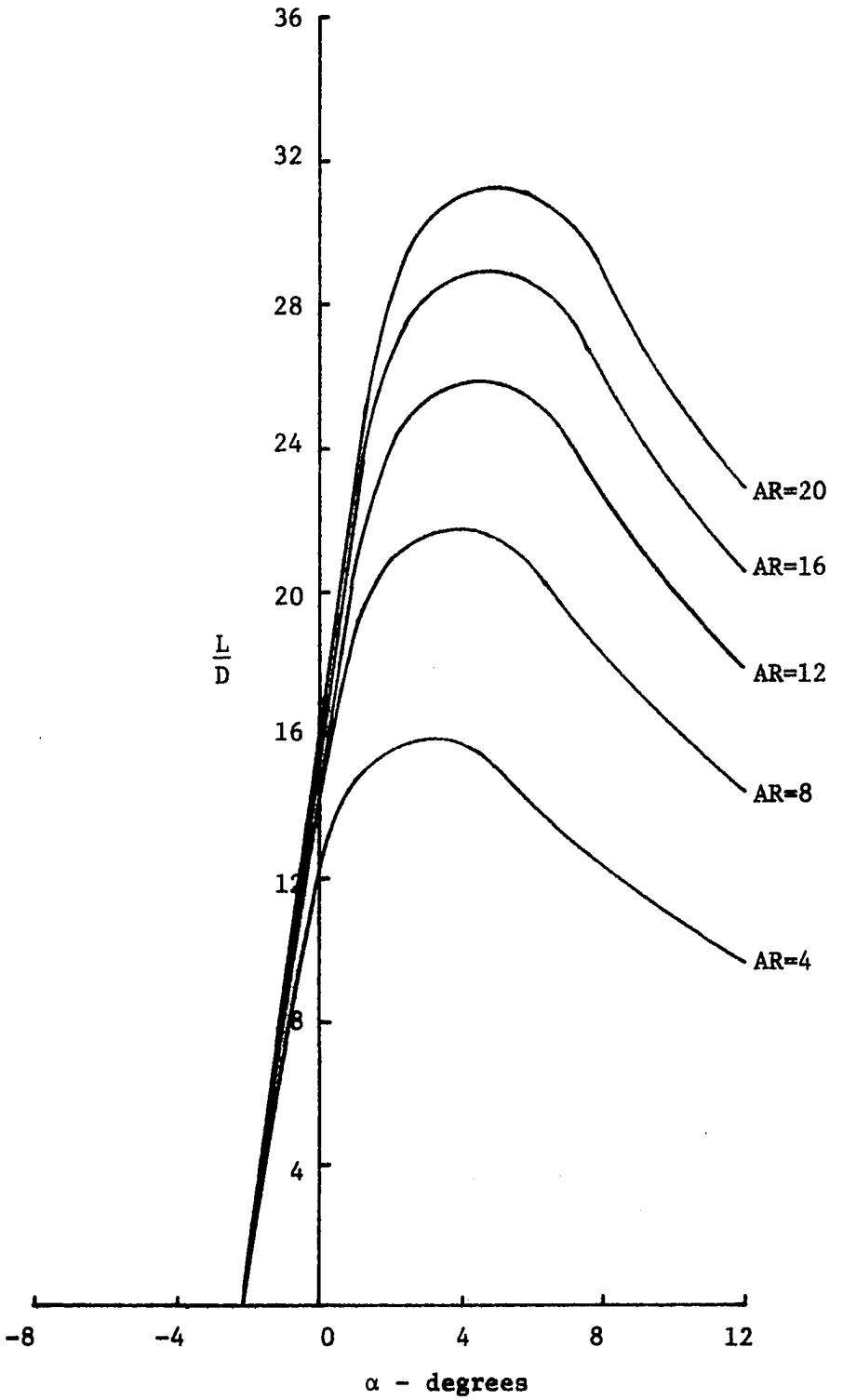

Figure 4.24 Wing L/D (e=.954)(NACA 2412 Airfoil)

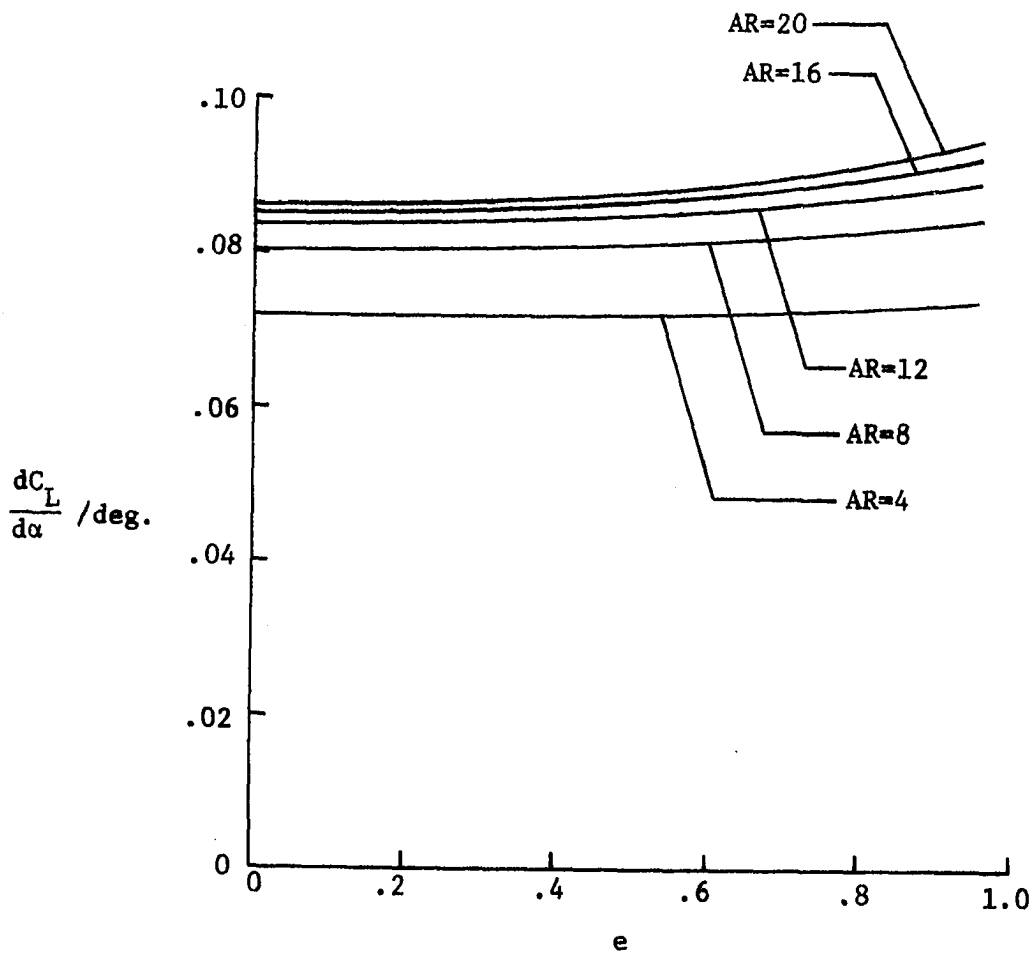

Figure 4.25 Lift Curve Slope vs. Eccentricity (NACA 4412 Airfoil)

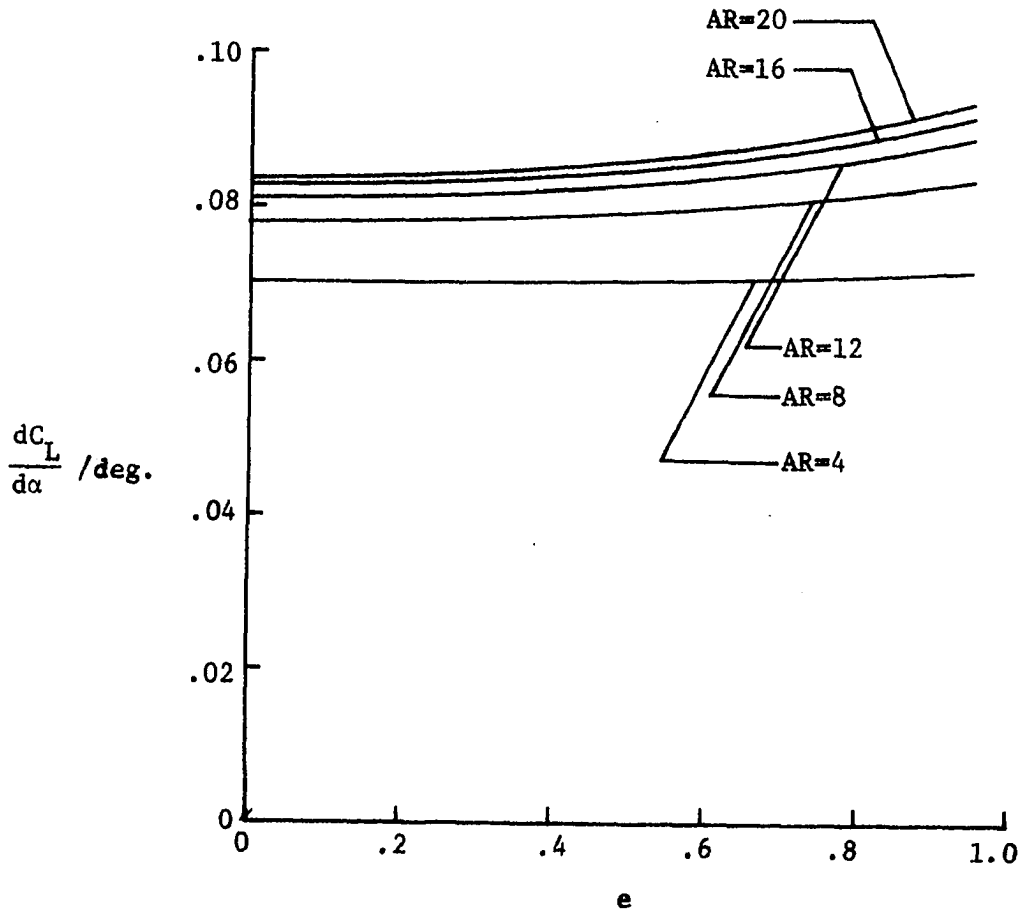

Figure 4.26 Lift Curve Slope vs. Eccentricity (NACA 2412 Airfoil)

For each wing of like aspect ratio and airfoil section the lift curve slope increases with eccentricity thus approaching the lift curve slope of a planar wing.

Efficiency Factor

The efficiency factor, k, can be calculated by

$$k = \frac{C_L^2}{\pi \, AR \, C_{D_i}} \tag{4.11}$$

In this manner the efficiency of an elliptically shaped wing can be compared to that of a planar wing having an elliptical circulation distribution (k=1). The efficiency factor was found to be independent of the angle of attack and the results are contained in figure 4.27. These results are compared to the optimum values calculated by Cone and the difference is discussed in Chapter V.

Generalized Power Required

A generalized power-required curve was developed using the expression developed by Perkins and Hage [15] for steady level flight. The expression is

$$\frac{P}{P_{L/D_{max}}} = \left[\frac{D}{D_{L/D_{max}}}\right] \left[\frac{U}{U_{L/D_{max}}}\right] \tag{4.12}$$

where P is the power required. The results were plotted for a wing composed of NACA 4412 airfoil sections (figure 4.28) and are independent of eccentricity.

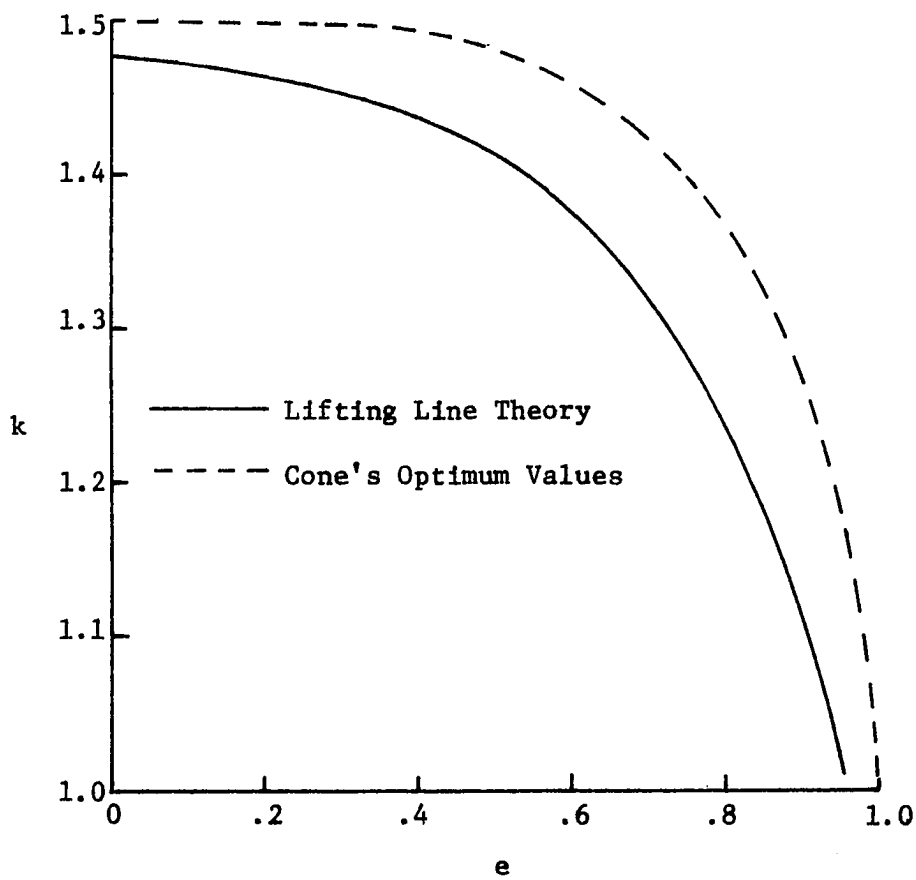

Figure 4.27 Efficiency Factor vs. Eccentricity
(NACA 4412 and NACA 2412 Airfoils)

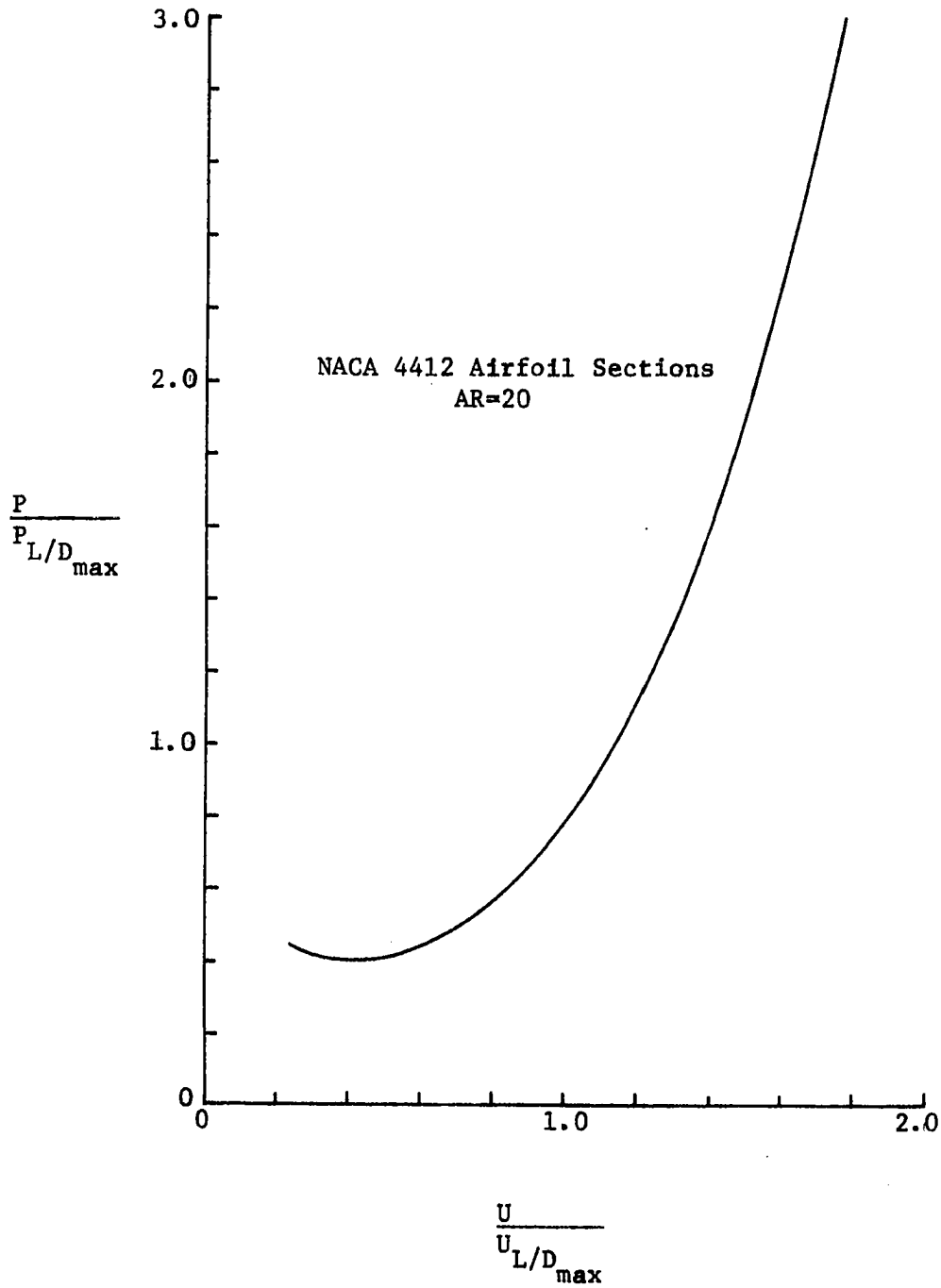

Figure 4.28 Generalized Power-Required for an Elliptical Wing

It must be remembered that the power ratio expressed here is that ratio required for overcoming the wing drag and makes no reference to the power required for a complete aircraft.

Endurance and Range

The contribution that each wing makes to increasing the endurance and range can best be expressed by first inspecting the equation for range and endurance.

For best endurance, it is assumed that the angle of attack is very small and therefore the lift equals the weight. For steady flight it is also assumed that the thrust equals the drag. Endurance then becomes

$$\text{Endurance} = \int_0^t dt$$

where t is the flight time. It is also possible to write

$$dt = \frac{dW}{\dot{W}_f} \tag{4.14}$$

where dW is the incremental change in the aircraft weight and $\dot{W}_f$ is the fuel rate of flow. The ratio $\frac{\dot{W}_f}{T}$ is normally referred to as the thrust specific fuel consumption and is given the symbol c. Therefore for a turbojet engine

$$\text{Endurance} = -\int_{W_i}^{W_f} \frac{1}{c}\frac{L}{D}\frac{dW}{W} \tag{4.15}$$

where W_i and W_f are the initial and final aircraft weights respectively. If, as in most cases, c is relatively constant for a turbojet engine, endurance is effected primarily by the ratio $\frac{L}{D}$ which should be maximized. For this reason the maximum lift to drag ratio is plotted against eccentricity for different aspect ratio wings in figure 4.29. As discussed before, the maximum lift to drag ratio increases with eccentricity and therefore maximum endurance will be reached as the eccentricity approaches that of a planar wing.

The range is a product of the endurance and the velocity and therefore equation 4.15 is modified to reflect this change. Range for a turbojet engine is then expressed as

$$\text{Range} = -\int_{W_i}^{W_f} \frac{U}{c}\frac{L}{D}\frac{dW}{W} \tag{4.16}$$

where the product $\frac{U}{c}\frac{L}{D}$ is commonly referred to as the range factor. The range factor must be maximized to produce the maximum range for a given aircraft and in general is a function of the altitude and the flight profile.

If the aircraft flies at a constant altitude, then equation 4.16 can be rewritten as

$$\text{Range} = -\int_{W_i}^{W_f} \frac{1}{c}\left[\frac{2}{\rho S}\right]^{1/2} \frac{C_L^{1/2}}{C_D}\frac{dW}{W^{1/2}} \tag{4.17}$$

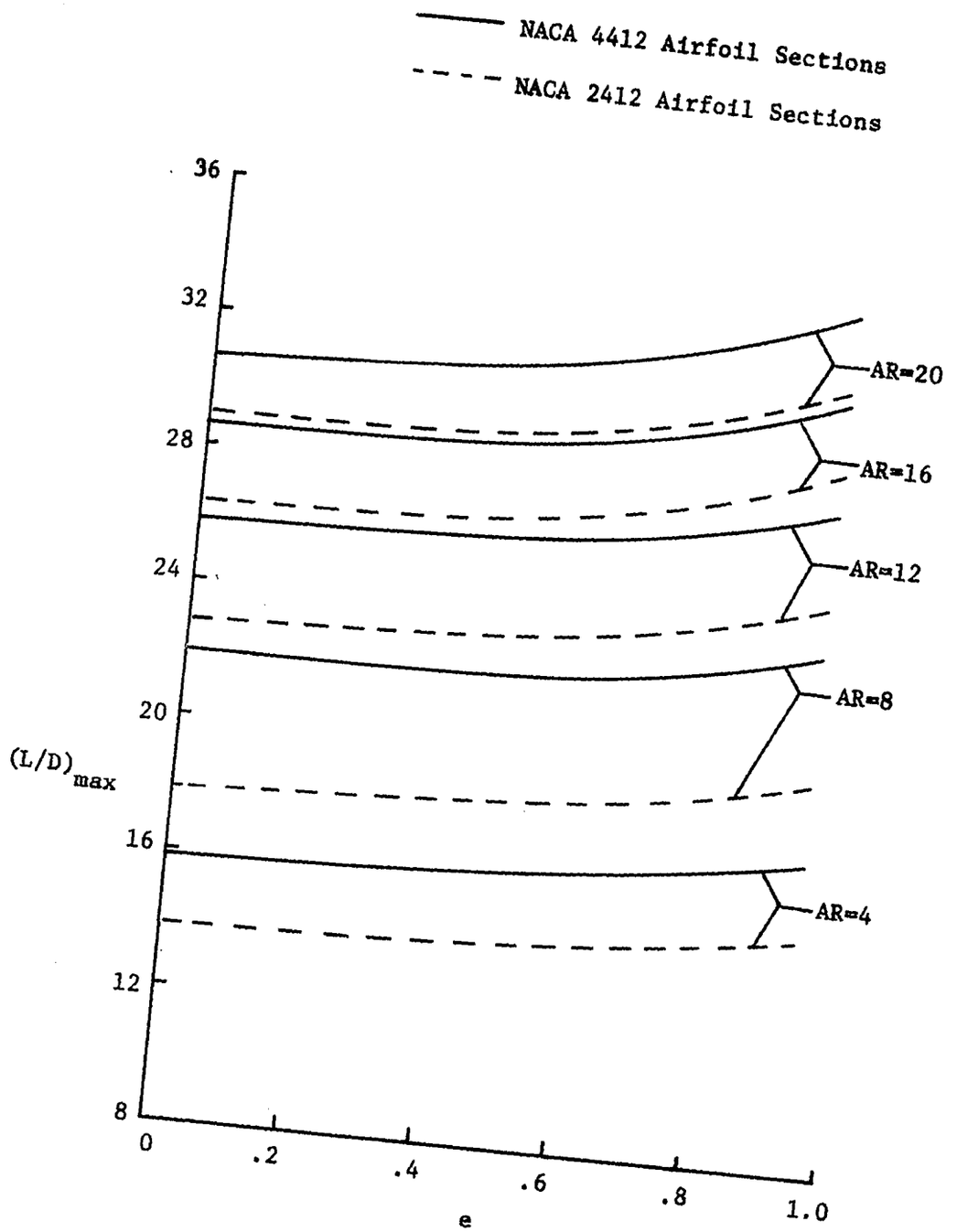

Figure 4.29 $(L/D)_{max}$ vs. Eccentricity

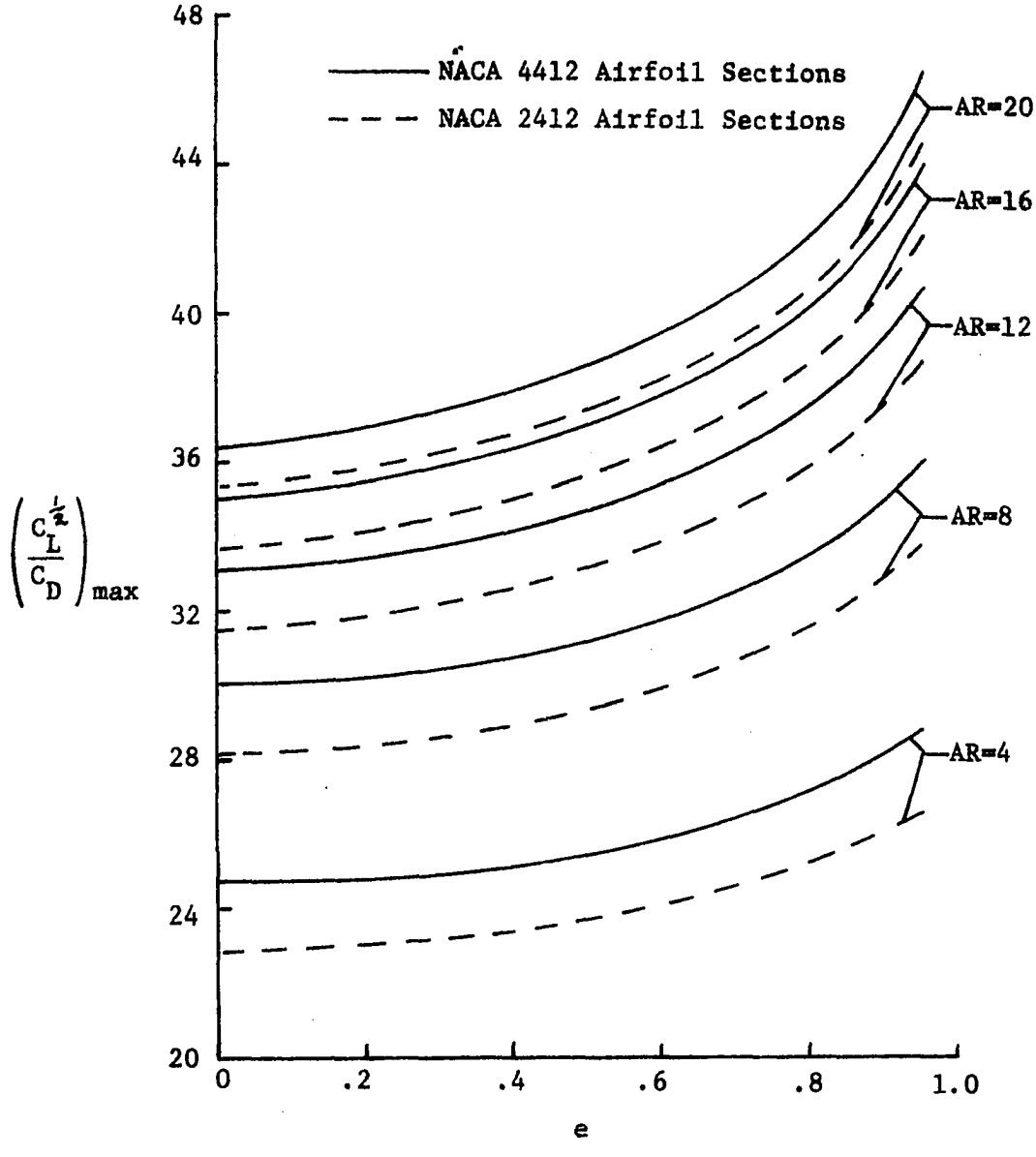

Figure 4.30 $\left(\frac{C_L^{\frac{1}{2}}}{C_D}\right)_{max}$ vs. Eccentricity

and maximum range will be attained when the ratio $C_L^{1/2}/C_D$ is a maximum. This of course assumes that the thrust specific fuel consumption, c, remains constant for a turbojet engine. Values for $\left(\frac{C_L^{1/2}}{C_D}\right)_{max}$ are plotted against eccentricity for different aspect ratio wings in figure 4.30. From these results it can be seen that the range also increases as eccentricity increases.

CHAPTER V

DISCUSSION OF RESULTS

The circulation distribution that is predicted by lifting line theory shows that the efficiency, in the classical sense, is greater for the semi-circular shape than for elliptical shapes of eccentricity greater than zero. This can be better understood by realizing that the circulation is a measure of the normal force on the wing and the accompanying induced drag. Lift, however, is the vertical component of this normal force and by increasing the circulation near the wing tip one merely increases the induced drag without substantially increasing the lift.

Three different wings were considered in Chapter III, each having a different airfoil section. The properties that were varied were the angle of zero lift and the lift curve slope. The NACA 2412 and 4412 airfoils have the same lift curve slope but different angles of zero lift. The third wing was composed of airfoil sections having an angle of zero lift equal to zero and a lift curve slope of 2π. It is interesting to note that the circulation distribution is effected more by the angle of zero lift than the lift curve slope. Decreasing the angle of zero lift on a non-planar wing has the same effect upon the circulation distribution as giving positive twist to a planar wing.

The efficiency factor, k, compares very favorably with that predicted by Cone for optimum shapes. No attempt was made to optimize the wings in this study so the efficiency factor is slightly less than the optimum value. In private communications with Mr. Roger Smith of Manchester, Missouri, it was determined that he had experimentally determined that the efficiency factor for a semi-circular wing composed of NACA 4412 airfoil sections was 1.48. This compares quite well with the theoretical value of 1.47 as determined by this study.

One must look further than the efficiency factor to measure the qualities of a non-planar wing. Considering wings of the same span, one finds that for small values of the lift coefficient the induced drag decreases as the elliptical wing tends toward a semi-circular wing while the profile drag increases with the resultant that the total drag increases coupled with a decrease in lift. The result is that the lift to drag ratio increases with an increases in eccentricity for small values of the lift coefficient. This is not to imply that the planar wing always has the best lift to drag ratio. The case studied in this report only involves wings that have a constant chord and constant airfoil sectional properties. A variation in these properties could possibly produce an elliptically shaped wing with a lift to drag ratio greater than that of a planar wing.

The value in the lifting line theory lies in its relative

simplicity. Although the required digital computer time is quite large (7000 seconds on a Burrough's 6700 for 20 collocation points) a matrix of the values from the singular integrals is independent of airfoil section, chord and the angle of attack and may be calculated for each eccentricity. Once this is accomplished, wings of the same eccentricity but with varying chord, airfoil section and angle of attack may be solved with relative ease.

Further study is needed in the area of the wing tip. It is obvious that the Fourier series does not properly describe the circulation distribution in this regime. Insight into this problem might be derived from applying singular perturbation techniques to the lifting surface theory associated with non-planar wings.

The use of propellers mounted in the elliptical wing sections obviously produces greater lift, as tests have shown. To determine the effect upon sections of differing eccentricity it would be beneficial to experimentally determine the pressure distribution over these wings with power-off and then to evaluate the change in pressure distribution produced by power-on. In this manner one may possibly be able to determine the predominant factors associated with propellers mounted in a channel with a large change in velocity across the propeller disk.

REFERENCES

1. Blick, E. F. "The Channel Wing - An Answer to the STOL Problem?" Shell Aviation News, No. 392, (1971).

2. Fasamanick, J. "Langley Full-Scale-Tunnel Tests of the Custer Channel Wing Airplane" NACA RM L53A09, (April 1953).

3. Young, D. W. "Tests of Two Custer Channel Wings Having a Diameter of 37.2 Inches and Lengths of 43 and 17.5 Inches" AAF Air Material Command, AAF TR 5568, (April 1947).

4. Young, D. W. "Custer U-Shaped Channel Wing" AAF Air Technical Service Command, AAF Memorandum Rept. TSEAL-2-4568-3-2, (July 1945).

5. Young, D. W. "Test of 1/3 Scale Powered Model of Custer Channel Shaped Wing - Five Foot Wind Tunnel Test No. 487" AAF Air Material Command, AAF TR 5142, (September 1944).

6. Crook, L. H. "Lift Forces on Custer Model Scoop with G-398 Airfoil Section" Aero. Rept. No. 571, January 1944, L. H. Crook Aero. Lab., Catholic Univ., Washington, D. C.

7. Crook, L. H. "Full Scale Static Lift Tests on Custer 72 Inch Diameter Channel Wing" Aero. Rept. No. 681, December 1947, L. H. Crook Aero. Lab., Catholic Univ., Washington, D. C.

8. Crook, L. H. "Full Scale Tests on CCW-2 Experimental Aircraft" Aero. Rept. No. 693, July 1951, L. H. Crook Aero. Lab., Catholic Univ., Washington, D. C.

9. Blick, E. F. "Power-On Channel Wing Aerodynamics" Journal of Aircraft, Vol. 8, No. 4, 234-238, (April 1971).

10. Hermes, M. E. "Aerodynamic Loads on Custer Channel Wing" DAS Report No. 553, February 1970, De Vore Aviation Service Corp., Roslyn Heights, New York.

11. Karamcheti, K. "Principles of Ideal-Fluid Aerodynamics" 538-547, John Wiley and Sons, Inc., (1966).

12. Ashley, H. and Landahl, M. "Aerodynamics of Wings and Bodies" 208-213, Addison-Wesley Publishing Company, Inc., (1965).

13. Cone, C. D. Jr. "The Theory of Induced Lift and Minimum Induced Drag of Nonplanar Lifting Systems" NASA TR R-139, (1962).

14. Abbott, I. H., et al. "Summary of Airfoil Data" NACA Report No. 824, (1945).

15. Perkins, C. D. and Hage, R. E. "Airplane Performance Stability and Control" 168-171, John Wiley and Sons, Inc., (1957).

APPENDIX A

Analysis of Lifting Line Theory using Lifting Surface Theory

Inspection of equation 2.11 shows that the downwash becomes infinite at the wing tips, a problem that is characteristic of lifting line theory. To investigate this problem further it is convenient to refer to lifting surface theory and make use of an expression for the downwash as developed by Ashley and Landahl [12].

The downwash, w, is expressed as

$$w(x,s) = \frac{1}{4\pi} \iint \gamma(x_1,s_1) K_{np}(x_0,y_0,z_{00}) dx_1 ds_1 \qquad (A.1)$$

where

$$K_{np} \doteq \frac{1}{y_0^2} \left\{ \sin\left[\psi(y) + \psi(y_1)\right] \frac{y_0^3 z_{00}}{r_1^4} \left[2 + \frac{2x_0^3 + 3x_0 r_1^2}{r_0^3} \right] \right.$$

$$- \cos\psi(y) \cos\psi(y_1) \frac{y_0^2 z_{00}^2}{r_1^2} \left[1 + \frac{x_0^3 + 2x_0 r_1^2}{r_0^3} \right.$$

$$\left. \left. - \frac{y_0^2}{z_{00}^2} \left(1 + \frac{x_0}{r_0} \right) \right] \right\}$$

$$- \sin \psi(y) \sin \psi(y_1) \frac{{y_0}^4}{{r_1}^4} \left[1 + \frac{{x_0}^3 + 2x_0 {r_1}^2}{{r_0}^3} - \frac{{z_{00}}^2}{{y_0}^2} \left(1 + \frac{x_0}{r_0} \right) \right] \Bigg\} \tag{A.2}$$

The variables x_0, y_0, z_{00}, r_1 and r_0 are defined by the following wxpressions and figure A.1.

$$x_0 = x - x_1 \tag{A.3}$$

$$y_0 = y - y_1 \tag{A.4}$$

$$z_{00} = z_0(y) - z_0(y_1) \tag{A.5}$$

$$r_1 = \left[{y_0}^2 + {z_{00}}^2 \right]^{\frac{1}{2}} \tag{A.6}$$

$$r_0 = \left[{x_0}^2 + {y_0}^2 + {z_{00}}^2 \right]^{\frac{1}{2}} \tag{A.7}$$

Since the ultimate goal will be to investigate the order of magnitude of certain terms in the neighborhood of various singularities it will suffice to assum a semi-circular shaped wing. Utilizing the geometry of a semi-circular wing the variables in equation A.1 and A.2 become

$$ds_1 = R d\eta \tag{A.8}$$

$$\psi(y) = \phi - \frac{\pi}{2} \qquad \psi(y_1) = \eta - \frac{\pi}{2} \tag{A.9}$$

$$z_0(y) = R(1-\sin\phi) \qquad z_0(y_1) = R(1-\sin\eta) \tag{A.10}$$

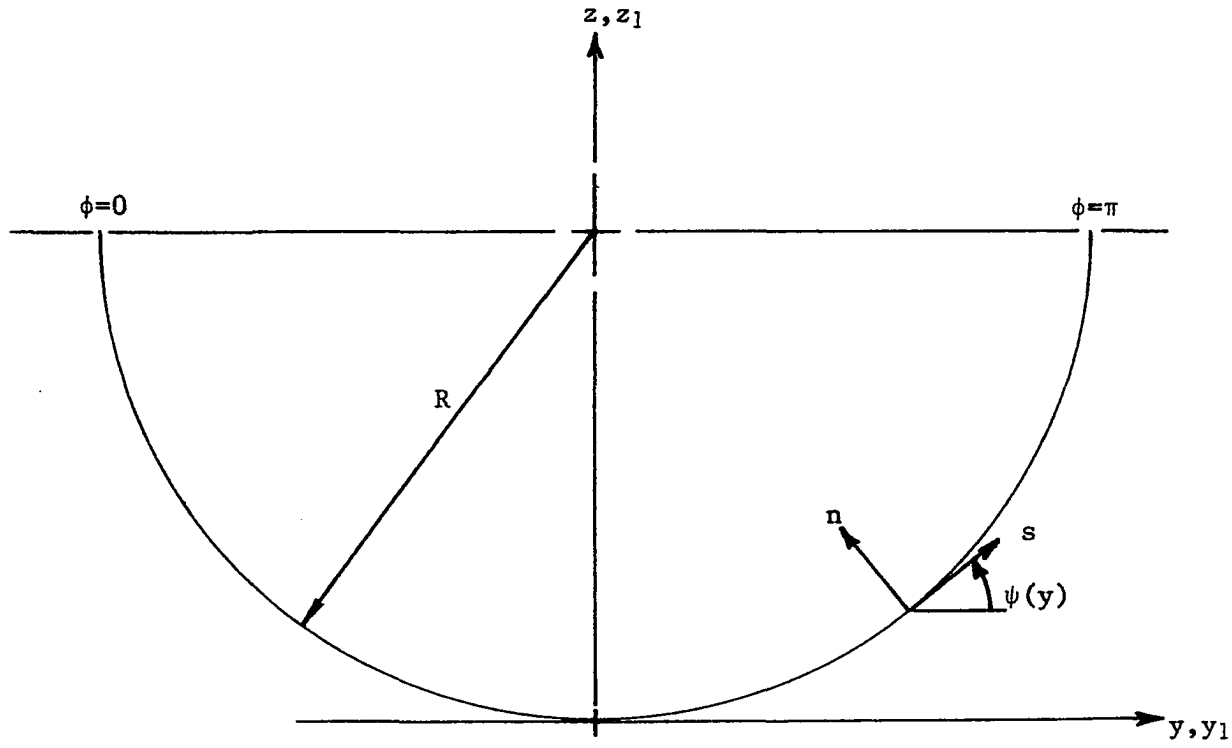

Figure A.1 Geometry of a Semi-circular Surface

$$z_{00} = R(\sin\eta - \sin\phi) \tag{A.11}$$

$$y = -R\cos\phi \qquad y_1 = -R\cos\eta \tag{A.12}$$

$$y_0 = R(\cos\eta - \cos\phi) \tag{A.13}$$

$$r_1 = R\left[2 - 2\cos(\phi-\eta)\right] \tag{A.14}$$

$$r_0 = \left[(x-x_,)^2 + R^2(2 - 2\cos(\phi-\eta))\right]^{1/2} \tag{A.15}$$

Substitution of these expressions into equations A.1 and A.2 yields

$$w(x,\phi) = \frac{R}{4\pi} \int_0^{\pi} \int_0^{c} \gamma(x_1,\eta) K_{np}\, dx_1 d\eta \tag{A.16}$$

and

$$K_{np} = \frac{1}{R^2\left[2 - 2\cos(\phi-\eta)\right]} \left\{ 1 + (x-x_1) \frac{\left[(x-x_1)^2 + R^2\left[4 - 4\cos(\phi-\eta) - (\sin\phi\cos\eta - \cos\phi\sin\eta)^2\right]\right]}{\left[(x-x_1)^2 + R^2(2-2\cos(\phi-\eta))\right]^{3/2}} \right\} \tag{A.17}$$

At this time it becomes convenient to evaluate the downwash at x=0. This is consistent with the assumptions made for the lifting-line analysis, in particular the assumption that the aspect ratio is very large. Upon non-dimensionalizing the variable x with the chord c, equation A.16 now becomes

$$w(0,\phi) = \frac{c}{4\pi R} \int_0^{\pi} \int_0^{1} \frac{\gamma(x_1,\eta)}{2-2\cos(\phi-\eta)} \left\{ 1 - x_1 \frac{\left[x_1^2+\frac{R^2}{c^2}\left[4-4\cos(\phi-\eta)-(\sin\phi\cos\eta-\cos\phi\sin\eta)^2\right]\right]}{\left[x_1^2+\frac{R^2}{c^2}\left[2-2\cos(\phi-\eta)\right]\right]^{3/2}} \right\} dx_1\, d\eta \quad (A.18)$$

where it should be understood that the variables x and x_1 are the new non-dimensional variables.

Now let the circulation distribution, γ, be represented by

$$\gamma(x_1,\eta) = \frac{2}{c}\left[1 - x_1\right] \gamma(\eta) \quad (A.19)$$

which assumes a chordwise distribution that is linear and devoid of a singularity at the leading edge. This is a reasonable assumption since chordwise integration is performed prior to making any of the order of magnitude assumptions. In rewriting equation A.18 it is also convenient to make the following substitutions.

$$\delta = \frac{c}{R} \qquad \xi = \eta - \phi$$

$$w(0,\phi) = \frac{1}{2\pi R} \int_{-\phi}^{\pi-\phi} \frac{\gamma(\phi+\xi)}{(2-2\cos\xi)} \int_0^{1} (1-x_1) \left\{ 1 - x_1 \frac{\left[x_1^2+\frac{1}{\delta^2}(4-4\cos\xi-\sin^2\xi)\right]}{\left[x_1^2+\frac{1}{\delta^2}(2-2\cos\xi)\right]^{3/2}} \right\} dx_1\, d\xi \quad (A.20)$$

At this point two parameters are of interest. First of all how does the expression for downwash behave when δ is much less than ξ, and secondly how does the expression behave for those values of ξ much less than δ?

To investigate the first of these questions it is assumed that

$$\delta << \xi$$

which is a valid assumption; being in consonance with the assumptions for lifting line theory. Expanding the integrand of equation A.20 for small values of $\frac{\delta}{\xi}$ and integrating across the chord gives

$$w(0,\phi) = \frac{1}{4\pi R} \int_{-\phi}^{\pi-\phi} \frac{\gamma(\phi+\xi)\, d\xi}{2-2\cos\xi} + \text{terms of order } \frac{\delta}{\xi} \qquad (A.21)$$

or

$$w(0,\phi) = \frac{1}{4\pi R} \int_{0}^{\pi} \frac{\gamma(\eta)\, d\eta}{2-2\cos(\phi-\eta)} + \text{terms of order } \frac{\delta}{\xi} \qquad (A.22)$$

The leading term of equation A.22 is of course identical to the downwash term in equation 3.6 if the proper substitution is made for the semi-circular shaped wing.

Since a semi-circular shaped wing has been assumed, it is necessary in the order of magnitude analysis to assume that

using the radius of the circle is analagous to using the radius of curvature for a non-circular section if the same order of magnitude analysis is to be carried forward to elliptical shaped wings. Figure A.2 shows the relationship between eccentricity and the radius of curvature at the wing tip. The tip is of course chosen since it represents the minimum radius of curvature for the wing. The radius of curvature, ρ, at the wing tip is expressed as

$$\rho = \frac{b\left[1 - 3e^2 + 3e^4 - e^6\right]^{3/2}}{(1-e^2)^{1/2}\left[1 - 2e^2 + e^4\right]} \tag{A.23}$$

The effect that the small values of radius of curvature at the tip will have on the overall circulation distribution is expected to be negligible but will have to be considered when tip effects are discussed.

The second aspect of the problem is a little more difficult to evaluate. First, equation A.20 will be divided into three intervals as follows.

$$w(0,\phi) = \frac{1}{2\pi R}\left\{ \int_{-\phi}^{-\varepsilon} \frac{\gamma(\phi+\xi)}{(2-2\cos\xi)} \int_{0}^{1} F(x_1,\xi)dx_1\, d\xi \right.$$

$$+ \int_{-\varepsilon}^{\varepsilon} \frac{\gamma(\phi+\xi)}{(2-2\cos\xi)} \int_{0}^{1} F(x_1,\xi)dx_1\, d\xi + \int_{\varepsilon}^{\pi-\phi} \frac{\gamma(\phi+\xi)}{(2-2\cos\xi)} \int_{0}^{1} F(x_1,\xi)dx_1\, d\xi$$

(A.24)

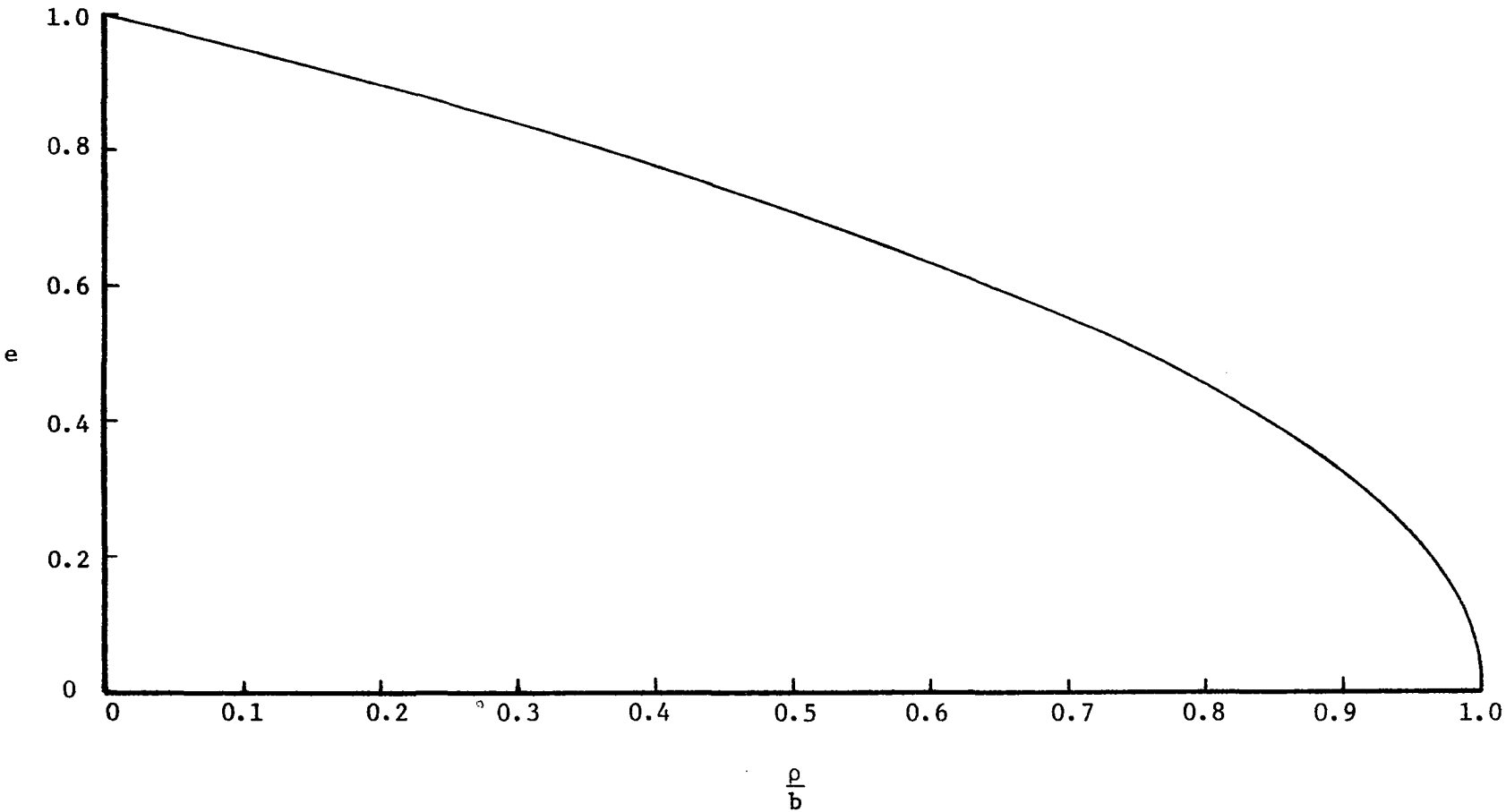

Figure A.2 The Ratio of Radius of Curvature to Span vs. Eccentricity (ϕ=0)

where

$$F(x_1,\xi) = (1 - x_1)\left\{1 - x_1\frac{\left[x_1^2 + \frac{1}{\delta^2}(4-4\cos\xi-\sin^2\xi)\right]}{\left[x_1^2 + \frac{1}{\delta^2}(2-2\cos\xi)\right]^{3/2}}\right\} \qquad (A.25)$$

Since the area of interest is when

$$\xi << \delta << 1$$

it is only necessary to evaluate the integral in the range $-\varepsilon$ to ε, assuming that ε is the same order of magnitude as ξ.

After performing the chordwise integration and then expanding for small values of $\frac{\xi}{\delta}$ the following expression results.

$$w(0,\phi) = \frac{1}{2\pi R}\left\{\int_{-\phi}^{-\varepsilon}\frac{\gamma(\phi+\xi)}{(2-2\cos\xi)}\int_0^1 F(x_1,\xi)dx_1d\xi\right.$$

$$+\int_{\varepsilon}^{\pi-\phi}\frac{\gamma(\phi+\xi)}{(2-2\cos\xi)}\int_0^1 F(x_1,\xi)dx_1d\xi$$

$$\left.+\int_{-\varepsilon}^{\varepsilon}\gamma(\phi+\xi)\left[\frac{1}{\delta\xi}+\frac{1}{2\delta^2}\ln\frac{\xi}{2\delta}-\frac{1}{4\delta^2}-\frac{7}{24}\frac{\xi^2}{\delta^2}\ln\frac{\xi}{2\delta}+\cdots\right]d\xi\right\} \qquad (A.26)$$

Assuming that $\gamma(\phi+\xi)$ is essentially constant for the small interval, $-\varepsilon$ to ε, the integration from $-\varepsilon$ to ε can then be performed and results in a correction term of order ε, a

correction term that is treated in more detail in appendix C.

The previous discussion assumes that all of the collocation points, points at which downwash is calculated, are interior points. If a collocation point is placed at the tip of the wing, say at $\phi=0$, then equation A.26 becomes

$$w(0,0) = \frac{1}{2\pi R}\left\{ \int_{\varepsilon}^{\pi} \frac{\gamma(\xi)}{(2-2\cos\xi)} \int_{0}^{1} F(x_1,\xi)\,dx_1\,d\xi + \int_{0}^{\varepsilon} \gamma(\xi)\left[\frac{1}{\delta\xi} + \frac{1}{2\delta^2} \ln\frac{\xi}{2\delta} - \frac{1}{4\delta^2} - \frac{7}{24}\frac{\xi^2}{\delta^2} \ln\frac{\xi}{2\delta} + \cdots \right] d\xi \right\} \quad \text{(A.27)}$$

It is quite evident from equation A.27 that the downwash becomes infinite at the tip of the wing, a result that is mathematically misleading. Physically this is not possible and several approaches to alleviating this impossibility may be considered.

An expression involving matched asymptotic expansions is a distinct possibility and would give the most detailed knowledge of the phenomena that are occurring in the neighborhood of the wing tip. This method is of course lengthy and does not seem warranted if the end result that is required is only

to find the circulation distribution as is the case for this study.

The downwash near the tip of the wing goes to infinity like the natural logarithim of the angular displacement from the tip as can be seen from equation A.27. The assumption that was made which led to the aforementioned result is of course that the circulation distribution can be adequately represented by a Fourier series. The downwash then becomes the integral of the curves shown in figure A.11. Two different curves are shown in this figure and both of them are meant to be only a graphical representation of the trend in data and not specific values for a particular wing. The area under the curve in case I represents the downwash at y=b and it is clearly evident that the value of the downwash is infinite at this point, the tip of the wing. The area under the curve in case II represents the downwash at an interior point of the wing and has a finite value. The implication is that the Fourier series does not adequately represent the circulation distribution, especially if a collocation point is to be placed near the tip of the wing.

Figures A.3 through A.10 show the effect of placing a collocation point too close to the tip of the wing. The collocation point that is the closest to the tip of the wing has an angular displacement of β radians from the tip of the wing. If the Fourier

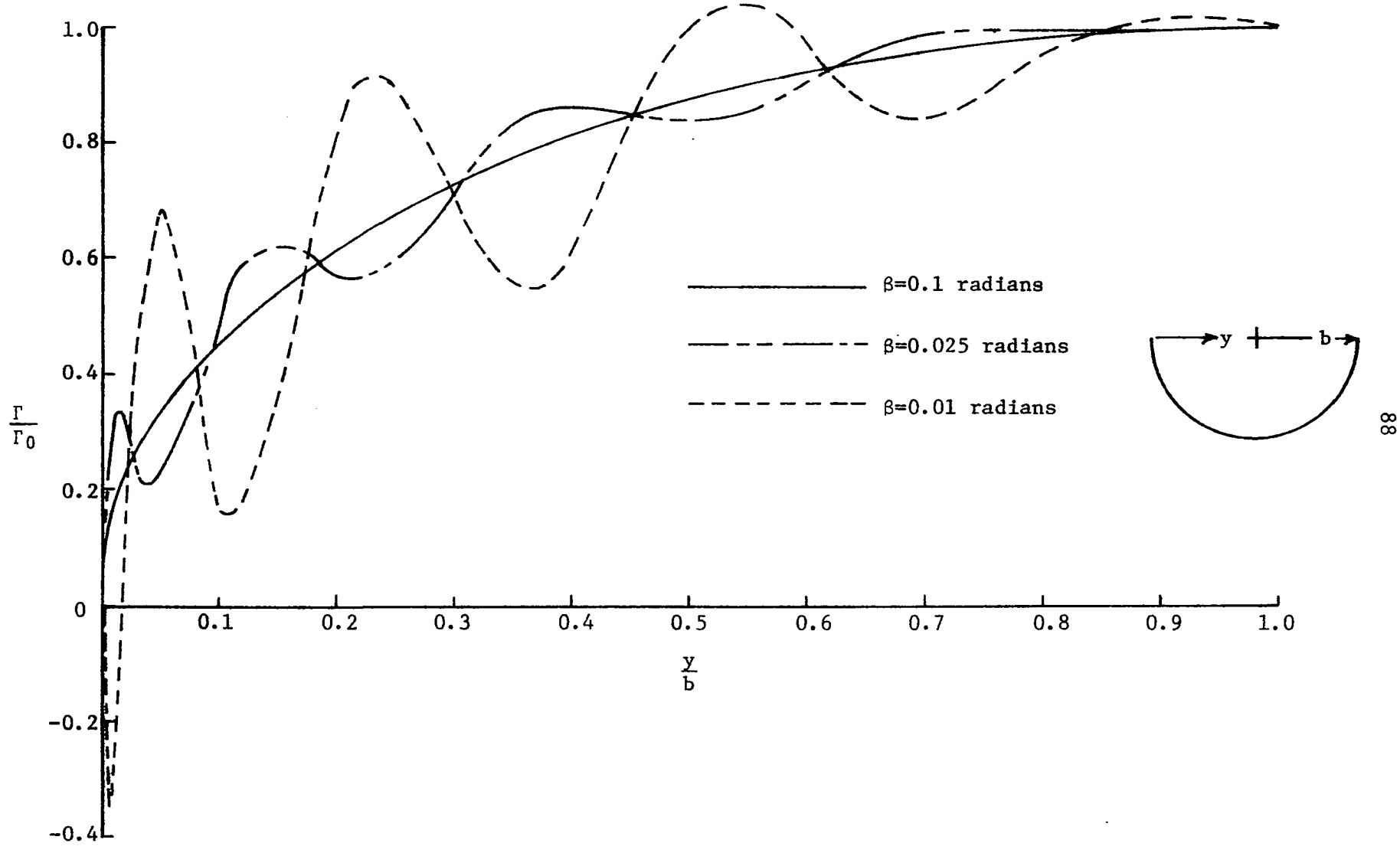

Figure A.3 Circulation Distribution (e=0) (AR=20)

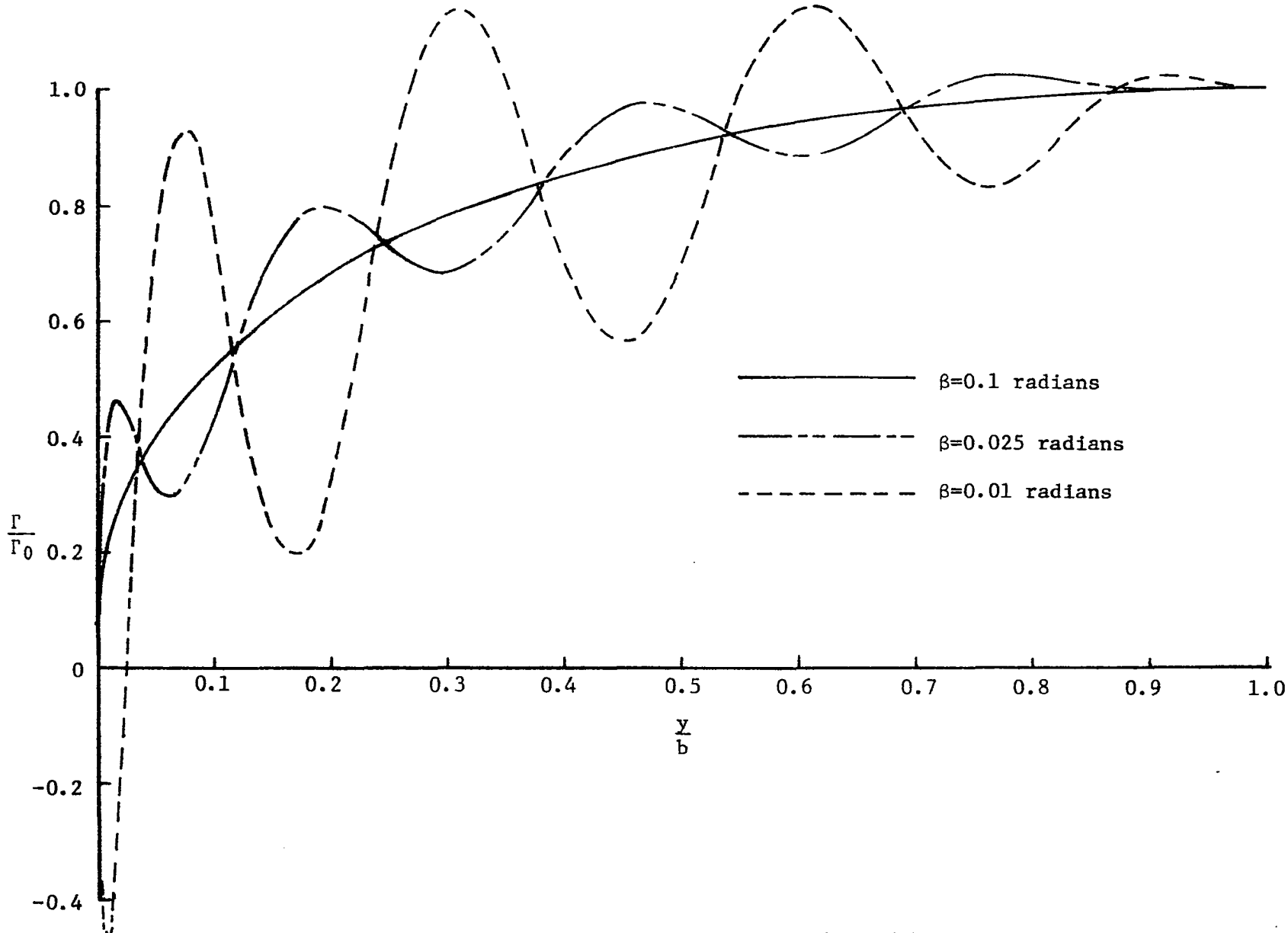

Figure A.4 Circulation Distribution (e=0.6)(AR=20)

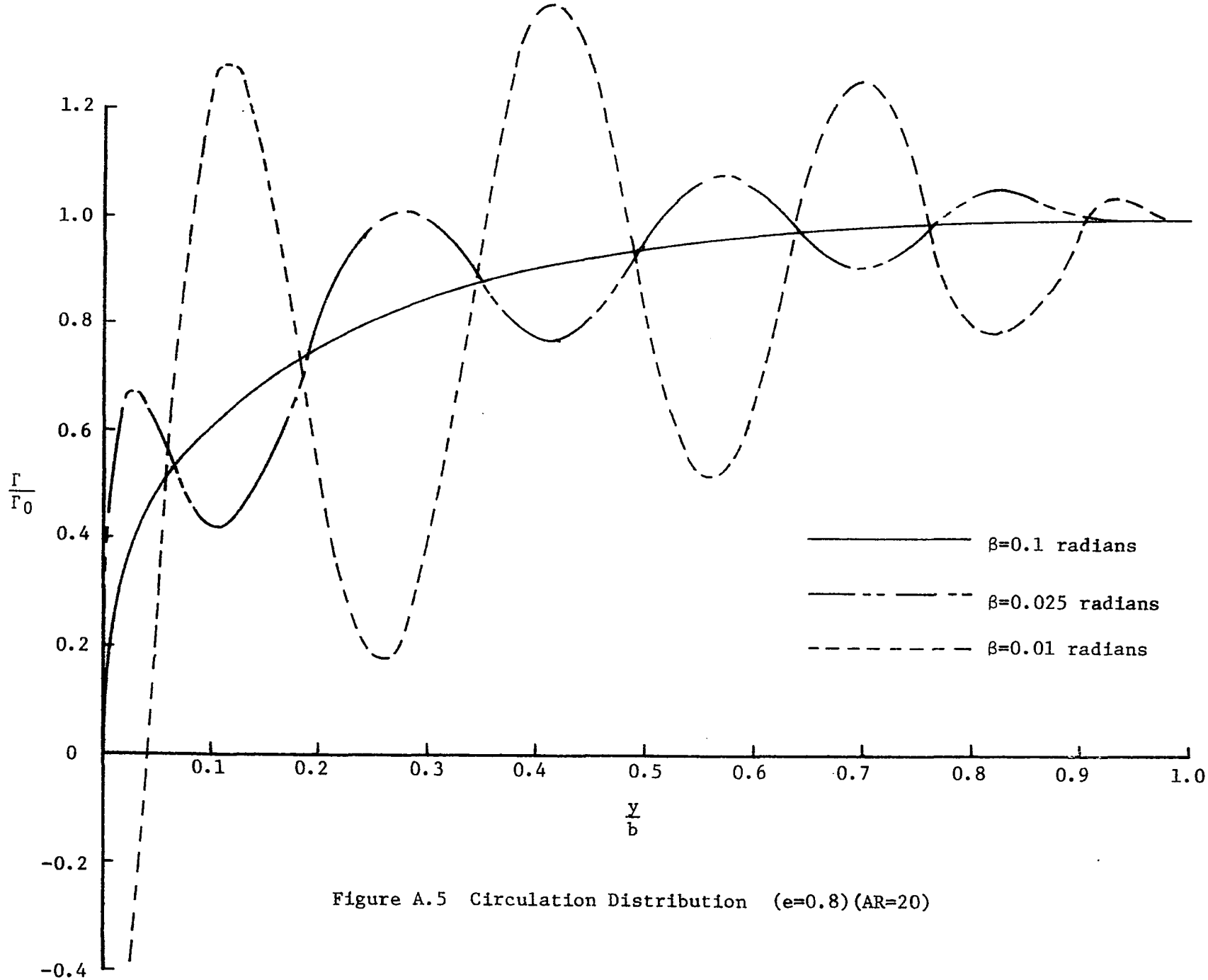

Figure A.5 Circulation Distribution (e=0.8)(AR=20)

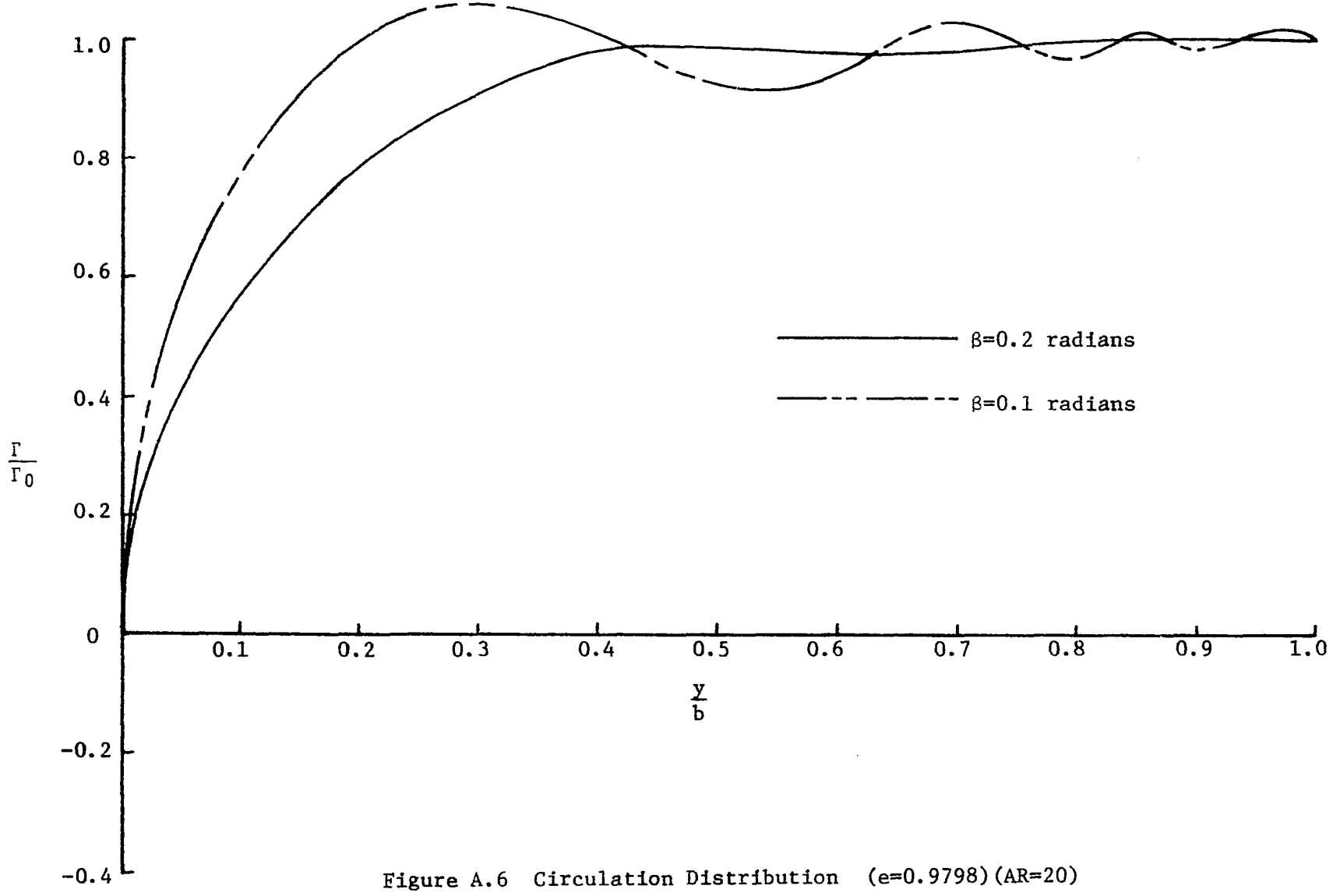

Figure A.6 Circulation Distribution (e=0.9798)(AR=20)

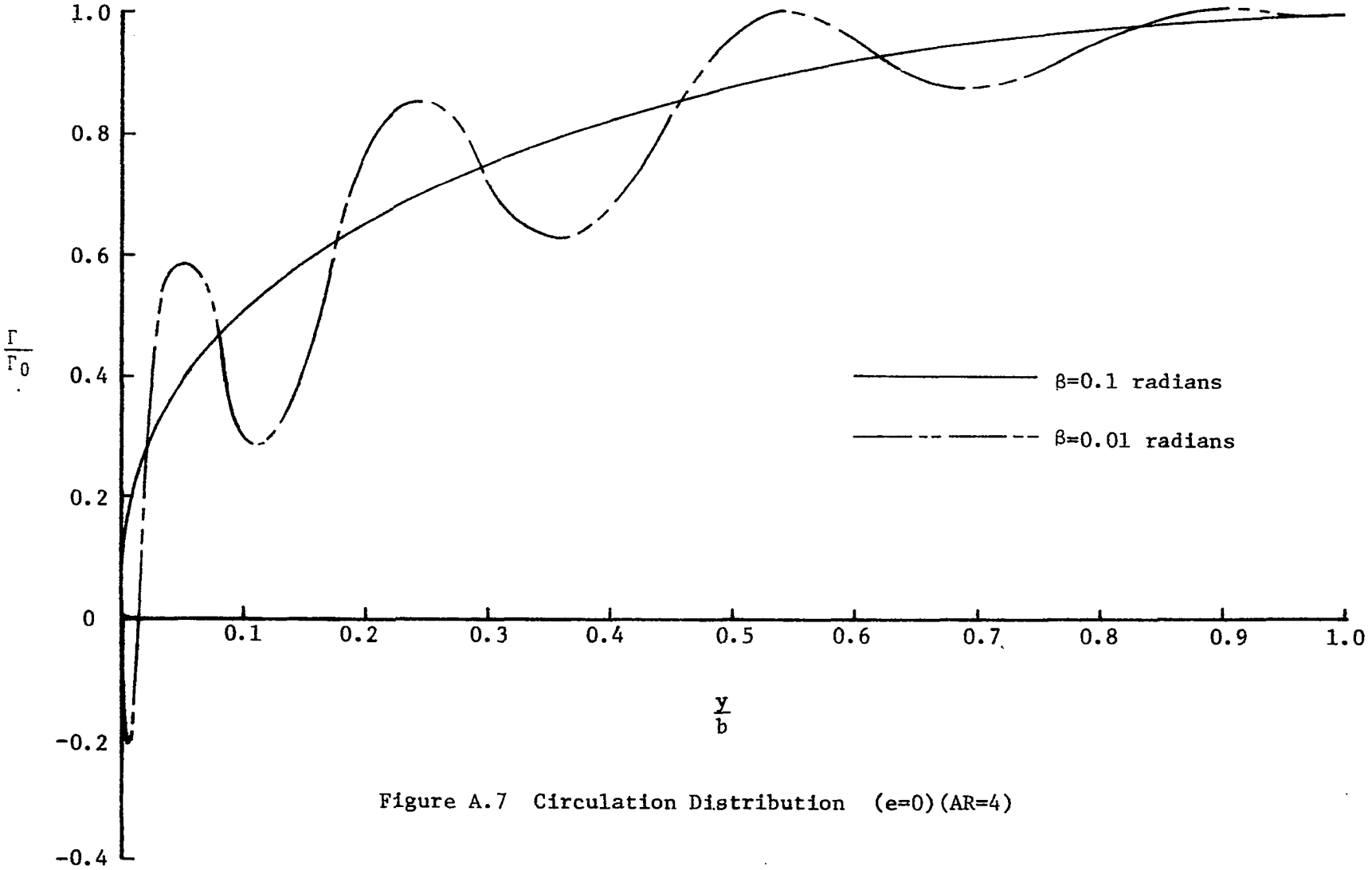

Figure A.7 Circulation Distribution (e=0)(AR=4)

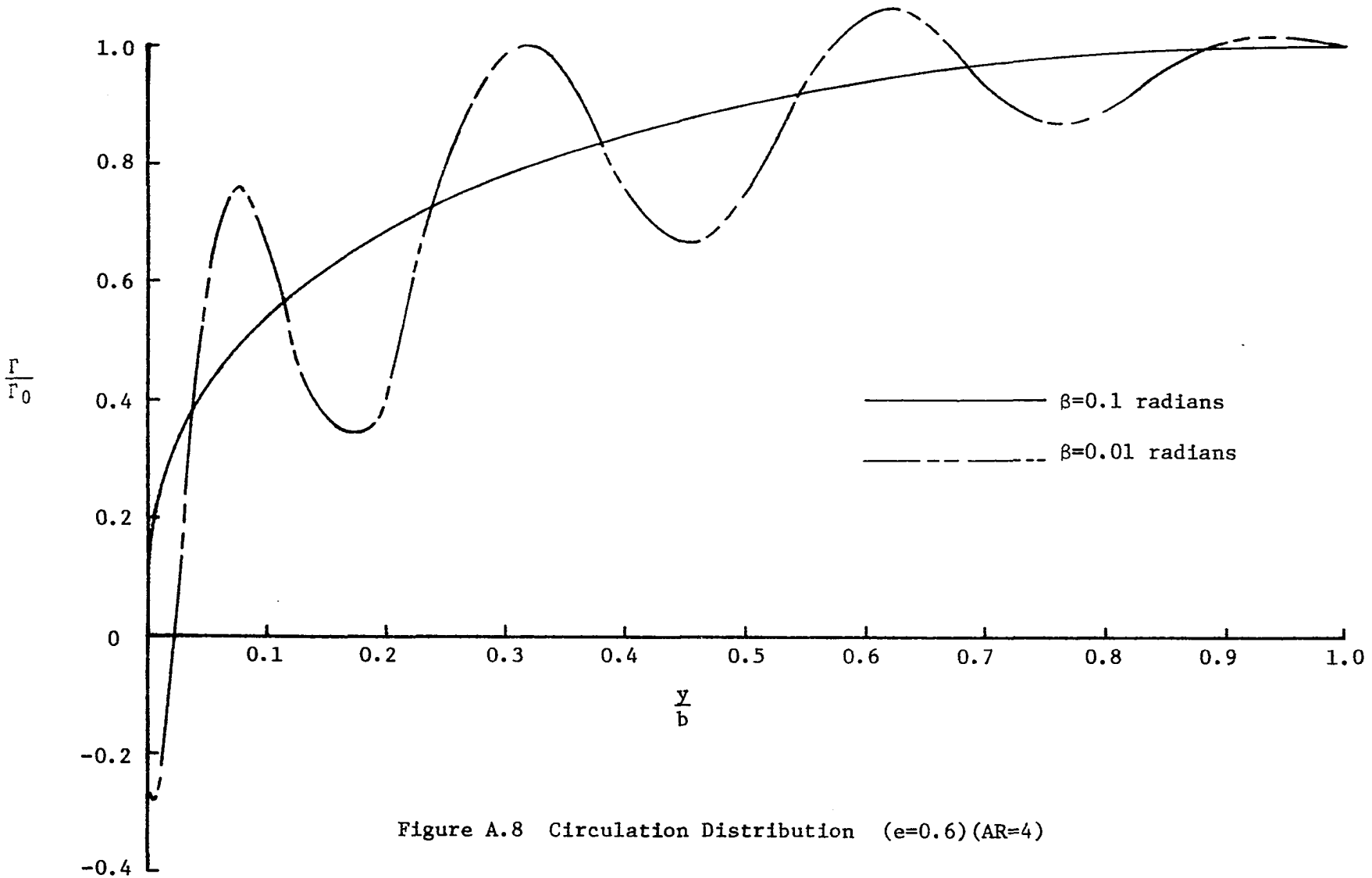

Figure A.8 Circulation Distribution (e=0.6)(AR=4)

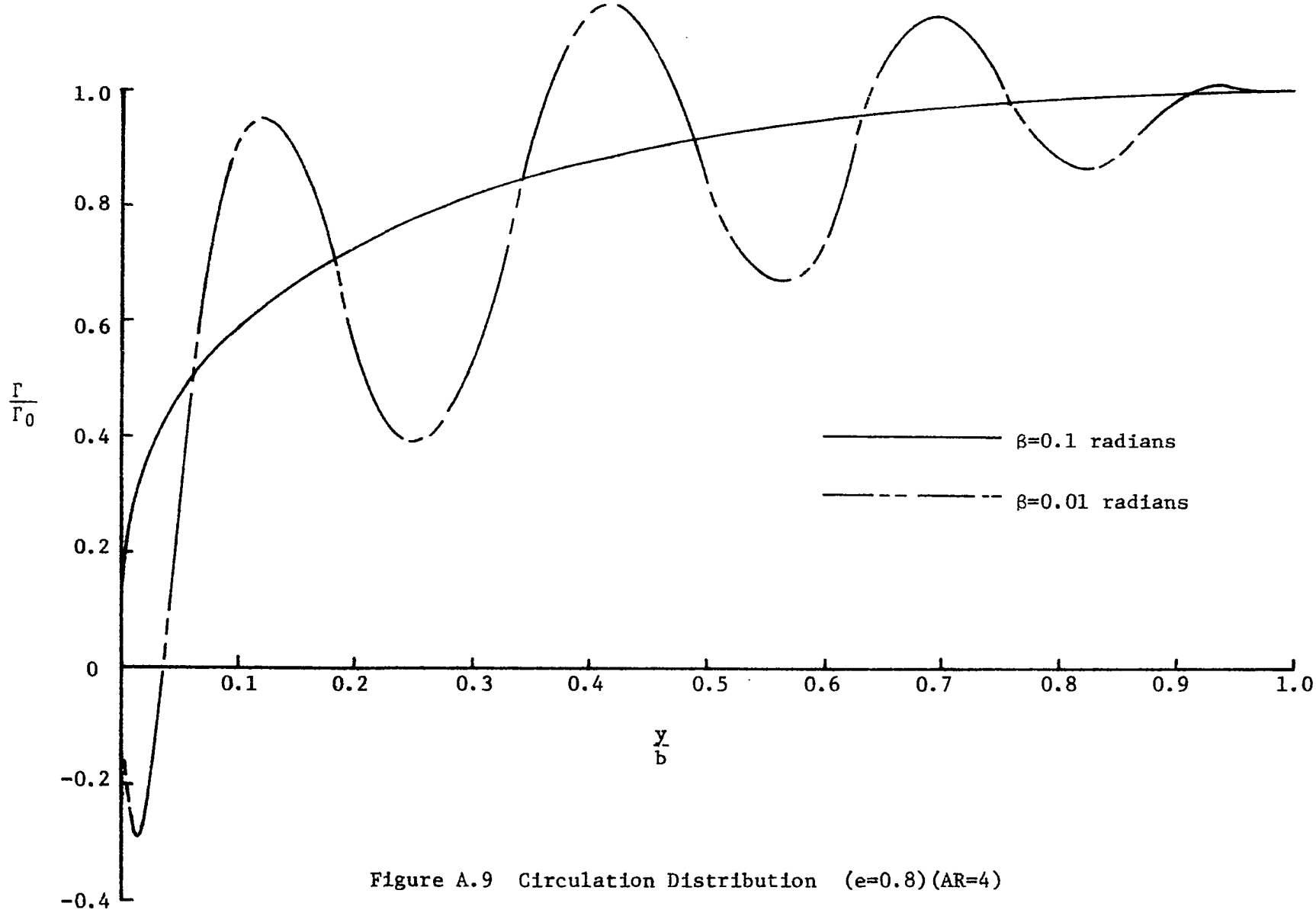

Figure A.9 Circulation Distribution (e=0.8)(AR=4)

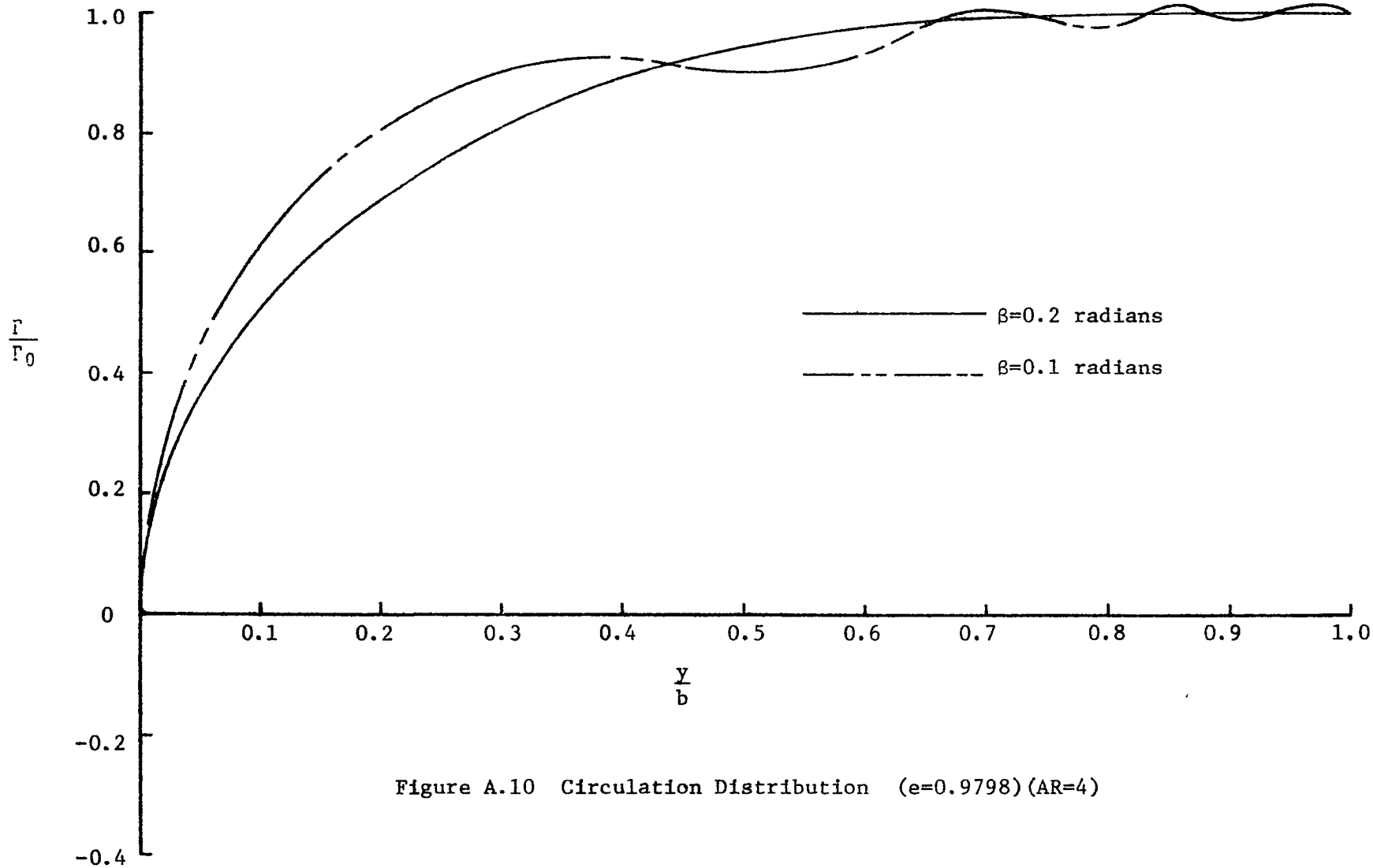

Figure A.10 Circulation Distribution (e=0.9798)(AR=4)

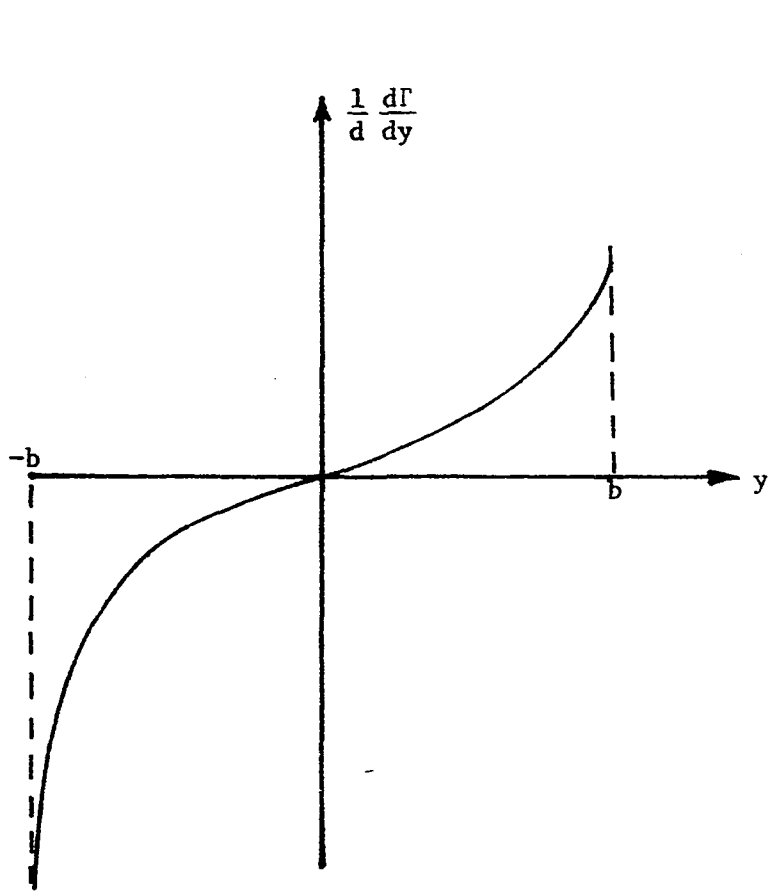

Case I Downwash Integral at y=-b

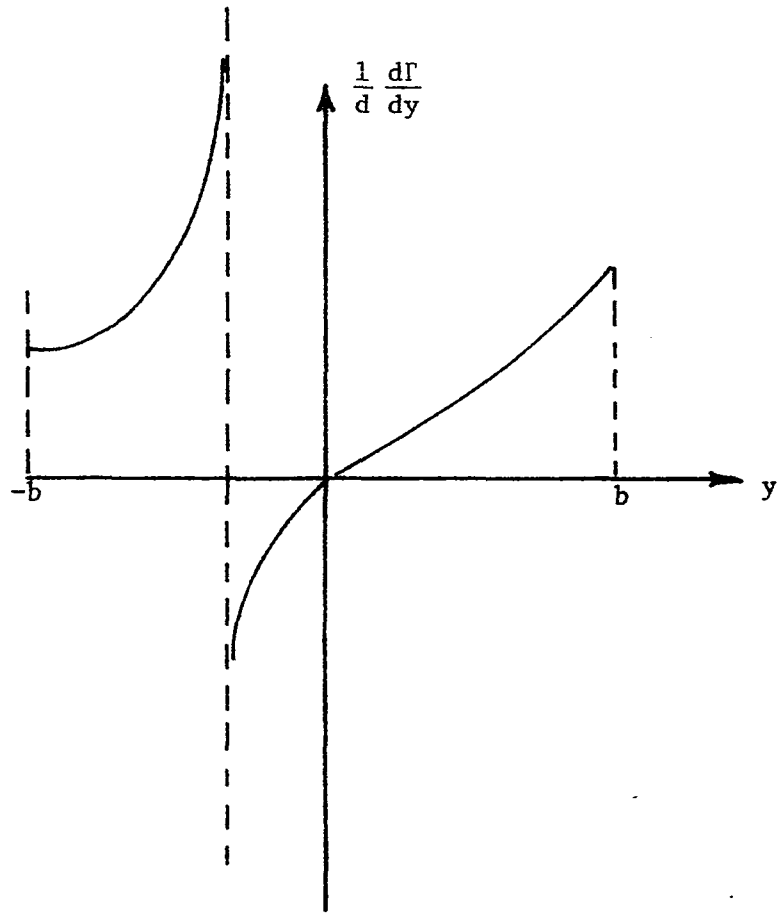

Case II Downwash Integral at -b<y<0

Figure A.11 Downwash Integrals at Different Spanwise Stations

series representation of the circulation distribution is to be used then certain steps must be taken to modify the usage of the lifting line theory.

For equation 3.15 to be completely valid, when the Fourier series approximation is used, the chord, c, between the wing tip and the last collocation point must be allowed to take values that will satisfy this equation. It is obvious from this equation that the chord must go to zero at the tip if the aforementioned equation is to be valid.

Two approaches were taken to investigate the manner in which the chord goes to zero at the tip of the wing. First of all the data presented in figures A.3 through A.10 imply that the chord may be assumed to have a constant value if the first collocation point is a minimum of 0.1 radians from the tip of the wing for all values of eccentricity. The Fourier coefficients that were obtained in this manner were then used to calculate the downwash at points between the wing tip and the first collocation point. These values of downwash were used to calculate a value for the distribution of the chord, c', that would satisfy equation 3.24 for the special case of a semi-circular channel. This is course an approximation since none of these values for the chord were in fact used to calculate the original values of the Fourier coefficients.

The second approach involves assuming a chord distribution from the wing tip (ϕ=0) to a value of ϕ=0.1 radians. Equation A.27

implies that the chord must go to zero as fast or faster than $1/\ell n\ \phi$ where ϕ is the angular displacement from the tip of the wing. Arbitrarily a chord distribution where

$$\frac{c'}{c} = \sin^2 \frac{\pi\phi}{2\beta} \tag{A.28}$$

was chosen for the span between the wing tip and the station where ϕ=0.1 radians. The remainder of the semi-span has a constant value for the chord, c. A comparison between this distribution and the one calculated using the lifting line theory is shown in figure A.12.

A further check on the method of assuming a chord distribution as described in equation A.28 was made by recomputing the Fourier coefficients by locating one of the collocation points at a point where ϕ/β=0.5. The value of the angle, β, was again chosen to be 0.1 radians. The Fourier coefficients and the resulting circulation distribution did not show any appreciable change from those values determined by having all collocation points at an angular displacement equal to or greater than o.1 radians. One may then conclude that either the assumed chord distribution is correct or that the contribution from the tip section is negligible and may be neglected. The latter explanation is more physically appealing and it is this method by which the final data will be collected. To further substantiate this reasoning the Fourier coefficients were again calculated but

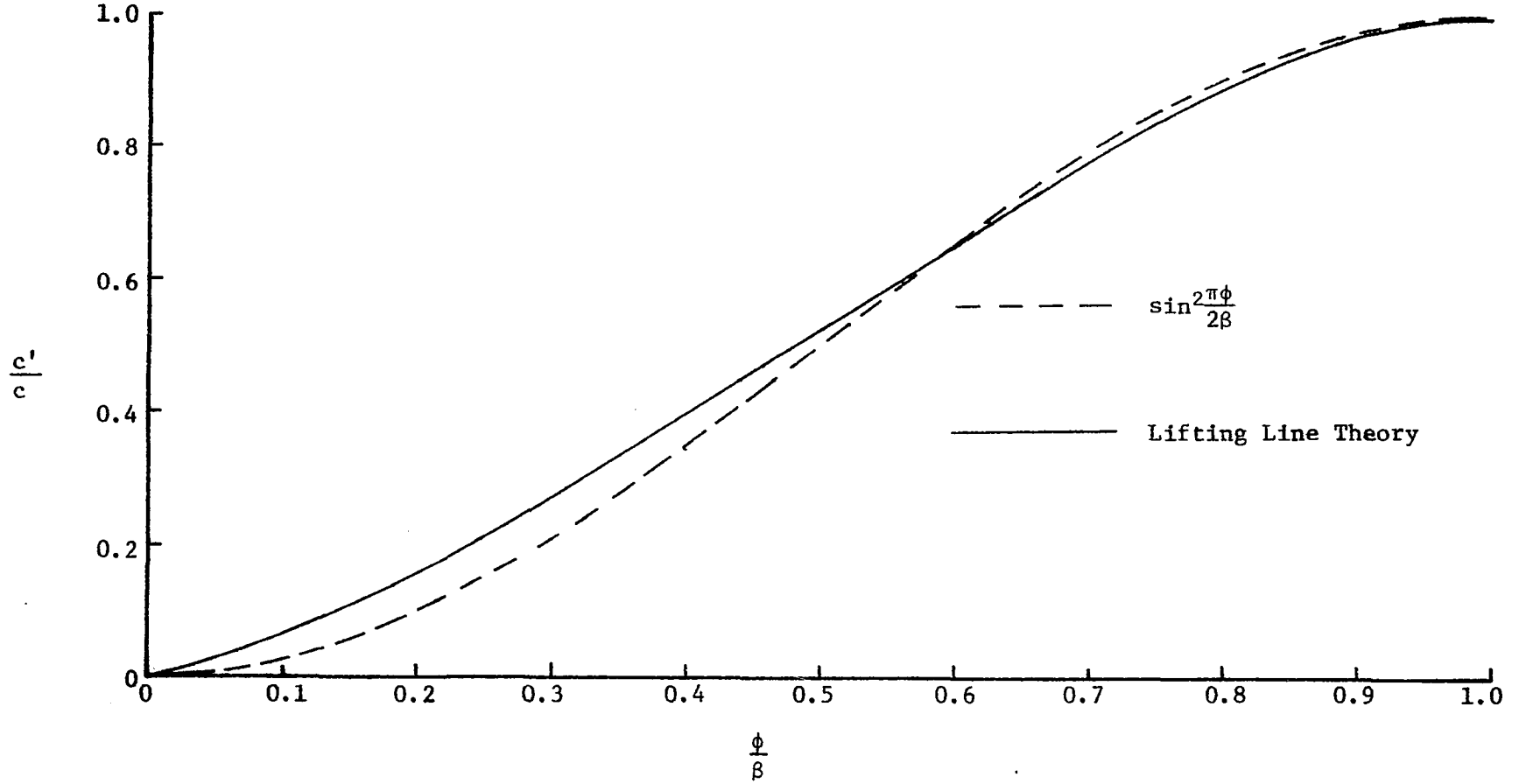

Figure A.12 Chord Distribution Near The Tip of the Wing

this time the rate of change of the circulation distribution was multiplied by a factor equal to

$$\sin^2 \frac{\pi\phi}{2\beta}$$

where again β was chosen to be 0.1 radians. One of the collocation points was again chosen to be at a point where $\phi/\beta=0.5$. The resulting data again showed no appreciable change.

Prior to concluding the discussion on the effect of the wing tip upon the wing it is convenient to again refer to the radius of curvature at the tip of the wing. To assume that the approach taken in equation A.22 is valid, the assumption is made that δ is much smaller than ξ, where ξ is of the order one in this expression. If ρ, the radius of curvature, becomes of the same order of magnitude as c then equation A.22 is no longer valid and therefore elliptical shapes with an eccentricity which permits the ratio c/ρ to become greater than say 0.1 should theoretically be excluded from this study. However, the effect of the small radius of curvature at the tip is localized and does not have an overall appreciable effect upon the results. Acceptable data has been obtained for values of c/ρ much greater than 0.1.

The final conclusion from this analysis is that the ideas associated with lifting line theory are applicable to non-planar surfaces. As in planar lifting line theory, the chord

distribution does play an important role in determining the validity of using a Fourier series for the circulation distribution. However, acceptable results are obtained for a non-planar wing having a constant chord if one is careful in the selection of the collocation points.

APPENDIX B

Circular Channels (e = 0)

In restricting equation 3.15 to the special case of a circular channel the algebraic expressions become greatly simplified.

Since

$$b=a \quad \text{i.e.} \quad K=1$$

it is found that

$$Q(\eta) = \frac{\sin(\phi-\eta)}{2\left[1-\cos(\phi-\eta)\right]}$$

and

$$\alpha_i(\phi) = \frac{1}{8\pi}\sum nB_n \oint_0^{\pi} \frac{\sin(\phi-\eta)\cos n\eta}{1-\cos(\phi-\eta)}\, d\eta$$

the integrand being singular in the limit as η approaches ϕ. A trigonometric identity allows the previous integral to be rewritten as

$$\alpha_i(\phi) = \frac{1}{8\pi}\sum nB_n \oint_0^{\pi} \cot\left(\frac{\phi-\eta}{2}\right)\cos n\eta\, d\eta$$

The evaluation of the singular integral is accomplished as follows.

$$\int_0^{\pi} \cot\left(\frac{\phi-\eta}{2}\right) \cos n\eta \, d\eta = \int_0^{\pi} \left[\cot\left(\frac{\phi-\eta}{2}\right) + \cot\left(\frac{\phi+\eta}{2}\right)\right] \cos n\eta \, d\eta$$

$$- \int_0^{\pi} \cot\left(\frac{\phi+\eta}{2}\right) \cos n\eta \, d\eta$$

Since it can be shown that

$$\int_0^{\pi} \cot\left(\frac{\phi-\eta}{2}\right) \cos n\eta \, d\eta = \int_{-\pi}^{0} \cot\left(\frac{\phi+\eta}{2}\right) \cos n\eta \, d\eta$$

it follows that

$$\int_0^{\pi} \cot\left(\frac{\phi-\eta}{2}\right) \cos n\eta \, d\eta = \int_{-\pi}^{\pi} \cot\left(\frac{\phi+\eta}{2}\right) \cos n\eta \, d\eta$$

$$- \int_0^{\pi} \cot\left(\frac{\phi+\eta}{2}\right) \cos n\eta \, d\eta$$

In evaluating the first integral on the right hand side of the previous equation it is necessary to make the following substitution.

Let

$$\lambda = \phi + \eta$$

therefore

$$\int_{-\pi}^{\pi} \cot\left(\frac{\phi+\eta}{2}\right) \cos n\eta \, d\eta = \int_{\phi-\pi}^{\phi+\pi} \cot\frac{\lambda}{2} \cos n(\lambda-\phi) \, d\lambda$$

$$= \cos n\phi \int_{\phi-\pi}^{\phi+\pi} \cot\frac{\lambda}{2} \cos n\lambda \, d\lambda + \sin n\phi \int_{\phi-\pi}^{\phi+\pi} \cot\frac{\lambda}{2} \sin n\lambda \, d\lambda$$

Since the integrand is an odd function for all values of n

$$\int_{\phi-\pi}^{\phi+\pi} \cot\frac{\lambda}{2} \cos n\lambda \, d\lambda = 0$$

and it follows that

$$\int_{-\pi}^{\pi} \cot\left(\frac{\phi+\eta}{2}\right) \cos n\eta \, d\eta = \sin n\phi \int_{\phi-\pi}^{\phi+\pi} \cot\frac{\lambda}{2} \sin n\lambda \, d\lambda$$

Now let

$$J_n = \int_{\phi-\pi}^{\phi+\pi} \cot\frac{\lambda}{2} \sin n\lambda \, d\lambda$$

and therefore

$$J_n - J_{n-1} = \int_{\phi-\pi}^{\phi+\pi} \cot\frac{\lambda}{2} \left[\sin n\lambda - \sin(n-1)\lambda\right] d\lambda$$

Upon evaluation it is found that

$$J_n - J_{n-1} = 0$$

and therefore

$$J_n = J_1 = 2\pi$$

which gives

$$\int_{-\pi}^{\pi} \cot\left(\frac{\phi+\eta}{2}\right) \cos n\eta \, d\eta = 2\pi \sin n\phi$$

The expression for the induced angle of attack is now

$$\alpha_i(\phi) = \frac{1}{8\pi} \sum nB_n \left[2\pi \sin n\phi - \int_0^{\pi} \cot\left(\frac{\phi+\eta}{2}\right) \cos n\eta \, d\eta \right]$$

In the remaining integral let

$$\lambda = \phi + \eta$$

and therefore

$$\int_0^{\pi} \cot\left(\frac{\phi+\eta}{2}\right) \cos n\eta \, d\eta = \cos n\phi \int_{\phi}^{\phi+\pi} \cot\frac{\lambda}{2} \cos n\lambda \, d\lambda + \sin n\phi \int_{\phi}^{\phi+\pi} \cot\frac{\lambda}{2} \sin n\lambda \, d\lambda$$

Now let

$$H_n = \int_{\phi}^{\phi+\pi} \cot \frac{\lambda}{2} \sin n\lambda \, d\lambda$$

and therefore

$$H_n - H_{n-1} = \int_{\phi}^{\phi+\pi} \cot \frac{\lambda}{2} \left[\sin n\lambda - \sin(n-1)\lambda \right] d\lambda$$

Upon evaluation of this integral it is found that

$$H_n - H_{n-1} = \frac{1}{n} \left[(-1)^n - 1 \right] \sin n\phi + \frac{1}{n-1} \left[1+(-1)^n \right] \left[\sin \phi \cos n\phi - \cos \phi \sin n\phi \right]$$

and

$$H_1 = \pi - 2 \sin \phi$$

Now let

$$I_n = \int_{\phi}^{\phi+\pi} \cot \frac{\lambda}{2} \cos n\lambda \, d\lambda \qquad (0 \leq \phi < \pi)$$

and evaluate as before finding that

$$I_n - I_{n-1} = \frac{1}{n}\left[(-1)^n - 1\right] \cos n\phi -$$

$$\frac{1}{n-1}\left[1+(-1)^n\right]\left[\cos\phi \cos n\phi + \sin\phi \sin n\phi\right]$$

where

$$I_1 = \ln\left[\frac{1 + \cos\phi}{1 - \cos\phi}\right] - 2\cos\phi$$

The final expression for the induced angle of attack is

$$\alpha_i(\phi) = \frac{1}{8\pi} \sum nB_n \left[2\pi \sin n\phi - I_n \cos n\phi - H_n \sin n\phi\right]$$

where the coefficients H_n and I_n are determined by the previously described recurrence relationships.

APPENDIX C

Convergence of $\oint_0^{\pi} Q(\eta)\, d\eta$

Equation 3.21 is usually evaluated in the following format.

$$\oint_0^{\pi} Q(\eta)\, d\eta = \lim_{\varepsilon \to 0} \left[\int_0^{\phi-\varepsilon} Q(\eta)\, d\eta + \int_{\phi-\varepsilon}^{\phi+\varepsilon} Q(\eta)\, d\eta + \int_{\phi+\varepsilon}^{\pi} Q(\eta)\, d\eta \right]$$

In the limit

$$\lim_{\varepsilon \to 0} \int_{\phi-\varepsilon}^{\phi+\varepsilon} Q(\eta)\, d\eta = 0$$

but for machine integrations it becomes necessary to investigate how this integral converges to zero for small values of ε.

Let

$$\lambda = \eta - \phi$$

and therefore

$$\oint_{\phi-\varepsilon}^{\phi+\varepsilon} Q(\eta)\, d\eta = \oint_{-\varepsilon}^{\varepsilon} Q(\lambda)\, d\lambda$$

Remembering that

$$Q(\eta) = \frac{MN^4 \sin(\phi-\eta) + \left[MN^2 \cos(\phi-\eta) - M^2N\right] \sin\phi \cos\phi \quad (K^2-1)}{M^2 + N^2 - 2MN \cos(\phi-\eta)}$$

where

$$M = (K^2 \sin^2\eta + \cos^2\eta)^{1/2}$$

and

$$N = (K^2 \sin^2\phi + \cos^2\phi)^{1/2}$$

Rewriting these expressions in the new variable λ gives

$$Q(\lambda) = \frac{-MN^4\sin\lambda + \left[MN^2\cos\lambda - M^2N\right] \sin\phi \cos\phi (K^2-1)}{M^2 + N^2 - 2MN \cos\lambda}$$

where

$$M = \left[K^2\sin^2(\lambda+\phi) + \cos^2(\lambda+\phi)\right]^{1/2}$$

Expanding M and powers of M in a Taylor series gives

$$M = \left[1 + \lambda \frac{(K^2-1)\sin\phi\cos\phi}{N^2} + \lambda^2 \left[\frac{(K^2-1)(\cos^2\phi-\sin^2\phi)}{2N^2} - \frac{(K^2-1)^2\sin^2\phi\cos^2\phi}{2N^4}\right] + \cdots\right] N$$

and

$$M^2 = \left[1 + \lambda \frac{2(K^2-1)\sin\phi\cos\phi}{N^2} + \lambda^2 \left[\frac{(K^2-1)(\cos^2\phi-\sin^2\phi)}{N^2}\right] + \cdots\right] N^2$$

Substituting these values into the expression for Q and remembering that

$$\sin \lambda = \lambda + O(\lambda^3)$$

and

$$\cos \lambda = 1 - \frac{\lambda^2}{2} + O(\lambda^4)$$

gives

$$Q(\lambda) = \frac{-N^3 \left[N^4+(K^2-1)^2\sin^2\phi\cos^2\phi\right]}{(K^2-1)^2\sin^2\phi\cos^2\phi + N^4} - \left\{\frac{N \sin\phi \cos\phi (K^2-1)}{2\left[(K^2-1)^2\sin^2\phi\cos^2\phi + N^4\right]}\right\}$$

$$\left\{3N^4 + N^2(K^2-1)(\cos^2\phi - \sin^2\phi)+(K^2-1)^2\sin^2\phi\cos^2\phi\right.$$

Integrating over the given limits gives

$$E(\phi) = \int_{-\varepsilon}^{\varepsilon} Q(\lambda)\, d\lambda = -\left[\frac{N\sin\phi \cos\phi (K^2-1)}{(K^2-1)^2\sin^2\phi\cos^2\phi + N^4}\right]$$

$$\left[3N^4 + N^2(K^2-1)(\cos^2\phi-\sin^2\phi) + (K^2-1)^2\sin^2\phi\cos^2\phi\right]\varepsilon$$

a correction term which renders equation 3.22 valid to within an order ε.

APPENDIX D

Computer Program

The computer program used in calculating the Fourier coefficients is a combination of integration schemes and a routine for solving a system of linear non-homogeneous equations.

Since the integration scheme is required to evaluate the Cauchy principle value of singular integrals, special care must be exercised. A distance of $\pm$ .001 radians was excluded around the singular point and from this limit to $\pm$ .1 radians a 32-point Gaussian quadrature method was used (DQG32). This method was chosen because of the steep slope of the function in this area. Outside of these limits a straight forward use of the trapezoidal rule (DQATR) was used. In using the trapezoidal rule, the step size must be small enough so that the oscillatory nature of the function is smoothed out and the value of the integral converges.

All variables within the program are denoted by using comment cards.

```
C     ENTIRE PROGRAM IS WRITTEN IN FORTRAN AND MAY BE MODIFIED TO
C     CHANGE THE GEOMETRIC PROPERTIES OF THE WING.
C
      IMPLICIT REAL*8(A-H,O-Z),INTEGER*4(I-N)
      EXTERNAL FCT
      EXTERNAL FNF
      DIMENSION BR(9,9),BC1(9),BC(9,9),BP(9,9),V(9)
      DIMENSION AX1(50),AX2(50),AX3(50)
      COMMON RK,PHI,RN,QN
      EPT=0.10
C     EPT IS THE ANGULAR DISPLACEMENT MEASURED IN RADIANS FROM THE
C     TIP OF THE WING TO THE FIRST COLLOCATION POINT
      NCOL=9
C     NCOL IS THE NUMBER OF COLLOCATION POINTS USED
      COL=NCOL-1
      FLIM=0.001
C     FLIM IS THE INTEGRATION TOLERANCE USED IN THE DQATR SUBROUTINE
      NDI=100
      PI=3.141592654
      DELT=(PI/2.-EPT)/COL
      DO 800 NE=1,9,2
      QNE=NE-1
      B99=1.0-0.1*QNE
      E=DSQRT(1.-B99**2)
C     E IS THE ECCENTRICITY OF THE ELLIPTICAL SHAPED WING
      B=1.0
C     B IS THE SEMI-SPAN OF THE WING
      A=B*B99
C     A IS THE DEPTH OF THE WING
```

```
      RK=B/A
  104 FORMAT(1H1)
      WRITE(6,104)
      DO 1 M=1,NCOL
      QM=M-1
      PHI=EPT+QM*DELT
      RN=DSQRT((RK**2)*((DSIN(PHI))**2)+(DCOS(PHI))**2)
      NCOB=2*NCOL-1
      DO 1 N=1,NCOB,2
      K=(N+1)/2
      QN=N
      S=0.0
      CALL DQATR(S,PI,FLIM,NDI,FCT,S1,IER,AX1)
      BR(M,K)=S1
  101 FORMAT(3X,I4,3X,I4,3X,I4,3X,E17.8)
    1 WRITE(6,101)IER,M,N,S1
      WRITE(6,104)
      DO 2 M=1,NCOL
      QM=M-1
      PHI=EPT+QM*DELT
      RN=DSQRT((RK**2)*((DSIN(PHI))**2)+(DCOS(PHI))**2)
      IF(PHI-0.1)50,50,51
   50 XL=0.0
      XU=PHI-.001
      CALL DQG32(XL,XU,FNF,S2)
      GO TO 52
   51 XL=0.0
      XU=PHI-0.1
      CALL DQATR(XL,XU,FLIM,NDI,FNF,S21,IER,AX2)
      XL=PHI-0.1
```

```
      XU=PHI-0.001
      CALL DQG32(XL,XU,FNF,S22)
   52 XL=PHI+0.001
      XU=PHI+0.1
      CALL DQG32(XL,XU,FNF,S31)
      XL=PHI+0.1
      XU=PI
      CALL DQATR(XL,XU,FLIM,NDI,FNF,S32,IER,AX3)
      ERR=(.001*(RK**2-1.)*DSIN(PHI)*DCOS(PHI)*RN**5*(3.0+(RK**2-1.)*
     1((DCOS(PHI))**2-(DSIN(PHI))**2)/(2.*RN**2)+((RK**2-1.)**2)*(DSIN(
     2PHI))**2*(DCOS(PHI))**2/(2.*RN**4)))/(RN**4+(RK**2-1.)**2*(DSIN(
     3PHI))**2*(DCOS(PHI))**2)
      IF(PHI-0.1)60,60,61
   60 BC1(M)=S2+S31+S32-ERR
  102 FORMAT(3X,4E17.8)
      WRITE(6,102)S2,S31,S32,ERR
      GO TO 2
   61 BC1(M)=S21+S22+S31+S32-ERR
  900 FORMAT(3X,5E17.8)
      WRITE(6,900)S21,S22,S31,S32,ERR
    2 CONTINUE
      DO 3 M=1,NCOL
      QM=M-1
      PHI=EPT+QM*DELT
      RMP=DSQRT((RK**4)*((DSIN(PHI))**2)+(DCOS(PHI))**2)
      DO 3 N=1,NCOB,2
      K=(N+1)/2
      QN=N
    3 BC(M,K)=(QN/(4.*PI*RMP))*(BR(M,K)+(DCOS(QN*PHI))*BC1(M))
```

```
  103 FORMAT(2X,6E17.8)
      WRITE(6,104)
      WRITE(6,103)((BC(M,N),N=1,NCOL),M=1,NCOL)
      AO=2.*PI
C     AO IS THE SLOPE OF THE LIFT CURVE (DCL/D ALPHA)
      C=0.1
C     C IS THE CHORD OF THE WING
      ALZ=0.0
C     ALZ IS ANGLE OF ZERO LIFT MEASURED IN DEGREES
      ALO=PI*ALZ/180.
      AZ=6.0
C     AZ IS THE ANGLE OF ATTACK OF THE CENTER SECTION OF THE WING
      DO 400 K9=1,2
      AL=PI*AZ/180.
      DO 4 M=1,NCOL
      QM=M-1
      PHI=EPT+QM*DELT
      ARG=RK**2*DSIN(AL)*DSIN(PHI)/(DCOS(AL)*DSQRT(RK**4*(DSIN(PHI))**2
     1+(DCOS(PHI))**2))
      DO 5 N=1,NCOB,2
      K=(N+1)/2
      QN=N
    5 BP(M,K)=DSIN(QN*PHI)+AO*C*BC(M,K)/(2.*B)
    4 V(M)=AO*C*(DATAN(ARG)-ALO)/(2.*B)
      WRITE(6,104)
      WRITE(6,103)((BP(M,N),N=1,NCOL),M=1,NCOL)
      WRITE(6,104)
      WRITE(6,103)(V(M),M=1,NCOL)
      CALL DIMQ(BP,V,NCOL,KS)
```

```
110 FORMAT(1H1,3X,23HSEMI-SPAN OF CHANNEL = ,F6.2,4X,
   119HDEPTH OF CHANNEL = ,F6.2,//,4X,15HECCENTRICITY = ,F10.8,
   27X,19HLIFT CURVE SLOPE = ,F10.6,//,4X,8HCHORD = ,F8.4,10X,
   321HANGLE OF ZERO LIFT = ,F8.4,//,4X,18HANGLE OF ATTACK = ,F8.4,
   4///)
111 FORMAT(4X,45HTHE FOURIER COEFFICIENTS FOR CIRCULATION ARE:,/)
    WRITE(6,110)B,A,E,AO,C,ALZ,AZ
    WRITE(6,111)
    WRITE(6,103)(V(M),M=1,NCOL)
    WRITE(6,104)
    GAMP=0.0
    DO 350 IX=1,NCOL
    QIX=IX
350 GAMP=GAMP+V(IX)*DSIN((2.*QIX-1.)*PI/2.)
    DO 300 IQ=1,51
    RIQ=IQ-1
    PHI=RIQ*PI/100.
    RAD=A*B/DSQRT((B*DSIN(PHI))**2+(A*DCOS(PHI))**2)
    SPAN=B-RAD*DCOS(PHI)
    GAM=0.0
    DO 799 M=1,NCOL
    QM=M
799 GAM=GAM+V(M)*DSIN((2.*QM-1.)*PHI)
    GAMR=GAM/GAMP
    WRITE(6,105)PHI,GAM,GAMR,SPAN
105 FORMAT(3X,4E17.8)
300 CONTINUE
400 AZ=-6.0
800 CONTINUE
    CALL EXIT
    END
```

```
      FUNCTION FNF(BETA)
      IMPLICIT REAL*8(A-H,O-Z),INTEGER*4(I-N)
      COMMON RK,PHI,RN
      RM=DSQRT((RK**2)*((DSIN(BETA))**2)+(DCOS(BETA))**2)
      FNF=(RM*RN**4*DSIN(PHI-BETA)+(RK**2-1.)*(RM*RN**2*DCOS(PHI-BETA)-
     1RN*RM**2)*DSIN(PHI)*DCOS(PHI))/(RM**2+RN**2-2.*RM*RN*DCOS(PHI-
     2BETA))
      RETURN
      END
```

```
      FUNCTION FCT(BETA)
      IMPLICIT REAL*8(A-H,O-Z),INTEGER*4(I-N)
      COMMON RK,PHI,RN,QN
      RM=DSQRT((RK**2)*((DSIN(BETA))**2)+(DCOS(BETA))**2)
      IF(PHI-BETA)200,201,200
  201 FCT=QN*DSIN(QN*BETA)*RN**3*(RN**4-((RK**2-1.)*DSIN(BETA)
     1*DCOS(BETA))**2)/(((RK**2-1.)**2)*((DSIN(BETA)*DCOS(BETA))**2)
     2+RN**4)
      RETURN
  200 FCT=(RM*RN**4*DSIN(PHI-BETA)+(RM*RN**2*DCOS(PHI-BETA)-RM**2*RN)*
     1DSIN(PHI)*DCOS(PHI)*(RK**2-1.))*(DCOS(QN*BETA)-DCOS(QN*PHI))/
     2(RM**2+RN**2-2.*RM*RN*DCOS(PHI-BETA))
      RETURN
      END
```

```
C
C     ..................................................................
C
C     SUBROUTINE DQATR
C
C
C     PURPOSE
C        TO COMPUTE AN APPROXIMATION FOR INTEGRAL(FCT(X), SUMMED
C        OVER X FROM XL TO XU).
C
C     USAGE
C        CALL DQATR (XL,XU,EPS,NDIM,FCT,Y,IER,AUX)
C        PARAMETER FCT REQUIRES AN EXTERNAL STATEMENT.
C
C     DESCRIPTION OF PARAMETERS
C        XL     - DOUBLE PRECISION LOWER BOUND OF THE INTERVAL.
C        XU     - DOUBLE PRECISION UPPER BOUND OF THE INTERVAL.
C        EPS    - SINGLE PRECISION UPPER BOUND OF THE ABSOLUTE ERROR.
C        NDIM   - THE DIMENSION OF THE AUXILIARY STORAGE ARRAY AUX.
C                 NDIM-1 IS THE MAXIMAL NUMBER OF BISECTIONS OF
C                 THE INTERVAL (XL,XU).
C        FCT    - THE NAME OF THE EXTERNAL DOUBLE PRECISION FUNCTION
C                 SUBPROGRAM USED.
C        Y      - RESULTING DOUBLE PRECISION APPROXIMATION FOR THE
C                 INTEGRAL VALUE.
C        IER    - A RESULTING ERROR PARAMETER.
C        AUX    - AUXILIARY DOUBLE PRECISION STORAGE ARRAY WITH
C                 DIMENSION NDIM.
C
C     REMARKS
C        ERROR PARAMETER IER IS CODED IN THE FOLLOWING FORM
C        IER=0  - IT WAS POSSIBLE TO REACH THE REQUIRED ACCURACY.
```

```
C                NO ERROR.
C        IER=1  - IT IS IMPOSSIBLE TO REACH THE REQUIRED ACCURACY
C                 BECAUSE OF ROUNDING ERRORS.
C        IER=2  - IT WAS IMPOSSIBLE TO CHECK ACCURACY BECAUSE NDIM
C                 IS LESS THAN 8, OR THE REQUIRED ACCURACY COULD NOT
C                 BE REACHED WITHIN NDIM-1 STEPS, NDIM SHOULD BE
C                 INCREASED.
C
C     SUBROUTINES AND FUNCTION SUBPROGRAMS REQUIRED
C        THE EXTERNAL DOUBLE PRECISION FUNCTION SUBPROGRAM FCT(X)
C        MUST BE CODED BY THE USER.  ITS DOUBLE PRECISION ARGUMENT X
C        SHOULD NOT BE DESTROYED.
C
C     METHOD
C        EVALUATION OF Y IS DONE BY MEANS OF TRAPEZOIDAL RULE IN
C        CONNECTION WITH ROMBERGS PRINCIPLE.  ON RETURN Y CONTAINS
C        THE BEST POSSIBLE APPROXIMATION OF THE INTEGRAL VALUE AND
C        VECTOR AUX THE UPWARD DIAGONAL OF ROMBERG SCHEME.
C        COMPONENTS AUX(I) (I=1,2,...,IEND, WITH IEND LESS THAN OR
C        EQUAL TO NDIM) BECOME APPROXIMATIONS TO INTEGRAL VALUE WITH
C        DECREASING ACCURACY BY MULTIPLICATION WITH (XU-XL).
C        FOR REFERENCE, SEE
C        (1) FILIPPI, DAS VERFAHREN VON ROMBERG-STIEFEL-BAUER ALS
C            SPEZIALFALL DES ALLGEMEINEN PRINZIPS VON RICHARDSON,
C            MATHEMATIK-TECHNIK-WIRTSCHAFT, VOL.11, ISS.2 (1964),
C            PP,49-54.
C        (2) BAUER, ALGORITHM 60, CACM, VOL.4, ISS.6 (1961), PP,255.
C
C     ..................................................................
C
```

```
      SUBROUTINE DQATR(XL,XU,EPS,NDIM,FCT,Y,IER,AUX)
C
C
      DIMENSION AUX(1)
      DOUBLE PRECISION AUX,XL,XU,X,Y,H,HH,HD,P,Q,SM,FCT,EPS
C
C     PREPARATIONS OF ROMBERG-LOOP
      AUX(1)=.5D0*(FCT(XL)+FCT(XU))
      H=XU-XL
      IF(NDIM-1)8,8,1
    1 IF(H)2,10,2
C
C     NDIM IS GREATER THAN 1 AND H IS NOT EQUAL TO 0.
    2 HH=H
      E=EPS/DABS(H)
      DELT2=0.
      P=1.D0
      JJ=1
      DO 7 I=2,NDIM
      Y=AUX(1)
      DELT1=DELT2
      HD=HH
      HH=.5D0*HH
      P=.5D0*P
      X=XL+HH
      SM=0.D0
      DO 3 J=1,JJ
      SM=SM+FCT(X)
    3 X=X+HD
      AUX(I)=.5D0*AUX(I-1)+P+SM
```

```
C     A NEW APPROXIMATION OF INTEGRAL VALUE IS COMPUTED BY MEANS OF
C     TRAPEZOIDAL RULE.
C
C     START OF ROMBERGS EXTRAPOLATION METHOD.
      Q=1.D0
      JI=I-1
      DO 4 J=1,JI
      II=I-J
      Q=Q+Q
      Q=Q+Q
    4 AUX(II)=AUX(II+1)+(AUX(II+1)-AUX(II))/(Q-1.D0)
C     END OF ROMBERG-STEP
C
      DELT2=DABS(Y-AUX(1))
      IF(I-8)7,5,5
    5 IF(DELT2-E)10,10,6
    6 IF(DELT2-DELT1)7,11,11
    7 JJ=JJ+JJ
    8 IER=2
    9 Y=H*AUX(1)
      RETURN
   10 IER=0
      GO TO 9
   11 IER=1
      Y=H*Y
      RETURN
      END
```

```
C
C     ..................................................................
C
C        SUBROUTINE DIMQ
C
C        PURPOSE
C           OBTAIN SOLUTION OF A SET OF SIMULTANEOUS LINEAR EQUATIONS.
C           AX=B
C
C        USAGE
C           CALL DIMQ(A,B,N,KS)
C
C        DESCRIPTION OF PARAMETERS
C           A - MATRIX OF COEFFICIENTS STORED COLUMNWISE.  THESE ARE
C               DESTROYED IN THE COMPUTATION.  THE SIZE OF MATRIX A IS
C               N BY N.
C           B - VECTOR OF ORIGINAL CONSTANTS (LENGTH N), THESE ARE
C               REPLACED BY FINAL SOLUTION VALUES, VECTOR X.
C           N - NUMBER OF EQUATIONS AND VARIABLES.  N MUST BE .GT. ONE.
C           KS - OUTPUT DIGIT
C                0 FOR A NORMAL SOLUTION
C                1 FOR A SINGULAR SET OF EQUATIONS
C
C        REMARKS
C           MATRIX A MUST BE GENERAL.
C           IF MATRIX IS SINGULAR, SOLUTION VALUES ARE MEANINGLESS.
C           AN ALTERNATIVE SOLUTION MAY BE OBTAINED BY USING MATRIX
C           INVERSION (MINV) AMD MATRIX PRODUCT (GMPRD).
C
```

```
C        SUBROUTINES AND FUNCTION SUBPROGRAMS REQUIRED
C           NONE
C
C        METHOD
C           METHOD OF SOLUTION IS BY ELIMINATION USING LARGEST PIVOTAL
C           DIVISOR. EACH STAGE OF ELIMINATION CONSISTS OF INTERCHANGING
C           ROWS WHEN NECESSARY TO AVOID DIVISION BY ZERO OR SMALL
C           ELEMENTS.
C           THE FORWARD SOLUTION TO OBTAIN VARIABLE N IS DONE IN
C           N STAGES. THE BACK SOLUTION FOR THE OTHER VARIABLES IS
C           CALCULATED BY SUCCESSIVE SUBSTITUTIONS. FINAL SOLUTION
C           VALUES ARE DEVELOPED IN VECTOR B, WITH VARIABLE 1 IN B(1),
C           VARIABLE 2 IN B(2).....VARIABLE N IN B(N).
C           IF NO PIVOT CAN BE FOUND EXCEEDING A TOLERANCE OF 0.0,
C           THE MATRIX IS CONSIDERED SINGULAR AND KS IS SET TO 1. THIS
C           TOLERANCE CAN BE MODIFIED BY REPLACING THE FIRST STATEMENT.
C
C     .....................................................................
C
      SUBROUTINE DIMQ(A,B,N,KS)
      IMPLICIT REAL*8(A-H,O-Z),INTEGER*4(I-N)
      DIMENSION A(1),B(1)
C
C     FORWARD SOLUTION
C
      TOL=0.0
      KS=0
      JJ=-N
      DO 65 J=1,N
      JY=J+1
      JJ=JJ+N+1
```

```
      BIGA=0
      IT=JJ-J
      DO 30 I=J,N
C
C     SEARCH FOR MAXIMUM COEFFICIENT IN COLUMN
C
      IJ=IT+I
      IF(DABS(BIGA)-DABS(A(IJ))) 20,30,30
   20 BIGA=A(IJ)
      IMAX=I
   30 CONTINUE
C
C     TEST FOR PIVOT LESS THAN TOLERANCE (SINGULAR MATRIX)
C
      IF(DABS(BIGA)-TOL) 35,35,40
   35 KS=1
      RETURN
C
C     INTERCHANGE ROWS IF NECESSARY
C
   40 I1=J+N*(J-2)
      IT=IMAX-J
      DO 50 K=J,N
      I1=I1+N
      I2=I1+IT
      SAVE=A(I1)
      A(I1)=A(I2)
      A(I2)=SAVE
C
C     DIVIDE EQUATION BY LEADING COEFFICIENT
C
```

```
   50 A(I1)=A(I1)/BIGA
      SAVE=B(IMAX)
      B(IMAX)=B(J)
      B(J)=SAVE/BIGA
C
C     ELIMINATE NEXT VARIABLE
C
      IF(J-N) 55,70,55
   55 IQS=N*(J-1)
      DO 65 IX=JY,N
      IXJ=IQS+IX
      IT=J-IX
      DO 60 JX=JY,N
      IXJX=N*(JX-1)+IX
      JJX=IXJX+IT
   60 A(IXJX)=A(IXJX)-(A(IXJ)*A(JJX))
   65 B(IX)=B(IX)-(B(J)*A(IXJ))
C
C     BACK SOLUTION
C
   70 NY=N-1
      IT=N*N
      DO 80 J=1,NY
      IA=IT-J
      IB=N-J
      IC=N
      DO 80 K=1,J
      B(IB)=B(IB)-A(IA)*B(IC)
      IA=IA-N
   80 IC=IC-1
      RETURN
      END
```

```
C
C     ..................................................................
C
C        SUBROUTINE DQG32
C
C        PURPOSE
C           TO COMPUTE INTEGRAL(FCT(X), SUMMED OVER X FROM XL TO XU)
C
C        USAGE
C           CALL DQG32 (XL,XU,FCT,Y)
C           PARAMETER FCT REQUIRES AN EXTERNAL STATEMENT
C
C        DESCRIPTION OF PARAMETERS
C           XL      - DOUBLE PRECISION LOWER BOUND OF THE INTERVAL.
C           XU      - DOUBLE PRECISION UPPER BOUND OF THE INTERVAL.
C           FCT     - THE NAME OF AN EXTERNAL DOUBLE PRECISION FUNCTION
C                     SUBPROGRAM USED.
C           Y       - THE RESULTING DOUBLE PRECISION INTEGRAL VALUE.
C
C        REMARKS
C           NONE
C
C        SUBROUTINES AND FUNCTION SUBPROGRAMS REQUIRED
C           THE EXTERNAL DOUBLE PRECISION FUNCTION SUBPROGRAM FCT(X)
C           MUST BE FURNISHED BY THE USER.
C
C        METHOD
C           EVALUATION IS DONE BY MEANS OF 32-POINT GAUSS QUADRATURE
C           FORMULA, WHICH INTEGRATES POLYNOMIALS UP TO DEGREE 63
C           EXACTLY. FOR REFERENCE, SEE
```

```
C           V.I.KRYLOV, APPROXIMATE CALCULATION OF INTEGRALS,
C           MACMILLAN, NEW YORK/LONDON, 1962, PP,100-111 AND 337-340.
C
C     ..................................................................
C
      SUBROUTINE DQG32(XL,XU,FCT,Y)
C
C
      DOUBLE PRECISION XL,XU,Y,A,B,C,FCT
C
      A=.5D0*(XU+XL)
      B=XU-XL
      C=.4986319309247407 8D0*B
      Y=.3509305004735048 3D-2*(FCT(A+C)+FCT(A-C))
      C=.4928057557726341 7D0*B
      Y=Y+.8137197365452835D-2*(FCT(A+C)+FCT(A-C))
      C=.4823811277937532 2D0*B
      Y=Y+.1269603265463103 0D-1*(FCT(A+C)+FCT(A-C))
      C=.4674530379688698 4D0*B
      Y=Y+.1713693145651071 7D-1*(FCT(A+C)+FCT(A-C))
      C=.4481605778830260 6D0*B
      Y=Y+.2141794901111334 0D-1*(FCT(A+C)+FCT(A-C))
      C=.4246838068662849 9D0*B
      Y=Y+.2549902963118808 8D-1*(FCT(A+C)+FCT(A-C))
      C=.3972418979839712 0D0*B
      Y=Y+.2934204673926777 4D-1*(FCT(A+C)+FCT(A-C))
      C=.3660910593701448 4D0*B
      Y=Y+.3291111138818092 3D-1*(FCT(A+C)+FCT(A-C))
      C=.3315221334651076 0D0*B
      Y=Y+.3617289705442425 3D-1*(FCT(A+C)+FCT(A-C))
```

```
C=.29385787862038116D0*B
Y=Y+.39096947893535153D-1*(FCT(A+C)+FCT(A-C))
C=.25344995446611470D0*B
Y=Y+.41655962113473378D-1*(FCT(A+C)+FCT(A-C))
C=.21067563806531767D0*B
Y=Y+.43826046502201906D-1*(FCT(A+C)+FCT(A-C))
C=.16593430114106382D0*B
Y=Y+.45586939347881942D-1*(FCT(A+C)+FCT(A-C))
C=.11964368112606854D0*B
Y=Y+.46922199540402283D-1*(FCT(A+C)+FCT(A-C))
C=.7223598079139825D-1*B
Y=Y+.47819360039637430D-1*(FCT(A+C)+FCT(A-C))
C=.24153832843869158D-1*B
Y=B*(Y+.48270044257363900D-1*(FCT(A+C)+FCT(A-C)))
RETURN
END
```